

Department of Environment, Land and Infrastructure Engineering (DIATI)

Master of Science in Environmental and Land Engineering

Spatiotemporal Analysis of Snow and Vegetation Dynamics Using Copernicus Sentinel-2 Imagery in the Maritime Alps

Candidate

Seyedeh Faezeh Sajjadi

Matricola: S307818

Supervisors:

Dr Francesca Matrone

Professor Fabio Giulio Tonolo

Declaration

I hereby declare that, except where specific reference is made to the work of others, the contents and organization of this dissertation constitute my own original work and does not compromise in any way the rights of third parties, including those relating to the security of personal data. This dissertation is entirely the result of my own work and includes nothing which is the outcome of work done in collaboration.

Seyedeh Faezeh Sajjadi

Acknowledgements

I would like to express my deepest gratitude to Dr. Francesca Matrone and Prof. Fabio Giulio Tonolo for their exceptional guidance, constant encouragement, and invaluable feedback throughout the course of this research. Their deep knowledge, intellectual generosity, and unwavering support have not only shaped the direction of this thesis but also deeply enriched my academic and personal growth. I am sincerely thankful for the time and attention they dedicated to every discussion, correction, and idea that helped transform this work into its final form.

My heartfelt appreciation goes to my family, whose unconditional love, trust, and encouragement have been the foundation of all my efforts. Although distance has often separated us, their presence has always been felt in every step of this journey. Their faith in me gave me the courage to persevere through challenges and the strength to move forward with confidence and hope.

I am profoundly grateful to my partner, whose patience, understanding, and unwavering belief in me have been a constant source of comfort and inspiration. Their presence has brought balance and light to the most demanding stages of this work, reminding me of the importance of love, support, and shared dreams.

I also wish to thank my friends, who stood beside me with kindness, humor, and encouragement, turning moments of stress into laughter and motivation. Their companionship made this journey more joyful and fulfilling.

Finally, to everyone who, in ways big or small, contributed to this achievement through words of encouragement, guidance, or silent support I extend my deepest gratitude. Your presence has made this experience truly meaningful and unforgettable.

Abstract

The research examines how vegetation and snow cover patterns change over time and space within the Maritime Alps (Western Italian Alps) which serves as a climate change and ecological transition hotspot. The research utilizes Sentinel-2 Level-2A multispectral imagery which underwent processing through two cloud-based Earth Observation (EO) platforms known as Google Earth Engine (GEE) and Sentinel Hub to track environmental changes from 2018 to 2024. Vegetation phenology and snow persistence were assessed using the Normalized Difference Vegetation Index (NDVI) and Normalized Difference Snow Index (NDSI).

A dual-threshold approach was applied: fixed thresholds (NDVI \geq 0.30, NDSI \geq 0.42) enabled temporal consistency, while adaptive Otsu thresholding addressed scene-specific spectral variability and topographic effects that typically reduce classification accuracy.

The validation process used four reference datasets which consisted of CORINE Land Cover 2018 and LUCAS 2022 and Carta degli Habitat and Copernicus Fractional Snow Cover (FSC) with their corresponding spatial scales and thematic precision levels. The evaluation of map accuracy included Overall Accuracy (OA) and Producer's and User's Accuracy (PA, UA) and Cohen's Kappa coefficient (κ) as statistical metrics. The results indicated that Otsu thresholds achieved superior results for detecting changes when the environment shifted between snowmelt and early vegetation growth but fixed thresholds delivered better results for monitoring long-term changes.

The cross-platform consistency between GEE and Sentinel Hub proved to be very high because both NDVI and NDSI products showed mismatch values under 15% which validated the reliability of the applied workflows. The NDVI data indicates that vegetation growth began earlier in years with short snow cover duration which supports the documented pattern of alpine vegetation moving to higher elevations (Lamprecht et al. 2018; Choler et al.,2021). The complete analysis of climate-driven landscape transformation emerges from studying vegetation and snow dynamics because it demonstrates how snowmelt impacts plant ecosystems.

This work presents a methodological approach which uses adaptive thresholding and multi-source validation and cloud-based processing to create a transferable and reproducible system for extended alpine monitoring. The research indicates GEE with Otsu adaptive thresholds provides the optimal combination of analytical consistency and scalability but Sentinel Hub delivers the most effective results for operational visualization and public dissemination of EO-based indicators. The dual-platform system provides support for upcoming climate monitoring and risk assessment and conservation planning activities in mountain areas with limited data availability.

Table of Contents

Abstract	4
Introduction	.10
1.1 Background and motivation	10
1.2 Problem statement	11
1.3 Objectives of the study	12
Project Framework	.13
2.1 Project framework: ACLIMO (Alpine Climate Monitoring)	13
2.2 Climate change impacts on vegetation and snow in the European Alps	13
2.2.1 Snow Cover Variability and Its Ecological Implications	14
2.2.2 Vegetation Dynamics and Phenological Shifts	14
2.2.3 Related Works and Research Context	14
2.3 Satellite imagery and data acquisition	15
2.3.1 Sentinel-2 Mission Overview	15
2.3.2 Data Characteristics and Preprocessing	16
2.4 Monitoring of vegetation and snow coverage through spectral indexes	21
2.4.1 Vegetation monitoring with NDVI	21
2.4.2 Snow monitoring with NDSI	24
2.5 Cloud-Based processing platforms	26
2.5.1 Google Earth Engine (GEE)	26
2.5.2 Planet Insight Browser (formerly Sentinel Hub EO Browser & APIs)	27
2.6 Otsu thresholding for NDVI and NDSI	28
2.7 Validation Approaches	30
2.7.1 Validation with LUCAS 2022	33
2.7.2 Validation with CORINE land cover 2018	33
2.7.3 Validation with Habitat Maps (Carta degli Habitat / Natura 2000)	34
2.7.4 Random-point validation	34
2.7.5 Validation with Copernicus Fractional Snow Cover	35

2.8 T	ransition to methodology	36
Preser	ntation Of Case Study37	,
3.1 T	he Maritime Alps as a Study Area	37
3.1	.1 Importance within ACLIMO Project	37
3.1	.2 Description of the Area	38
3.1	.3 Geological setting	39
3.1	.4 Climatic conditions	39
3.1	.5 Ecological and biodiversity value	39
3.1	.6 Historical and environmental events	40
3.2. (Considered Services for Sentinel-2 NDVI and NDSI Access	41
3.3 S	entinel Hub and Google Earth Engine: Vegetation and Snow Monitoring	44
3.3	.1 Overview and Functionality	44
3.3	.2 Comparative Strengths and Weaknesses	45
3.3	.4 Practical Applications and Workflow Examples	46
3.3	.5 Data Quality and Coverage Considerations	46
3.4 N	Iormalized Difference Indices: NDVI and NDSI	47
3.4	.1 Normalized Difference Vegetation Index (NDVI)	47
3.4	.2 Normalized Difference Snow Index (NDSI)	48
3.5 D	Pata Access and Processing Workflows for NDVI and NDSI	48
3.5	.1 Sentinel Hub workflow	49
3.5	.2 GEE workflow (cloud-side and post-processing)	51
3.5	.3 Definition of the monthly mean	52
3.5	.4 Definition of the robust Otsu threshold	53
3.5	.5 Cloud/shadow masking and mosaicking	53
3.5	.6 Equivalence and minor differences between platforms	55
3.5	.7 Deriving NDVI and NDSI Maps in QGIS	56
3.6 V	alidation Approaches!	57
3.6	.1 Validation of NDVI with CORINE Land Cover 2018	57
3.6	.2 Validation of NDVI with LUCAS 2022 and Confusion Matrix	62
3.6	.3 Post-Validation Evaluation and Sensitivity Analysis	65
3.6	4 Validation of NDVI with Carta deali Habitat	66

3.6.5 Validation of NDSI Results
Data, Processing, Results70
4.1 NDVI Dynamics from Google Earth Engine70
4.2 NDVI Dynamics from Google Earth Engine79
4.3 NDVI Dynamics from Sentinel Hub API82
4.4 NDVI Dynamics from Sentinel Hub API90
4.5 Validation of NDVI (2018) with CORINE Land Cover 201892
4.6 NDVI Threshold Optimization with CORINE 2018 (Google Earth Engine and Sentinel Hub)90
4.7 Validation of NDVI (2022) with LUCAS Data100
4.8 NDVI Threshold Optimization with LUCAS 2022 (Google Earth Engine and Sentinel Hub)104
4.9 Validation of NDVI (2018) with Carta degli Habitat109
4.10 NDSI Dynamics from Google Earth Engine113
4.11 NDSI Dynamics from Sentinel Hub123
4.12 NDSI Validation with Fractional Snow Cover (FSC) using Google Eartl Engine and Sentinel Hub133
4.13 Manual NDSI Validation (Google Earth Engine and Sentinel Hub, 2022) 143
Discussion
5.1 NDVI Thresholding and Vegetation Dynamics149
5.1.1 Fixed vs. Adaptive Thresholding
5.1.2 Validation with CORINE 201814
5.1.3 Validation with LUCAS 2022
5.1.4 Validation with Carta degli Habitat
5.1.5 Synthesis for NDVI
5.2 NDSI Thresholding and Snow Dynamics152
5.2.1 Seasonal Dynamics
5.2.4 Synthesis for NDSI
5.3 Cross-Platform Comparison (GEE vs Sentinel Hub)152
5.4 Ecological and Climatic Implications153

5.5 Methodological Recommendations 15	3
Conclusion155	
References158	

Introduction

1.1 Background and motivation

Mountain ecosystems represent some of the most active and climate-vulnerable regions which exist on Earth. The European Alps have experienced a major temperature increase which now stands at +2°C above late 19th century levels and exceeds global warming rates (Marty et al., 2017; Sven Kotlarski, Andreas Gobiet, Samuel Morin, Marc Olefs, Jan Rajczak & Raphaëlle Samacoïts, 2022.)The climate change has resulted in shorter snow cover duration and earlier snowmelt and altered plant growth patterns (Matiu et al., 2021).The changes in climate patterns produce two negative impacts on water circulation and energy transport systems which simultaneously damage mountainous ecosystems through biodiversity decline and increased natural disaster occurrences (Beniston et al., 2018).

The Maritime Alps (Piedmont Region, Northwestern Italy) experience these processes at their most extreme because of its steep climate differences and diverse landscape features and its position between Mediterranean and alpine bioclimatic zones. The duration of snow cover affects vegetation growth patterns and plant development which leads to changes in carbon storage and soil water content and slope stability. Scientists can create successful ecosystem-based climate adaptation plans through their research of these interactions while assessing the extended stability of alpine ecosystems.

Earth Observation (EO) advancements together with open-access satellite imagery data now enable environmental monitoring through their delivery of continuous spatial data that occurs frequently over time while maintaining reproducibility. The Copernicus Sentinel-2 mission serves as a primary EO data source because it provides multispectral optical imagery at 10–20 m resolution which enables precise monitoring of snow and vegetation and surface processes through its 5-day revisit cycle (M. Drusch a, et al., 2012). The EO data analysis and visualization capabilities of Google Earth Engine (GEE) and Sentinel Hub operate through cloud-based platforms which eliminate the need for users to possess local computing resources.

The ACLIMO (Alpine Climate Monitoring) Project under ARPA Piemonte serves as a key regional organization for establishing common methods to monitor alpine

areas. The ACLIMO system achieves harmonized climate monitoring through the combination of satellite data with in-situ meteorological networks and field

validation to analyze NDVI vegetation dynamics and NDSI snow-cover variability and geomorphological responses to climate forcing (Bonardi et al. 2010; ARPA Piemonte, 2023; JRC, 2023). The present research depends on this project for its conceptual and operational framework to improve the accuracy and consistency of Earth Observation-based alpine monitoring techniques.

1.2 Problem statement

The two indicators NDVI and NDSI show strong potential for vegetation and snow monitoring, yet threshold-based classification techniques continue to generate classification uncertainties. Research studies depend on established threshold values (NDVI \geq 0.30 and NDSI \geq 0.42) which (ROUSE JW, 1973) originally defined for low- to mid-latitude areas. 1974; (Hall et al., 1995.)The fixed threshold system allows for both reproducible results and time-based analysis yet it fails to identify changes in spectral patterns which result from variations in illumination and surface roughness and snow cover and canopy density that commonly occur in alpine regions. The combination of different land cover types in transitional zones which include snowmelt areas and rocky outcrops and sparse vegetation results in frequent classification mistakes (Verrelst et al., 2015).

The Otsu method (Otsu, 1979.). serves as an adaptive thresholding approach which determines the best threshold value through analysis of pixel value distributions that show bimodal characteristics. The data-driven thresholds automatically adapt to changes in spectral patterns which leads to better detection results in challenging conditions. The application of these methods in alpine monitoring faces restrictions because of insufficient standardization which creates difficulties when researchers attempt to validate and compare their results.

A second major challenge exists with validation datasets. The reference data sets CORINE Land Cover, LUCAS and Carta degli Habitat present distinct characteristics through their varying scales and thematic precision and acquisition techniques. points although it lacks sufficient density. The comparison between satellite-derived classifications and reference data produces discrepancies because of differences in scale and mixed pixel effects and time-based data misalignment. Research has not fully evaluated the cross-platform reproducibility between GEE

and Sentinel Hub systems because these platforms continue to gain popularity in Earth Observation operational workflows.

1.3 Objectives of the study

The overarching aim of this research is to develop and evaluate a dual-threshold remote-sensing methodology for integrated snow and vegetation monitoring in the Maritime Alps, leveraging multi-platform Sentinel-2 processing.

The specific objectives are:

- 1. To quantify temporal variations in vegetation (NDVI) and snow cover (NDSI) across the 2018–2024 period using Sentinel-2 Level-2A data processed in both GEE and Sentinel Hub.
- 2. To compare fixed and adaptive (Otsu) thresholding methods, identifying their strengths, weaknesses, and suitability under different environmental conditions.
- 3. To validate the classification results using multi-source reference datasets (CORINE, LUCAS, Carta degli Habitat, and FSC) and assess the reliability of each as ground-truth data.
- 4. To evaluate cross-platform consistency between GEE and Sentinel Hub, analyzing differences due to compositing, cloud masking, and data handling.
- 5. To provide methodological recommendations for alpine EO studies, defining best practices for threshold selection, validation strategies, and platform use.
- 6. To link spectral dynamics to ecological interpretation, examining how snow duration affects vegetation productivity and spatial distribution patterns in the Maritime Alps.

Through these objectives, the study contributes to refining EO-based monitoring frameworks and improving the reliability of vegetation—snow interaction analyses in mountain environments.

Project Framework

2.1 Project framework: ACLIMO (Alpine Climate Monitoring)

The ACLIMO (Alpine Climate Monitoring) Project under ARPA Piemonte coordination with academic and regional partners served as the research framework for this study. The project uses satellite Earth Observation data and insitu meteorological networks to track Western Italian Alps environmental and climatic patterns through geohazard field validation.

ACLIMO enables researchers to access standardized data and common methods for studying NDVI vegetation changes and NDSI snow cover patterns and climate-induced landslides and debris flows. The project framework provides the scientific basis for this research while maintaining methodological consistency that enables comparison with other Alpine monitoring studies (ARPA Piemonte, 2023; JRC, 2023; Bonardi et al., 2008).

2.2 Climate change impacts on vegetation and snow in the European Alps

Climate change has profoundly affected the cryosphere and vegetation dynamics across the European Alps. The region's mean annual temperature has significantly increased, the length of snow cover has decreased, and the growing season has begun earlier in recent decades (Matiu et al., 2021; Kotlarski et al., 2022). In particular, at high elevations where the snow—rain transition is most susceptible to temperature anomalies, these changes are changing species composition, reshaping alpine ecosystems, and impacting hydrological regimes.

Snow cover is essential for controlling soil moisture, energy balance, and the phenological stages of plants in alpine regions. Early soil exposure and, as a result, earlier vegetation greening are caused by shorter snow durations (Choler, 2021; Lamprecht et al., 2018). The way that alpine vegetation responds to these changes varies geographically, though; some areas are more productive because of longer growing seasons, while others are stressed because of less water available and more frequent drought events (Brunetti et al., 2009; Gobiet et al., 2014). Therefore, one of the most important indicators of ecological resilience to changing climatic conditions is the interaction between snow persistence and vegetation activity.

2.2.1 Snow Cover Variability and Its Ecological Implications

Variability in snow cover affects the environment directly as well as indirectly. It directly affects overwintering species and soil microbial communities by changing the insulation of soil and root systems. Snow indirectly affects downstream ecosystems, water resource availability, and runoff regimes (Marty et al., 2017). In many Alpine regions, especially at mid-elevations, satellite-based observations show that the average duration of snow cover has decreased by about 8.4% every ten years (Kotlarski et al., 2022). An upward shift in the snowline and a change from snow-dominated to rain-dominated precipitation regimes are frequently observed in conjunction with this decline.

2.2.2 Vegetation Dynamics and Phenological Shifts

Numerous in situ and remote sensing studies have documented how vegetation is responding to climate change. Although these changes vary with altitude, aspect, and species composition, earlier leaf-out and delayed senescence have prolonged the vegetation period throughout the Alps (Vitasse et al., 2018; Choler, 2021). Greenness trends are on the rise, according to NDVI-based analyses, especially in subalpine and montane zones where temperature constraints are most noticeable. High-elevation ecosystems, however, are getting close to ecological thresholds, beyond which changes in species dominance or moisture stress brought on by warming may lower productivity (Gamon et al., 2015; Senf et al., 2020).

2.2.3 Related Works and Research Context

. Prior research has evaluated vegetation and snow cover interactions by combining field observations, climate data, and satellite imagery. For example, Gascoin et al. (2020) examined Sentinel-2-derived NDSI to estimate snow persistence across mountain regions, and Choler (2021) used Sentinel-2 time series to track vegetation phenology in snow-controlled alpine grasslands.

Similarly, to measure snow-vegetation feedbacks in the Alps, Notarnicola et al. (2020) combined Sentinel-2 and MODIS data. These results demonstrate how crucial multispectral Earth Observation (EO) data are for identifying environmental changes with high temporal and spatial resolution. Building on this background, the Sentinel-2 satellite mission and the data collection method used for the study's vegetation and snow monitoring are explained in section 2.3.



Figure 2.1 Earth observation missions developed by ESA, Source: ESA,2023

2.3 Satellite imagery and data acquisition

Satellite Earth Observation provides a consistent and reproducible means of monitoring dynamic environmental processes such as snow and vegetation cover. In this research, Sentinel-2 Level-2A imagery was selected for its high spatial, spectral, and temporal resolution, which make it particularly suitable for mountainous environments characterized by complex terrain and rapid seasonal changes.

2.3.1 Sentinel-2 Mission Overview

The Sentinel-2 mission, which is a component of the European Space Agency's (ESA) Copernicus Program, is made up of two identical polar-orbiting satellites (Sentinel-2A and Sentinel-2B) that are 180° apart and in the same sun-synchronous orbit. According to Drusch et al. (2012), the mission offers worldwide coverage every two to three days at mid-latitudes and every five days at the equator. The Multispectral Instrument (MSI), carried by Sentinel-2, has spatial resolutions of 10 m, 20 m, and 60 m depending on the band. It can acquire 13 spectral bands, from visible to shortwave infrared (SWIR) (Table 2.1). Each MSI band's spectral configuration and spatial resolution are compiled in Table 2.1. Table 2.1 shows the spatial resolution and spectral bands of the Sentinel-2 MSI.

2.3.2 Data Characteristics and Preprocessing

The Sentinel-2 Level-2A product provides atmospherically corrected surface reflectance through the Sen2Cor processor, which includes correction for atmospheric, topographic, and adjacency effects. For this study, only bands relevant to vegetation and snow monitoring were retained specifically, the Red (B4), Near-Infrared (B8), and Shortwave Infrared (B11) bands. Cloud and shadow masking was applied using the Scene Classification Layer (SCL) and QA60 cloud mask to ensure high-quality input data.

The Multispectral Instrument (MSI) of Sentinel-2 operates as its core component to measure reflectance data through 13 bands which span from visible to short-wave infrared wavelengths as shown in Figure 2.2.

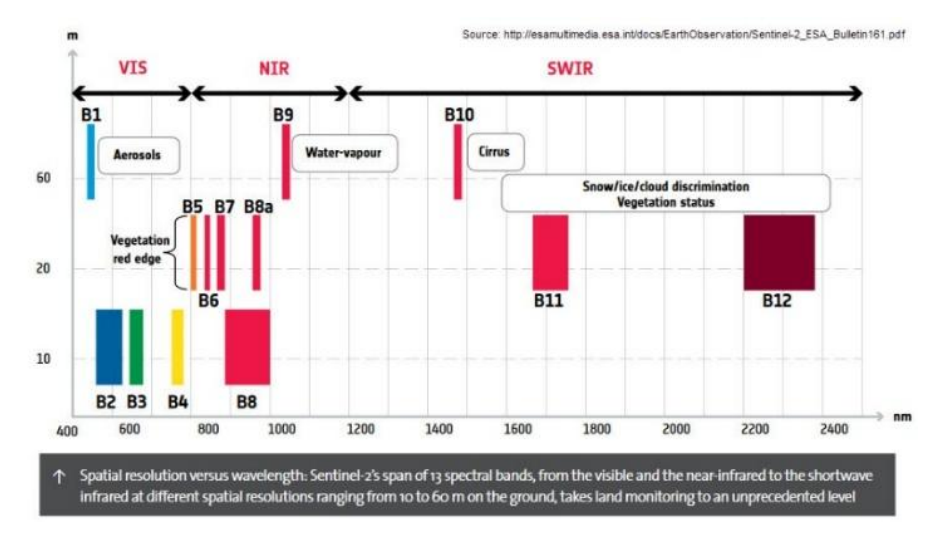


Figure 1.2 Sentinel-2 spectral bands (VIS, NIR, SWIR) and their main applications, Source: ESA (2015), Introducing Sentinel-2, ESA Bulletin 161.

The bands of Sentinel-2 provide optimal measurements for Earth surface and atmospheric physical properties which enables effective monitoring of vegetation health and soil and water moisture levels and snow cover and atmospheric conditions. The system operates at three native spatial resolutions which correspond to its designated measurement functions.

- 10 m bands (B2-Blue, B3-Green, B4-Red, B8-NIR): These bands deliver high spatial resolution data that scientists use to map land cover and study vegetation and urban environments. The NDVI index which serves as a key tool for vegetation monitoring requires the combination of data from the red (B4) and near-infrared (B8) bands.
- 20 m bands (B5–B7 red-edge series, B8A–narrow NIR, B11–SWIR-1, B12–SWIR-2): The additional spectral data from these bands enables detection of vegetation stress and provides information about canopy structure as well as soil and vegetation moisture and snow or burned area identification. The snow index (NDSI) uses the green band (B3 at 10 m) and SWIR-1 band (B11 at 20 m) to create its measurement.
- 60 m bands (B1-coastal aerosol, B9-water vapor, B10-cirrus): The bands serve mainly for atmospheric correction purposes to achieve accurate reflectance measurements across different wavelengths although they do not support detailed surface mapping applications.

The process of data preparation requires a fundamental step to merge bands recorded at different resolutions (10 m and 20 m) for NDVI and NDSI index calculations. The standard practice for data analysis involves two methods to handle band resolution differences: analysts either resample 10 m bands to match 20 m resolution, or they use pan-sharpening and super-resolution techniques to improve the detail of coarser bands. The application of Generative Adversarial Networks in deep learning technology has shown successful results for reducing 20 m and 60 m band resolution to 10 m which results in detailed vegetation and snow monitoring without compromising spectral accuracy (Romero et al., 2016)

The primary remote sensing data source for this research uses Sentinel-2 to study vegetation and snow patterns in the Maritime Alps. The combination of Sentinel-2's detailed spectral data with its high spatial resolution and regular data collection schedule makes it an ideal tool for studying the diverse snow and vegetation patterns and ecological shifts in this climate-vulnerable area.

Band	Description & Example Use	Central λ (nm)	Resolution
B1	Coastal aerosol, mainly for atmospheric correction and coastal water studies.	443	60 m
B2	Blue detects shallow water, turbidity, and atmospheric scattering. Combined with B3 and B4 to produce "true color" images.	490	10 m
В3	Green, useful for vegetation monitoring and in water indices such as NDWI (B3/B11). Also sensitive to snow reflectance.	560	10 m
B4	Red, strong chlorophyll absorption; crucial in NDVI (B8/B4) for vegetation productivity.	665	10 m
B5	Red-edge 1 enhances detection of chlorophyll content and crop differentiation.	705	20 m
В6	Red-edge 2, increases sensitivity to vegetation stress and canopy structure.	740	20 m
В7	Red-edge 3, valuable in forestry for phenology and long- term canopy health monitoring.	783	20 m
B8	NIR (broad), widely used for vegetation biomass and phenology, forms the basis of NDVI.	842	10 m
B8A	NIR (narrow), complements red-edge bands to discriminate subtle changes in vegetation condition.	865	20 m
В9	Water vapor detects absorption features of water vapor for atmospheric correction.	945	60 m
B10	Cirrus identifies thin, high-altitude cirrus clouds, improving cloud masking.	1375	60 m
B11	SWIR-1, sensitive to soil and vegetation moisture, also used in snow mapping (NDSI) and burn indices (NBR).	1610	20 m
B12	SWIR-2 provides information for geology, soils, and burned area assessment. (NBR).	2190	20 m

Table 2.1 Sentinel-2 MSI bands, their spectral characteristics, spatial resolution, and example applications.

During data preparation, 10 m and 20 m bands were merged to align the spatial resolution used for NDVI and NDSI calculations. This resampling step ensures consistency between vegetation and snow indices.

Sentinel-2 products are distributed in two main levels: Level-1C (Top-of-Atmosphere) and Level-2A (Bottom-of-Atmosphere) reflectance. Level-2A data, corrected by the Sen2Cor processor, remove atmospheric effects to provide surface reflectance values that are essential for accurate NDVI and NDSI computation in mountainous terrain ("ESA, 2023,".).

Overall, the Sentinel-2 mission provides a reliable and versatile dataset for Alpine environmental monitoring. Its combination of high spatial resolution, frequent revisit, and broad spectral depth makes it particularly suitable for tracking vegetation and snow dynamics in the Maritime Alps.

The overall workflow of this research from data acquisition to classification and validation is summarized in Figure 2.3. The detailed methodological description of each step, including index calculation, threshold selection, mosaicking, and accuracy assessment, is provided in Chapter 3.

The figure outlines the sequence from Sentinel-2 data acquisition and cloud filtering to NDVI/NDSI computation, thresholding (fixed and Otsu), validation with reference datasets, and final analysis of vegetation and snow trends.

The following section explains how these spectral capabilities are applied to monitor vegetation and snow using NDVI and NDSI indices.

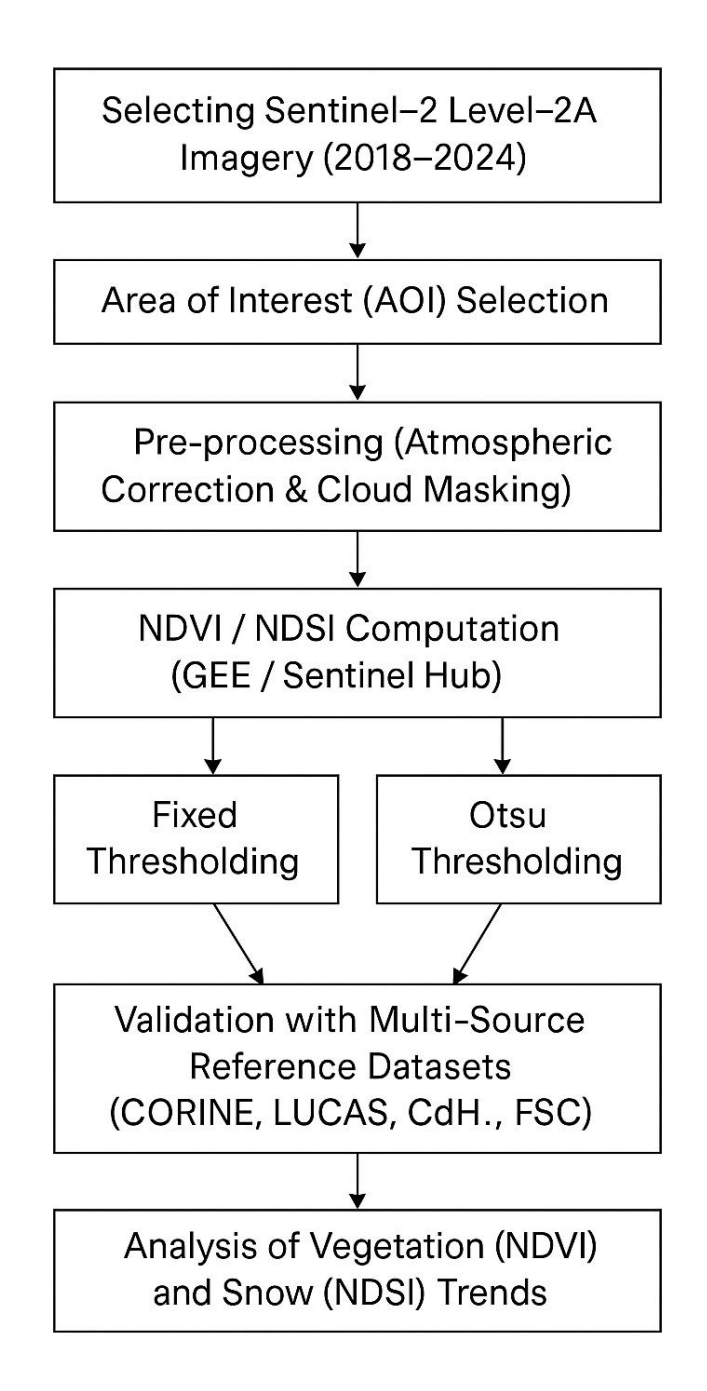


Figure 2.3 General workflow of the study showing the sequence from Sentinel-2 data acquisition to spectral index computation, threshold classification (Fixed and Otsu), validation using multi-source datasets, and analysis of vegetation and snow trends.

2.4 Monitoring of vegetation and snow coverage through spectral indexes

Monitoring vegetation and snow dynamics through spectral indexes is essential for understanding ecosystem responses to climatic variability in alpine regions. Among the available Earth Observation techniques, spectral indices derived from Sentinel-2 imagery particularly the Normalized Difference Vegetation Index (NDVI) and the Normalized Difference Snow Index (NDSI) provide robust tools for quantifying changes in vegetation greenness and snow-cover extent. This section presents an overview of the methodological framework used for index-based monitoring, including a comparative review of recent studies and the integration of cloud-based processing platforms.

2.4.1 Vegetation monitoring with NDVI

The Normalized Difference Vegetation Index (NDVI), which uses red absorption and near-infrared reflectance data, serves as one of the most widely adopted indicators for photosynthetic activity and green biomass estimation (Tucker, 1979). It is calculated using the following equation:

$$NDVI = \frac{(NIR - RED)}{(NIR + RED)}$$

where *NIR* and *RED* correspond to the near-infrared and red reflectance bands of the Sentinel-2 imagery. NDVI values range from –1 to +1, with high positive values representing dense vegetation and negative values corresponding to non-vegetated surfaces such as water, snow, or clouds.

As described in Section 2.3.2, Sentinel-2 provides 10–20 m spatial resolution and a 5-day revisit frequency, which together enable detailed temporal tracking of vegetation growth. These characteristics make NDVI especially suitable for Alpine studies characterized by steep gradients and mixed land-cover types.

Recent studies have emphasized that using multi-temporal NDVI stacks rather than single-date imagery. For instance, (Notti et all.,2023), demonstrated that Sentinel-2 NDVI time-series features enhance the discrimination of vegetation. Similarly, (Lasaponara et al., 2022)reported that NDVI trajectories from Google Earth Engine (see Section 2.5) improve reproducibility in Alpine vegetation mapping.

An example of NDVI-based vegetation classification in Alpine terrain is shown in Figure 2.4, where Sentinel-2 imagery captures spectral differences among forest, grassland, and shrubland habitats (Wakulińska and Marcinkowska-Ochtyr, 2020). Although the Giant Mountains differ geographically from the Maritime Alps, both regions share similar alpine ecological gradients and vegetation—snow interactions, making this study comparable in methodological approach and environmental relevance.

Beyond single-index analysis, NDVI can be complemented by derivative metrics such as the Normalized Difference Moisture Index (NDMI) (Gao, 1996) and Tasseled Cap Wetness (TCW) (Crist; Cicone, 1984), which enhance sensitivity to vegetation moisture and canopy structure. In addition, red-edge bands from Sentinel-2 (e.g., B5, B6, B7) have been incorporated to improve the detection of subtle chlorophyll variations and phenological trends (Parisi et al.,2023;Delegido et al., 2011)NDMI is computed as (NIR – SWIR) / (NIR + SWIR), indicating vegetation moisture content, while TCW derives from a linear combination of reflectance bands emphasizing soil and canopy wetness.

The NDVI is still the most reliable and interpretable indicator for vegetation monitoring in mountain ecosystems, even with its well-known drawbacks, such as saturation in dense canopies and sensitivity to topographic illumination. This is especially true when using multi-temporal and multi-platform frameworks for analysis.

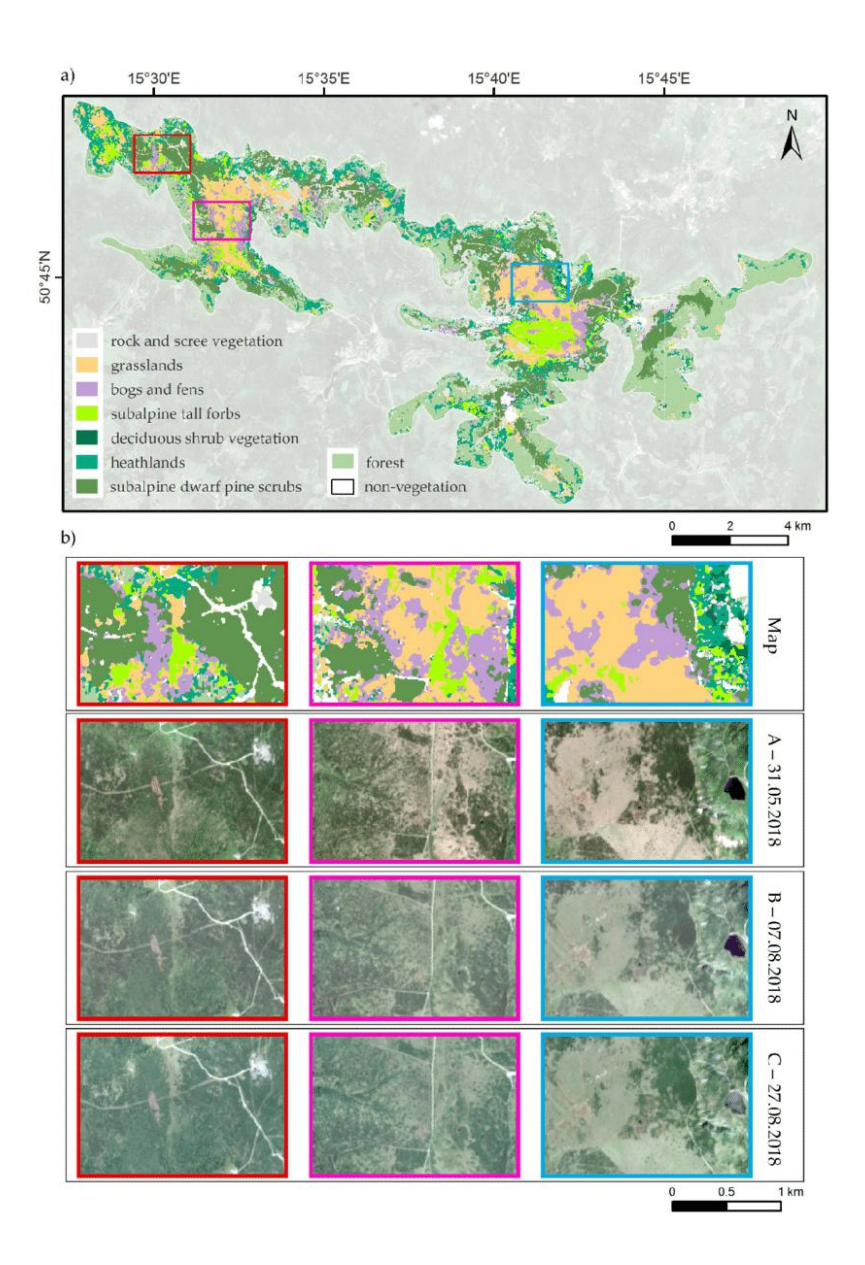


Figure 2.4 Vegetation types of the Giant
Mountains, based on Sentinel-2 imagery (natural
RGB composition), Source: Wakulińska &
Marcinkowska-Ochtyra (2020).

2.4.2 Snow monitoring with NDSI

The Normalized Difference Snow Index (NDSI) is widely used for quantifying snow-cover extent and monitoring its seasonal and inter-annual variability. Introduced by (Hall et al., 1995), NDSI exploits snow's high reflectance in the visible green wavelengths and its strong absorption in short-wave infrared (SWIR) to distinguish snow from bright surfaces such as clouds or bare soil. It is expressed as:

$$NDSI = \frac{(GREEN - SWIR)}{(GREEN + SWIR)}$$

where *GREEN* represents reflectance in the visible green band (Sentinel-2 Band 3, 0.56 μ m) and *SWIR* corresponds to the short-wave infrared band (Band 11, 1.61 μ m). High NDSI values (close to +1) indicate snow-covered areas, while lower or negative values correspond to water, cloud, or bare surfaces.

As described in section 2.3.2, the 10–20 m spatial resolution of Sentinel-2 enables fine-scale snow mapping and captures spatial heterogeneity previously unresolved by coarser sensors such as MODIS (250–500 m). Studies have demonstrated that Sentinel-2 NDSI time-series provide robust detection of snow persistence and seasonal transitions at catchment scales (Mazzotti et al.,2019; Dumont et al., 2020)When combined with the Scene Classification Layer (SCL), NDSI improves snow–cloud separation and refines seasonal snow cover metrics (Drolon et al., 2017).

The integration of multi-sensor archives (Landsat + Sentinel-2) and cloud-based infrastructures such as Google Earth Engine and Planet Insight Browser (see Section 2.5) has further enhanced temporal coverage, producing dense datasets for regional and continental snow monitoring. Automated pipelines on these platforms support near-real-time snow product generation and visualization (Mohammadi et al., 2023; Puliti a et al., 2017).

Observations across the European Alps show that snow extent has been decreasing, especially at mid-elevations, where rising temperatures accelerate snowmelt and shorten seasonal duration (Marty et al., 2017; Terzago et al., 2023). Model-based syntheses confirm that temperature, more than precipitation, is the dominant control on snow variability, highlighting the sensitivity of Alpine snow to ongoing warming (Kotlarski et al., 2023).

Despite improvements in data processing, NDSI analyses in mountainous terrain remain challenged by topographic shadows, forest canopy interference, and short-lived clouds, which can affect snow detection accuracy. Nonetheless, advanced correction techniques, such as terrain normalization and multi-date compositing, have considerably enhanced the reliability of Sentinel-2–based snow monitoring in complex landscapes.

As illustrated in Figure 2.5, the Sentinel-2 NDSI maps effectively distinguish snow and glacier cover, while advanced classifiers such as SVM and XGB refine the separation between ice and non-ice surfaces (Mohammadi et al., 2023).

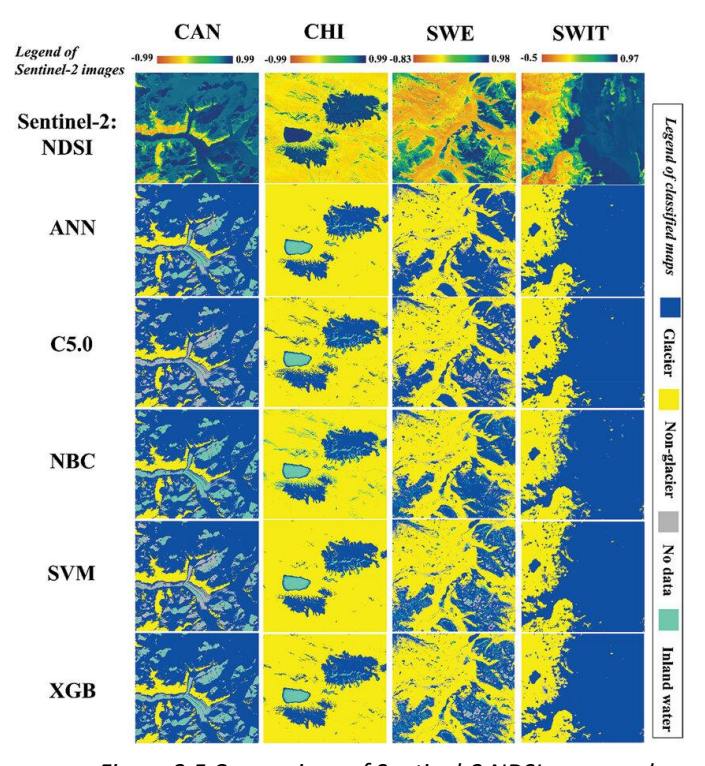


Figure 2.5 Comparison of Sentinel-2 NDSI maps and machine learning classifiers (ANN, C5.0, NBC, SVM, XGB) for glacier and snow detection across test sites in Canada (CAN), Chile (CHI), Sweden (SWE), and Switzerland (SWIT). Blue areas represent glaciers.

In addition to binary classification, the Copernicus Fractional Snow Cover (FSC) product provides 20 m resolution estimates of the percentage of snow within each pixel across Europe. This fractional metric serves as a key validation dataset because it quantifies partially snow-covered areas that NDSI may classify as either snow or no-snow. As a result, FSC complements NDSI by enhancing accuracy assessment in complex mountainous terrain and mixed pixels, making it the preferred reference for snow-related validation in this study (see Chapter 3 for details on its implementation).

To process these spectral indices efficiently across multiple years, cloud-based platforms were adopted, as described in the next section.

2.5 Cloud-Based processing platforms

The Sentinel-2 satellite imagery growth demands cloud-based systems to manage data access and processing and visualization operations at high performance levels. Users can access and process large Earth Observation (EO) datasets through online systems which eliminate the need for storage space and powerful computing equipment.

Both Google Earth Engine (GEE) and Planet Insight Browser (formerly Sentinel Hub EO Browser) operate with Sentinel-2 Level-2A surface-reflectance products, ensuring consistent input data. Their main differences arise from the mosaicking, cloud-masking, and data-processing pipelines applied within each system.

This section presents two major platforms widely adopted in environmental and cryospheric studies: Google Earth Engine and Planet Insight Browser (previously known as Sentinel Hub EO Browser).

2.5.1 Google Earth Engine (GEE)

Fully automated analyses using JavaScript or Python scripting are made possible by the Google Earth Engine (GEE) platform, which offers petabyte-scale access to multispectral, radar, and climate datasets. Without downloading raw imagery, GEE's cloud computing enables scalable Sentinel-2 processing, mosaicking, and timeseries generation.

By combining cloud-free composites and surface reflectance correction, GEE allows users to compute NDVI and NDSI over wide regions and extended periods of

time. The system is perfect for creating repeatable pipelines and validation procedures because of its scripting flexibility.

Prior research has shown that GEE is useful for Alpine monitoring, such as phenological evaluations in mountain ecosystems (Rösch et al., 2022) and NDVI trajectory analysis for landslides and wildfires (Lasaponara et al., 2020; Notti et al., 2023). The platform offers free access for research purposes and outputs data in several formats (GeoTIFF, CSV, and JSON) (see Figure 2.6 for interface overview).



Figure 2.6 Google Earth Engine Code Editor

interface, Source: Science Park Study Group (2015).

2.5.2 Planet Insight Browser (formerly Sentinel Hub EO Browser & APIs)

The Planet Insight Browser now operates under Planet Labs since the Sentinel Hub service transition while offering quick visualization and analysis capabilities for Sentinel-2 data within the Copernicus program. The interface enables users to view multispectral imagery and create NDVI and NDSI composites and obtain processed layers through its web interface or Application Programming Interfaces (APIs).

Unlike the previous open access Sentinel Hub Statistical API, the new Planet Insight API requires user registration and authentication via an access token. The free version of the service has restrictions on the number of requests and data volume, but professional subscriptions provide access to bigger workflows. The system provides data outputs through standard formats which include Geo TIFF and PNG and JSON metadata.

The platform excels in interactive visualization and figure generation, making it particularly suitable for rapid assessments and communication with non-technical audiences. However, compared to GEE, its restricted scripting and automation capabilities limit its use for large-scale time-series or validation studies.

The flexible cloud-based architecture of Planet Insight, shown in (Figure 2.7), demonstrates how web-based and API workflows can integrate with GIS software and Python or JavaScript environments for on-demand visualization and data delivery.

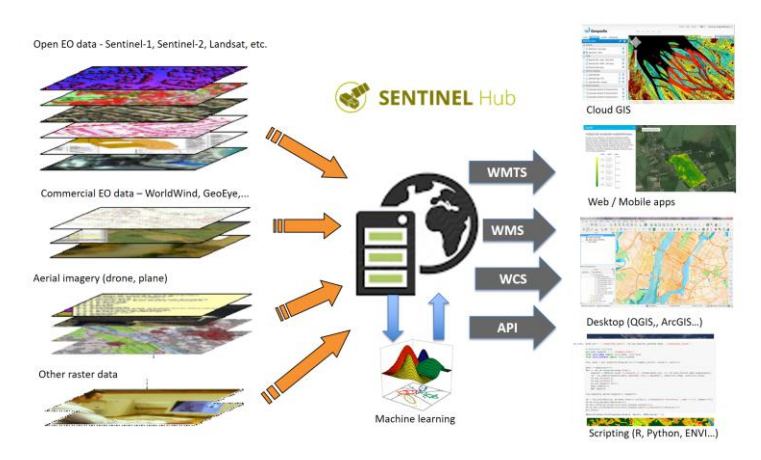


Figure 2.7 Planet Insight (formerly Sentinel Hub) data architecture and application. Source: ESA (2019).

2.6 Otsu thresholding for NDVI and NDSI

The conversion of continuous spectral indices like NDVI and NDSI into binary classes (vegetated/non-vegetated or snow/no-snow) needs automated threshold selection methods which produce consistent results across different environmental conditions.

Unlike fixed thresholds that rely on predetermined values, the Otsu approach computes an optimal threshold (t) directly from the image histogram, maximizing the variance between classes while minimizing variance within each class. This data-driven process removes human subjectivity in threshold definition and ensures consistent classification across different environmental settings.

The method analyses the histogram of pixel values and finds the separation point that best divides two distinct distributions, for example, vegetated vs. non-vegetated or snow-covered vs. bare areas based on reflectance differences. The optimal threshold is located at the lowest point between the two peaks of the frequency distribution, as shown in Figure 2.8.

$\sigma B2(t) = \omega 1(t)\omega 2(t)[\mu 1(t) - \mu 2(t)]2$

where σ_B^2 is the between-class variance, ω_1 and ω_2 are the probabilities of the two classes, and μ_1 and μ_2 are their mean values. The optimal threshold t^* is found where $\sigma_B^2(t)$ is maximized.

For large-scale or multi-temporal analyses, where manual selection would be inconsistent, automated thresholding works especially well.

The Otsu algorithm is perfect for studies that span several years or climatic conditions because it can adjust to scene-specific conditions like illumination, snow albedo, or vegetation density. To maintain methodological consistency across all years and validation datasets, Otsu thresholding was applied to both the NDVI and NDSI datasets in this study.

Because Otsu thresholding creates stable binary masks that reduce class overlap under different illumination conditions, it is advantageous for NDVI classification (Xue et al., 2021; Zhou, 2020).

Likewise, for NDSI, this approach outperforms static thresholds in high-reflectance or shaded terrain and successfully separates snow from other bright surfaces (such as ice or clouds) (Gascoin et al., 2019; Härer et al., 2018) For example, Otsu thresholding effectively extracted snow extent in the Pyrenees and Mount Erciyes, even in the presence of variable illumination (Gascoin et al., 2018).

Research literature suggests several guidelines for optimal Otsu implementation:

- Apply Otsu thresholding to specific time periods or spatial subsets where snow or vegetation presence is expected to vary.
- Integrate cloud and shadow masks to minimize atmospheric and topographic artifacts.
- Document threshold sensitivity between months or seasons to identify environmental shifts.

These best practices were adopted throughout this study to ensure comparability between vegetation (NDVI) and snow (NDSI) analyses.

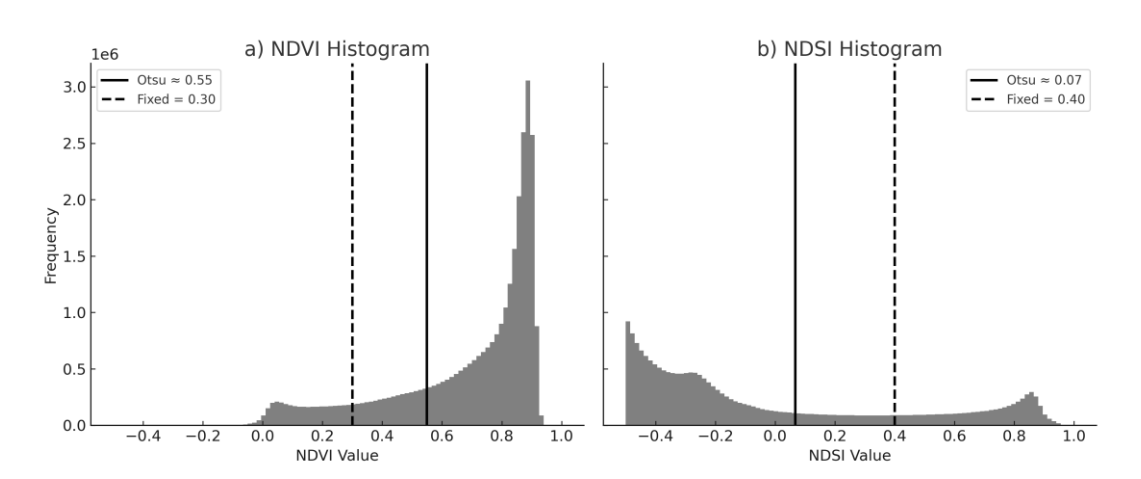


Figure 2.8 Greyscale histograms of (a) NDVI June 2022 and (b) NDSI showing Otsu thresholds (solid lines) April 2022 GEE compared with fixed thresholds (dashed).

2.7 Validation Approaches

The reliability of interpreting NDVI and NDSI derived products depends on validation processes.

Validation ensures that index-derived classifications (vegetation and snow) accurately represent real-world conditions by comparing them with independent reference datasets.

The European region depends on two primary datasets for this work, including CORINE Land Cover (CLC) and LUCAS (Land Use/Cover Area Frame Survey). In addition, ecological frameworks such as the Carta degli Habitat and the Natura 2000 network, developed under the EU Habitats Directive, provide reference maps for validating the *ecological significance* of EO-derived vegetation and snow-cover changes.

These frameworks extend validation beyond simple land-cover classification, linking spectral indices (NDVI, NDSI) to real habitat conditions and conservation status. (György Büttner, 2014).

• **CORINE Land Cover (CLC):** Provides continental-scale land-cover maps at 100 m resolution with a minimum mapping unit of 25 ha.

- **LUCAS:** Offers in-situ field observations at point locations across the EU, serving as accurate ground-truth samples for pixel-level validation.
- Carta degli Habitat (CdH): Supplies polygon-based habitat delineations derived from ecological surveys, mainly used for qualitative assessment.

Using these complementary datasets allowed the analysis to combine spatial consistency (CLC), point precision (LUCAS), and ecological context (CdH).

The accuracy evaluation used confusion matrices to measure the agreement between classification outputs and reference data according to (Congalton, Green, 2019) and (Foody, 2002). The matrix compares predicted versus reference classes and summarizes correct (true) and incorrect (false) classifications, enabling computation of multiple statistical indicators:

- **User's Accuracy (UA)** measures the likelihood that a specific pixel classification matches its actual ground-based classification.
- The Producer's Accuracy (PA) measures the likelihood that reference pixels match their corresponding map classifications.
- Overall Accuracy (OA) represents the total number of correctly classified pixels in relation to the complete dataset.
- The Kappa Coefficient (K) evaluates the degree of agreement between classification results and reference data by removing random classification errors.

These metrics were computed separately for NDVI (vegetation/non-vegetation) and NDSI (snow/no-snow) classifications to ensure cross-index comparability.

The same validation structure was applied across all datasets and years, ensuring methodological consistency.

Each validation dataset (CLC, LUCAS, CdH) provided independent samples, and NDVI/NDSI predictions at corresponding locations were extracted for accuracy computation.

Reference Data	Vegetation (1)	Non-Vegetation (0)	Total
Predicted Vegetation (1)	TP	FP	TP+FP
Predicted non- vegetation (0)	FN	TN	FN+TN
Total	TP+FN	FP+TN	N

Table 2.1 Structure of a binary confusion matrix illustrating the relationship between predicted and reference vegetation classes used for accuracy assessment.

Where TP, FP, FN, and TN denote true positives, false positives, false negatives, and true negatives respectively.

Applying this standardized approach across both NDVI and NDSI ensures consistent accuracy comparison between vegetation and snow-monitoring analyses.

An example of a confusion matrix used in this process is shown in Figure 2.9, which visually demonstrates the distribution of correct and incorrect classifications.

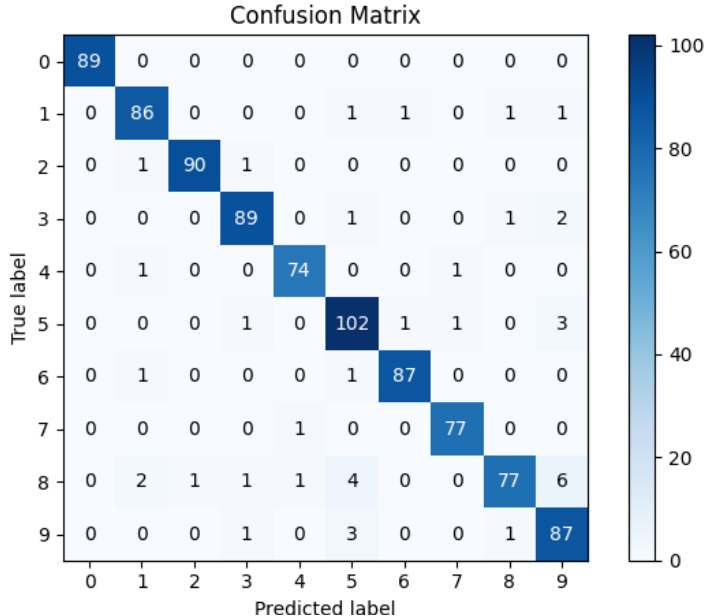


Figure 2.9 Example of a binary confusion matrix used to evaluate classification accuracy, Source: adapted from the Scikit-learn documentation (Pedregosa et al., 2011).

2.7.1 Validation with LUCAS 2022

The LUCAS (Land Use/Cover Area Frame Survey) dataset provides high-precision, ground-based observations collected across Europe. Its point-based design offers reliable validation for pixel-level classification accuracy. Research integrating Sentinel-2 NDVI data with LUCAS points demonstrates its effectiveness for mapping vegetation dynamics.

For instance, the research by (d'Andrimont et al., 2021) combined Sentinel-2 NDVI time series data with LUCAS reference points to create European-scale crop type maps which achieved more than 85% overall accuracy through confusion matrix analysis that showed most errors occurred between similar types. Similarly, research by (Malinowski et al., 2020) evaluated NDVI-based land-cover mapping in Poland through LUCAS sample validation which produced high accuracy for forest and cropland classes but lower accuracy for transitional and mosaic core(Drolon et al.,2017) applied Sentinel-2 NDVI data in GEE to classify categories.

Such results highlight LUCAS as a robust reference for vegetation-related validation due to its direct field observations and precise geolocation.

2.7.2 Validation with CORINE land cover 2018

The CORINE Land Cover (CLC) dataset provides a harmonized European land-cover inventory with a 100 m spatial resolution, making it well suited for class-based validation at regional and continental scales. (Belcore et al., 2024)) used CLC to validate Alpine NDVI classifications, reporting an overall accuracy of 94.5%, confirming clear spectral separability between grasslands, shrubs, and forest areas. Similarly, (Varga et al., 2020) observed distinct NDVI patterns among CLC Level-1 categories (forest, cropland, urban), supporting its reliability for vegetation-type evaluation.

For snow mapping, several studies have applied confusion-matrix validation to CLC-based or in-situ datasets. (Häre et al., 2019) evaluated Otsu and fixed NDSI thresholds for Turkey's Mount Erciyes, finding that Otsu improved snow detection but occasionally underestimated snow extent. In the (Pyrenees, Gascoin et al., 2018) validated Sentinel-2 NDSI using in-situ snow depth measurements, showing that adaptive thresholding enhanced performance under variable illumination conditions.

These findings confirm that CLC supports class-wise validation of both NDVI and NDSI, though its coarse resolution limits fine-scale pixel accuracy compared to LUCAS. Consequently, this study adopted CORINE for categorical validation and LUCAS for point-level validation, ensuring complementary accuracy evaluation.

2.7.3 Validation with Habitat Maps (Carta degli Habitat / Natura 2000)

Building upon the CORINE and LUCAS-based validation, the *Carta degli Habitat* framework aligned with the EU Habitats Directive and the Natura 2000 network serves as an ecological labelling system that enhances land-cover inventory and conservation assessments.

The ecological processes of structure and species composition and conservation status make these frameworks suitable for validating the ecological significance of EO-derived greenness changes that extend beyond basic cover types.

Sentinel-2-derived NDVI trajectories and identified habitat types can be compared thanks to the CdH database. For instance, (Čahojová et al.,2022) and (Pesaresi et al., 2020) identified unique forest phenology patterns within Annex I habitats using time-series NDVI and functional principal component analysis (FPCA), with accuracies of up to 87.5% in temperate and Mediterranean regions.

Furthermore, it was shown by (Moravec et al., 2023) that Natura 2000 polygons exhibiting aberrant spectral behavior can be identified using a combination of Sentinel-1 and Sentinel-2 features, which leads to targeted field verification.

The NDSI method finds limited use in habitat validation but remains important for snow-dependent habitats because snow duration acts as a vital ecological factor. The existing research shows that combining NDSI-based snow duration measurements with NDVI phenology analysis would create a dual ecological assessment system for habitats that require both snow presence and growing season duration for their identification and condition assessment.

2.7.4 Random-point validation

When ground-truth data are scarce or dispersed unevenly, a common validation technique is random or stratified point sampling.

In order to extract predicted classes (such as vegetation/non-vegetation or snow/no-snow) from NDSI or NDVI maps, representative sampling points are randomly generated within the Area of Interest (AOI).

Accuracy metrics like user and producer accuracy are then calculated by comparing these sampled values with reference datasets (such as CORINE and LUCAS). Due to its ability to objectively and reproducibly evaluate classification performance across large or complex terrains, this approach has gained widespread adoption (Olofsson et al., 2014; Congalton, 1991).

Random sampling has been used in Alpine applications to assess spatial variability in snow cover and guarantee statistical robustness on MODIS and Landsat snow maps.

Its reliability mainly depends on two factors:

- 1. The representativeness and spatial density of the sampled points, and
- 2. The accuracy of the reference data used for comparison.

Random-point validation complements the other datasets by ensuring classification consistency across the AOI, particularly where in-situ data are scarce.

2.7.5 Validation with Copernicus Fractional Snow Cover

The Copernicus Fractional Snow Cover (FSC) product serves as the primary quantitative reference for snow-cover validation in this study.

FSC data, available at 20 m resolution since 2016, represent the proportion of snow within each pixel providing a fractional rather than binary view of snow extent (Nagler et al., 2015; Salomonson & Appel, 2004).

This capability is especially valuable for mixed or partially snow-covered pixels that traditional NDSI classification may mislabel.

FSC data are widely used to validate or complement NDSI-derived snow products in mountain regions because they supply frequent, spatially detailed updates (Gascoin et al., 2019; Dumont et al., 2020). Research has shown that FSC supports two complementary validation pathways:

1. Binary validation, where pixels with FSC ≥ 50 % are interpreted as snow; and

2. Fractional validation, in which continuous NDSI-FSC relationships are analysed through correlation or RMSE metrics.

The integration of Sentinel-2 data with Copernicus FSC ensures spatial consistency and temporal continuity, making FSC an optimal external benchmark for Alpine snow-monitoring studies (Puliti et al., 2021; Mohammadi et al., 2023).

To evaluate classification accuracy, the study adopted a confusion-matrix framework (introduced in Section 2.7), which summarizes agreement between predicted and reference snow classes (Figure 2.9).

2.8 Transition to methodology

The scientific and technical basis of this study was laid out in the previous sections, which described how Sentinel-2 spectral indices (NDVI and NDSI), thresholding techniques (fixed and Otsu), and a multi-layer validation framework are used for vegetation and snow monitoring in Alpine regions.

These elements work together to create an integrated Earth Observation (EO) approach that is intended to assess the spatiotemporal evolution of snow cover and vegetation greenness under varying climatic conditions.

While the integration of CORINE, LUCAS, Carta degli Habitat, and Copernicus FSC datasets provides complementary validation scales from continental land-cover consistency to ground-truth precision and ecological relevance the combination of fixed and adaptive thresholds allows for the detection of both year-specific variability and stable long-term trends.

Moreover, the use of cloud-based platforms (Google Earth Engine and Sentinel Hub) ensures efficient data acquisition, processing, and reproducibility across multiple years.

Chapter 3 builds upon this conceptual framework by presenting the operational workflow employed in this thesis. It details the step-by-step procedures for data acquisition, pre-processing, index computation, threshold application, and validation, as illustrated in the graphical methodology diagram. This transition from theoretical foundation to applied methodology ensures that the analysis is both scientifically grounded and operationally reproducible across the Western Italian Alps.

Presentation Of Case Study

3.1 The Maritime Alps as a Study Area

3.1.1 Importance within ACLIMO Project

The ACLIMO (Alpine Climate Monitoring) Project is an INTERREG cross-border initiative coordinated by ARPA Piemonte in collaboration with academic and regional partners from Italy and France. The project aims to establish a harmonized framework for monitoring Alpine environmental dynamics by integrating satellite Earth Observation data, in-situ measurements, and geohazard field validation.

The main objectives of ACLIMO are to enhance understanding of Alpine climate change impacts on snow cover, vegetation phenology, and slope stability, while supporting long-term ecosystem and hazard management strategies. Through the development of multiscale and multi sensor methodologies, the project promotes consistent data acquisition, thresholding, and validation approaches across representative Alpine sites.

To achieve these objectives, ACLIMO applies a standardized methodological framework that combines optical and radar satellite imagery with meteorological and ground-based datasets, enabling spatial and temporal analyses of snow- and vegetation-related processes. This multilevel approach allows for both local-scale assessments and regional-scale comparisons of climatic responses across the Western Alps.

Within this framework, the present study contributes to the first analytical component of ACLIMO, focusing on small-scale and satellite-based investigations of vegetation and snow dynamics. By implementing Sentinel-2 Level-2A imagery and dual-thresholding methods (fixed vs. adaptive), the research strengthens the project's overarching goal of monitoring climate-driven transformations in Alpine ecosystems and validating methodological consistency across border areas between Italy and France.

3.1.2 Description of the Area

The Maritime Alps represent the southernmost section of the Alpine arc which connects northwestern Italy (Piedmont and Liguria) to southeastern France (Provence-Alpes-Côte d'Azur). The mountain range reaches from the Col de Tende in the southern part to the Stura di Demonte Valley in the northern section with elevations that span from 500 meters of foothills to peaks higher than 3,000 meters including Monte Argentera at 3,297 meters. The area presents a distinctive Alpine landscape with deep valleys and glacial basins and steep mountain slopes which create an intricate mountainous terrain (Bonardi et al. (2010); COMOGLIO et al., 2003)Figure 3.1 provides a detailed topographic view of the Maritime Alps, while Figure 3.2 situates the ACLIMO Project study area along the Italy–France border within the Aree Protette Alpi Marittime and Mercantour National Park regions.

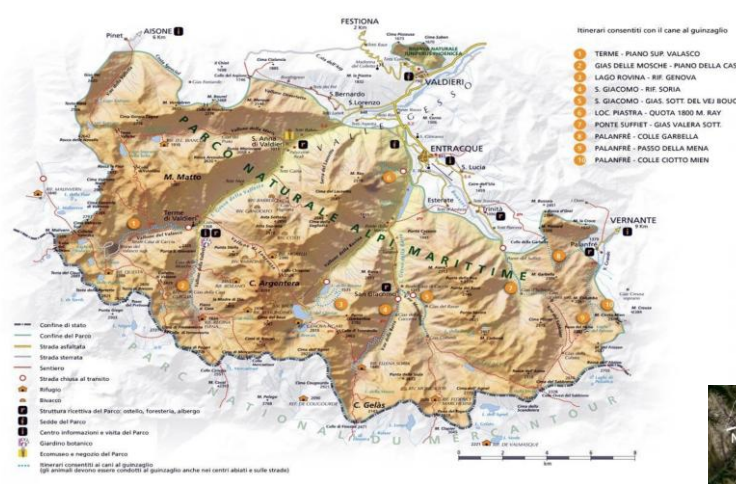


Figure 3.1 Detailed view of Maritime Alps, Source:

Mohseni (Mapping Snow and Vegetation Coverage Using

Multitemporal Open Satellite Imagery: Case Study of Maritime

Alps, Politecnico di Torino



Figure 3.2. ACLIMO Project study area located along the Italy–France border within the Maritime Alps, encompassing the Aree Protette Alpi Marittime and Mercantour National Park regions. Source: ACLIMO Project, Politecnico di Torino (2024).

3.1.3 Geological setting

The Maritime Alps form part of the southern Alpine mountain range because they exist where European and Adriatic tectonic plates meet. The area consists of gneisses and schists and granites which alternate with sedimentary rock layers of limestone and marl (Comoglio et al., 2003). The diverse geological foundation creates extensive landscape variability because it produces unstable steep rock faces and glacial deposits in valley basins and karstic systems within carbonate-rich areas. The geological structure determines both the formation of the landscape and the development of soils and water systems and slope activities which directly influence plant growth and snow accumulation patterns.

3.1.4 Climatic conditions

The Maritime Alps function as a transitional area between Mediterranean climate zones and Alpine climate zones. The Mediterranean climate pattern of mild winters and dry summers dominates the lower valley areas but the higher mountain regions experience Alpine weather with heavy snowfall and prolonged snow cover and cool summer temperatures (Comoglio et al., 1978; JRC, 2023). The mountainous terrain creates enhanced precipitation patterns which result in more than 2000 mm of annual rainfall in certain drainage areas.

Recent climate studies indicate that this region exhibits high sensitivity to warming trends, with snow seasons starting later and ending earlier, leading to a measurable reduction in snow duration and depth (Marty et al., 2017; Terzago et al., 2023). These shifts have major implications for hydrology, vegetation phenology, and slope stability in Alpine catchments.

3.1.5 Ecological and biodiversity value

The Maritime Alps qualify as Europe's most biodiverse region because they combine Mediterranean and Alpine biological regions. The region contains many unique species and different environments which range from Mediterranean shrublands to alpine tundra and permanent snow areas (Casazza et al., 2005). The area contains numerous protected Natura 2000 sites and regional parks that safeguard its diverse ecosystems including Parco Naturale Alpi Marittime in Italy and Parc National du Mercantour in France. The ecosystems face high sensitivity to snow regime changes because snowbed communities face extinction from reduced snow

periods while forest ecosystems move to higher elevations (Cornelissen et al., 2007).

This ecological variability makes the Maritime Alps a key natural laboratory for studying climate impacts on vegetation—snow interactions using Earth Observation data.

3.1.6 Historical and environmental events

Scientists have been studying the Maritime Alps because these mountains show high sensitivity to natural climate and geological changes. The historical documentation (Comoglio, 2003). The 1994 Piedmont flood and subsequent Little Ice Age ended with glacial retreat which became more rapid during the 20th century according to floods in 2020 triggered numerous landslides and debris flows throughout the region because heavy rainfall events make steep slopes highly susceptible to failure (Castellaro et al., 2014). The region demonstrates how climate changes affect snow conditions and vegetation growth which in turn creates new hazards.

Building upon this regional and historical context, the following section presents the remote sensing datasets and satellite processing services employed for quantifying vegetation and snow-cover dynamics in the Maritime Alps.

3.2. Considered Services for Sentinel-2 NDVI and NDSI Access

Sentinel-2 was selected for this study because it provides open-access multispectral data with 10–20 m spatial resolution and a five-day revisit frequency, which are particularly suitable for detecting vegetation and snow dynamics in mountainous terrain. Its long temporal coverage (2018–2024) also ensures compatibility with previous satellite time series such as Landsat and MODIS, facilitating trend continuity and inter-sensor comparison for long-term Alpine monitoring.

The evaluation of Sentinel-2 imagery requires selecting efficient Earth Observation (EO) services capable of managing large datasets and performing preprocessing operations for NDVI and NDSI analysis.

The process of downloading and processing large Sentinel-2 Level-1C and Level-2A products through ESA's Copernicus Open Access Hub becomes inefficient for time-series studies in mountainous regions (Gorelick et al., 2017)Therefore, this study focused on cloud-based platforms that automate atmospheric correction, mosaicking, and spectral index generation.

The Climate Engine platform provides browser-based access to pre-computed NDVI time-series data from Landsat, Sentinel-2, and MODIS satellites (https://climateengine.org). The study by Huntington et al. (2017) demonstrated its utility for large-scale vegetation anomaly and drought index analysis, though it lacks pixel-level precision.

The Agri4Cast service, developed by the Joint Research Centre (JRC) of the European Commission, generates dekadal NDVI composites for agricultural monitoring from 2000 onwards (https://agri4cast.jrc.ec.europa.eu). However, its aggregated data resolution is insufficient for detailed Alpine terrain analysis (Baruth et al., 2007).

The NASA Earthdata LP DAAC distributes MODIS and VIIRS snow and vegetation products at global scale (https://lpdaac.usgs.gov). While it ensures long-term temporal consistency, its spatial resolution (250–500 m) limits application in small Alpine catchments (Hall & Riggs, 2007; Gascoin et al., 2018).

The ARPA Piemonte Geoportal provides regional NDVI layers for the Piemonte Alps but lacks access to raw raster datasets required for quantitative analysis (https://www.arpa.piemonte.it).

Currently, the two most adaptable platforms for Sentinel-2 data processing are the Planet Insight Browser (formerly Sentinel Hub EO Browser) and Google Earth Engine (GEE). Both enable fast data visualization, atmospheric correction, and spectral index generation for vegetation and snow monitoring (Belcore et al., 2024; Phiri et al., 2020)).

- Planet Insight Browser enables rapid online visualization and NDVI/NDSI computation through an intuitive interface and API access.
- **Google Earth Engine** provides powerful scripting capabilities (JavaScript and Python) for batch processing, multi-temporal analysis, and integration with validation datasets.

Previous studies (Belcore et al., 2024; Mohammadi et al., 2023) confirm that GEE-based pipelines achieve high accuracy (94–95 %) in Alpine NDVI/NDSI mapping and can efficiently scale to continental snow-monitoring workflows.

For this thesis, Sentinel Hub was used for visual inspection, cloud filtering, and scene selection, while GEE managed automated computation, thresholding, and validation steps. This dual-platform strategy optimized both efficiency and accuracy, ensuring reproducibility for long-term vegetation and snow monitoring in the Maritime Alps.

Materials & Methods

Platform	Strengths	Limitations	Suitability for study
Climate Engine	Simple browser interface; automatic temporal aggregation (mean, anomalies, trends); supports Sentinel, Landsat, MODIS	Limited polygon flexibility; restricted raw data export; results often pre-aggregated	Useful for quick time- series checks, but not selected as a core tool
Nasa Earthdata LP DAAC	Validated MODIS/VIIRS NDVI and NDSI products; global, long-term consistency	Coarser resolution (250–500 m); limited flexibility in thresholding and AOI clipping	Complementary background dataset, but not primary tool
Agri4Cast	Dekadal NDVI composites; long time series since 2000; CSV outputs at regional scale	Only aggregated statistics, no raster export; limited spatial detail	Good for regional-scale vegetation trends, not local analysis
ARPA Piemonte Geoportal	Regional NDVI visualizations for Piedmont; useful for qualitative validation	Provides static maps only (no raw rasters, no thresholding)	Used as contextual reference only
Sentinel Hub (EO Browser & APIs)	Direct access to Sentinel- 2NDVI/NDSI layers; custom scripts; rapid visualization; time-lapse; supports Statistical API for aggregation	EO Browser requires manual image selection; advanced features (Statistical API) need subscription	Selected as one of two main platforms (rapid analysis & visualization)
Google Earth Engine	Free for research; planetary-scale datasets (Sentinel, Landsat, MODIS, etc.); cloud masking; thresholding; reproducible scripted workflows; area statistics	Requires programming skills; steep learning curve for beginners	Selected as one of two main platforms (scalable, reproducible analyses)

Table 3.2 Comparison of selected Earth Observation platforms used for NDVI and NDSI data access and analysis. Adapted from Huntington et al. (2017); Baruth et al. (2007); Hall & Riggs (2007); Gascoin et al. (2018); Belcore et al. (2020); Fernández et al. (2023); Radic et al. (2020); ARPA Piemonte (2023).

3.3 Sentinel Hub and Google Earth Engine: Vegetation and Snow Monitoring

The research depends on Sentinel Hub and Google Earth Engine (GEE) to access, process and analyze Sentinel-2 NDVI and NDSI data through their cloud-based platforms. The two platforms work together to provide complete functionality for fast visualization and pre-processing to large-scale computation and validation supporting long-term monitoring of vegetation and snow patterns in the Alpine region.

3.3.1 Overview and Functionality

The Sentinel Hub platform (EO Browser & APIs) provides users with immediate access to Sentinel-1 and Sentinel-2 and Landsat and MODIS data through its browser-based interface. Users can access real-time vegetation and snow index calculations (NDVI and NDSI) through the platform which also supports automated time-lapse sequence generation without requiring local data storage. The Statistical API and Evalscript environment of Sentinel Hub enables users to create customized band operations and temporal statistics aggregation which makes it ideal for small to medium Alpine studies that need fast validation and inspection. (Milcinski et al., 2017; Sentinel Hub Documentation, 2024.)

Google Earth Engine (GEE), by contrast operates as a cloud-based computing system which contains a vast multi-petabyte database of Sentinel and Landsat and MODIS satellite data. The platform supports complex algorithm development through its JavaScript and Python APIs which also enable multi-sensor data fusion and time-based analysis for large-scale NDVI/NDSI calculations and climate variable integration. The platform enables researchers to perform large-scale vegetation pattern studies and snow cover duration assessments through its reproducible analysis capabilities. (Gorelick et al., 2017; (Chang et al., 2023).

In this thesis, Sentinel Hub was used for quick inspection, mosaicking, and cloud-free composite generation, while GEE handled statistical analysis, Otsu thresholding, and validation.

This complementary use of the two systems ensures both efficiency in data access and depth in analytical modeling for snow and vegetation monitoring.

3.3.2 Comparative Strengths and Weaknesses

The two platforms operate with different methods to handle Sentinel-2 data although they access the same upstream data source. The point-and-click interface of Sentinel Hub allows users to perform fast visual inspections and generate small-area products for export purposes, which makes it suitable for exploratory work and validation tasks. The system requires programming skills to operate but provides extensive processing abilities and global data access and automated workflow management for multi-temporal analysis.

Table 3.3 summarizes the main comparative features of both platforms in relation to NDVI/NDSI processing efficiency and analytical suitability.

Aspect	Sentinel Hub EO Browser	Google Earth Engine
Mode of access	Web interface, on-the-fly processing	Code-driven (JS/Python APIs)
Data Catalog	Copernicus + curated datasets	90+ PB global catalog
Vegetation Monitoring	Quick NDVI/NDRE maps, timelapses	Long-term NDVI/EVI trends, ML pipelines
Snow Monitoring	Built-in NDSI & Snow Classifier	Custom NDSI metrics, multi- sensor fusion
Cloud Masking	s2cloudless convenience bands	Cloud probability dataset (LightGBM)
Scalability	Small/medium AOIs; rapid exports	Regional to global scale analyses
Learning Curve	Low; suitable for non- programmers	Moderate–high; coding required
Cost/Licensing	Free basic access; API plans required for heavy use	Free for research/education; commercial options via Google Cloud

Table 3.3 Comparative strengths and weakness of Sentinel Hub and Google Earth Engine, Sources: Milcinski et al. (2017); Gomes et al. (2020); Sentinel Hub Docs (2024); Google Earth Engine Docs (2024).

3.3.4 Practical Applications and Workflow Examples

The Sentinel Hub EO Browser system lets users obtain NDVI data at field level by choosing areas of interest followed by running NDVI scripts and exporting results as images or statistics. Users can perform fast on-demand vegetation pattern assessments across their chosen scenes for initial research purposes.

Sentinel Hub was mainly utilized in this study for scene visualization, mosaic creation, and manual cloud-free condition verification prior to automated processing. Preliminary validation of NDSI-derived maps was made easier by the Snow Classifier tool in the EO Browser, which allowed visual inspection of snow extent and short-term snow persistence.

The same process in GEE demands scripting yet enables users to conduct extensive large-scale analysis. The defined workflows in GEE enable users to retrieve and process NDVI and NDSI data sets across different spatial areas which range from small catchments to the complete Alpine region.

The automated workflow in GEE allows for consistent application of thresholding and validation steps, reducing subjectivity during index interpretation.

A recent example by (Adrián Melón-Nava, 2024) illustrates the effectiveness of similar GEE-based methods, where Sentinel-2 surface reflectance data combined with cloud-probability layers were used to create daily snow persistence maps for Alpine regions. This reinforces the reliability of using GEE for automated and reproducible large-area processing.

3.3.5 Data Quality and Coverage Considerations

The two platforms utilize Sentinel-2 Level-2A data which present identical restrictions because of cloud cover and terrain shadow effects and missing data in mountainous areas. Research by (Dirk Tiede a et al., 2021) shows that high cloud detection rates decrease the number of available pixels for analysis.

To address these limitations, the study implemented a compositing and filtering strategy that harmonized the NDVI and NDSI datasets from both platforms.

In Sentinel Hub, rapid visual inspection and cloud-free mosaic generation allowed the creation of preliminary reference composites. In GEE, more advanced filtering was applied through automated cloud-masking and temporal compositing scripts, ensuring consistency in pixel selection across months and years.

These combined approaches ensured data quality uniformity and reduced noise from illumination differences, topographic shadows, and residual clouds an essential step for accurate NDVI and NDSI threshold calibration, as emphasized by (Sudmanns et al., 2019) and (Gomes et al. 2020).

3.4 Normalized Difference Indices: NDVI and NDSI

The NDVI and NDSI indices are operationally applied in this study to analyze vegetation and snow-cover dynamics throughout the Maritime Alps, building on the conceptual overview and formulas provided in Sections 2.6 and 2.7. To ensure uniformity in spatial and temporal coverage, both indices were generated from Sentinel-2 Level-2A surface reflectance data and processed using a single workflow in Google Earth Engine (GEE) and Sentinel Hub.

3.4.1 Normalized Difference Vegetation Index (NDVI)

The NDVI was used as a stand-in for phenological variability and vegetation greenness.

To capture vegetation change over time, composites were created for the peak growing seasons of June 2018 and June 2022. As explained in Section 4.4, both Otsu-adaptive thresholds and a fixed threshold (t = 0.3) were used to classify pixels as vegetated or non-vegetated.

3.4.2 Normalized Difference Snow Index (NDSI)

Snow persistence and seasonal extent were mapped using NDSI. Composites representing late-winter to early-spring conditions were created for April 2018 and April 2022. For comparison with NDVI-derived vegetation classifications, the classification used both fixed threshold (t = 0.42) and Otsubased methods (for more information, see Section 4.4).

3.5 Data Access and Processing Workflows for NDVI and NDSI

The only preprocessing steps that separate NDVI and NDSI are spectral bands and threshold parameters.

GEE and Sentinel Hub were used to access Sentinel-2 imagery, which was then mosaicked into monthly composites after being filtered for less than 10% cloud cover.

Following cloud and shadow masking, these composites were harmonized to a spatial resolution of 10 m and categorized using the appropriate index thresholds.

Vegetation and snow analyses are methodologically aligned and directly comparable across platforms and years thanks to the harmonized workflow. Whereas low or negative index values indicate bare or inactive areas like soil or water bodies, positive values indicate surfaces that are vegetated or covered in snow.

3.5.1 Sentinel Hub workflow

Objective.

Implement Sentinel Hub's Process API to generate NDVI and NDSI composites for each selected month and Area of Interest (AOI) in the Maritime Alps. The workflow reproduces cloud-filtered Sentinel-2 L2A image retrieval, index computation through EvalScripts, and binary classification using both fixed and Otsu-adaptive thresholds.

Procedure:

Masking and indices:

Custom EvalScripts were written to compute NDVI and NDSI from Sentinel-2 L2A bands while masking clouds and shadows through the Scene Classification Layer (SCL: classes 3, 8, 9, 10 masked; 11 retained for snow).

Daily mosaics:

Sentinel Hub retrieves all valid scenes below the specified cloud-cover threshold (< 10 %) within each AOI and month. Daily NDVI/NDSI rasters are generated and mosaicked on-the-fly into 10 m grids (UTM 32 N).

Monthly mean:

Daily mosaics are aggregated using mean values to obtain monthly composites clipped to each AOI (e.g., NDVI_YYYY_MM_mean_SH.tif).

• Robust Otsu:

Percentile-trimmed (2nd–98th %) NDVI/NDSI values are scaled to 8-bit (0–255) and processed through the Otsu algorithm to compute adaptive thresholds, later converted back to index units for classification masks. This trimming reduces the influence of outlier values such as residual clouds or noise before threshold optimization.

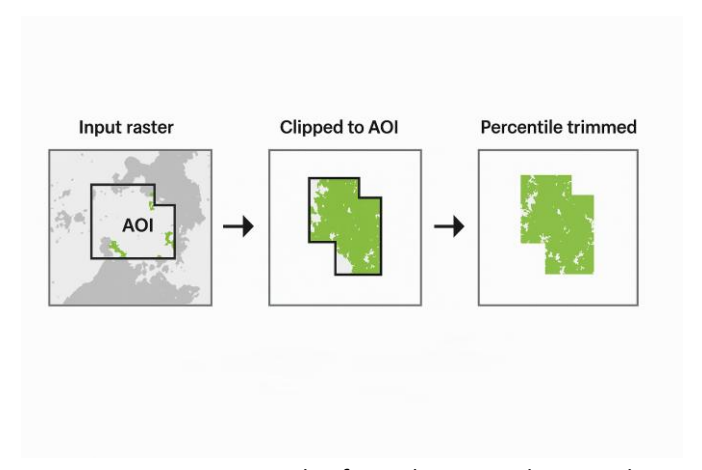


Figure 3.3 Example of AOI clipping and percentile trimming applied to NDVI/NDSI raster

• Masks and metrics:

Fixed (NDVI \geq 0.30; NDSI \geq 0.42) and Otsu masks are produced; area (km²) and mismatch (%) between methods are calculated.

• Exports:

Outputs include monthly means, Otsu and fixed masks, XOR difference layers, and summary metrics (masked area, mismatch %).

All results are exported as GeoTIFF (10 m, EPSG:32632) and PNG visualizations.

3.5.2 GEE workflow (cloud-side and post-processing)

Objective.

Replicate the Sentinel Hub logic within Google Earth Engine (GEE) using the *COPERNICUS/S2_SR_HARMONIZED* collection to produce equivalent NDVI and NDSI composites under identical conditions.

Procedure:

Masking and indices:

Cloud and shadow pixels were masked using SCL classes 3, 8, 9, 10, retaining snow (class 11).

NDVI and NDSI were computed through the normalizedDifference() function.

Daily mosaics:

Sentinel-2 images were filtered by AOI, date, and cloud cover (< 10 %) and processed to generate daily NDVI/NDSI rasters mosaicked at 10 m resolution (UTM 32N).

Monthly mean:

Daily mosaics were averaged using .mean() to create monthly composites clipped to the AOI, following the same temporal scheme as Sentinel Hub.

Robust Otsu:

The same percentile-trimmed Otsu algorithm was implemented server-side to derive adaptive thresholds directly from the NDVI/NDSI histograms.

Masks and metrics:

Fixed and Otsu masks were generated. Area (km²) and mismatch (%) were computed via pixelArea() for cross-platform comparison.

Exports:

Monthly means, masks, and difference layers were exported as GeoTIFFs (10 m, EPSG:32632) to Google Drive.

Post-processing (Python): Offline scripts recomputed robust Otsu thresholds for quality assurance, generated triptychs, and summarized metrics.

3.5.3 Definition of the monthly mean

For a given pixel p in month M, the monthly mean of NDVI or NDSI is computed as the arithmetic average of all valid daily mosaics:

$$\overline{I}_{p,M} = \frac{1}{n_p} \sum_{d \in M} x_{p,d}, \quad n_p = \#\{: x_{p,\cdot} \text{ is valid}\},$$

where I denotes NDVI or NDSI, and $x_{p,d}$ are daily index values within the range [-1,1]. Invalid pixels (e.g., clouds, shadows, or missing data) are excluded from both the sum and the count.

This averaging approach follows best practices in satellite index compositing (Gorelick et al., 2017) and ensures that the resulting monthly means represent robust averages of valid clear-sky observations, rather than isolated single-date scenes.

This method was selected because it minimizes the influence of short-term atmospheric variation and provides stable temporal indicators of vegetation and snow dynamics across complex Alpine terrain.

It should be noted, however, that while the arithmetic mean is optimal for assessing seasonal and interannual trends, alternative compositing strategies such as maximum-value compositing—may be more suitable for estimating maximum snow extent or peak vegetation greenness under specific study objectives.

3.5.4 Definition of the robust Otsu threshold

The classical Otsu method (Otsu, 1979) identifies the threshold that maximizes the between-class variance on a histogram to separate two spectral classes (e.g., snow/non-snow or vegetation/non-vegetation).

To minimize sensitivity to outliers and histogram tails, a robust variant was applied as follows:

- Extract valid monthly mean NDVI or NDSI values within the AOI, i.e., pixels not flagged as cloud, shadow, or snow by the Scene Classification Layer (SCL).
- 2. Compute the 2nd and 98th percentiles (p_2, p_{98}) to remove extreme values.
- 3. Clamp (limit) all data to the interval $[p_2, p_{98}]$, effectively discarding values outside this range to stabilize threshold computation.
- 4. Linearly rescale the clamped values to an 8-bit range (0–255).
- 5. Apply the Otsu algorithm to obtain a threshold T_8 in 8-bit units.
- 6. Convert this threshold back to the original index scale using:

$$t^{*} = p_2 + \frac{T_8}{255}(p_{98} - p_2)$$

where t^* represents the final Otsu threshold value expressed in NDVI or NDSI units.

This approach ensures that the computed threshold is robust against extreme outliers while maintaining sensitivity to genuine spectral transitions in snow or vegetation classes.

3.5.5 Cloud/shadow masking and mosaicking

Both workflows (Sentinel Hub and GEE) apply cloud and shadow masking based on the Sentinel-2 Level-2A Scene Classification Layer (SCL), which labels each pixel according to surface or atmospheric conditions.

To ensure accurate index values, the following classes were filtered:

- Rejected: SCL 3 (cloud shadow), 8 (cloud), 9 (high cloud), 10 (cirrus)
- Retained: SCL 11 (snow) used for NDSI; vegetated classes (4–6) for NDVI

After masking, each day's valid imagery was composited into a single daily mosaic:

- **Sentinel Hub:** Utilized the *MosaickingOrder.SIMPLE* mode, which automatically prioritizes the least-cloudy scenes after SCL filtering.
- Google Earth Engine (GEE): Used the .mosaic() function, ordering images by ascending cloud probability to produce a single clear-sky composite per day.

One daily mosaic was thus produced for each valid observation date, which then contributed to the monthly mean composites described in Section 3.5.3.

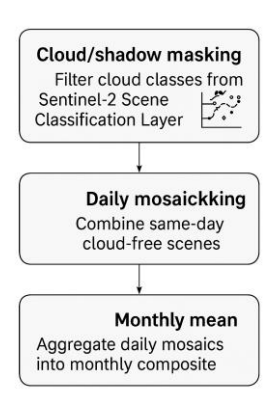


Figure 3.4 Sentinel Hub cloud/shadow masking and mosaicking workflow for NDVI/NDSI processing.

3.5.6 Equivalence and minor differences between platforms

Both Sentinel Hub and GEE ultimately produce equivalent results cloud-masked daily mosaics aggregated into monthly means and thresholded NDVI/NDSI maps.

However, small technical differences arise from internal data handling:

- Resampling: Sentinel Hub explicitly resamples each mosaic to a 10 m grid before monthly averaging. GEE performs averaging natively and applies resampling only at export.
- Mosaic tie-breaks: When multiple valid scenes overlap on the same date, each platform may prioritize slightly different pixels (e.g., by acquisition time or scene order), causing minor local variation.

These differences are negligible at the monthly scale and appear only as minimal area mismatches (%) in the Otsu vs. fixed-threshold comparison diagnostics.

Both systems therefore maintain methodological equivalence in terms of cloud-masking logic, compositing, and temporal aggregation. The tie-break procedures, illustrated in Figure 3.3, highlight how Sentinel Hub prioritizes sequence order while GEE prioritizes image clarity an operational difference that becomes negligible once daily mosaics are averaged into monthly means.

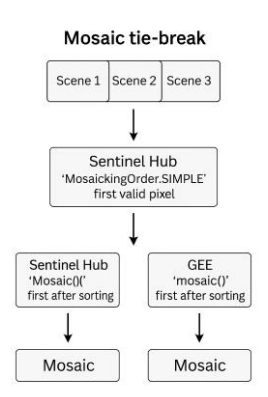


Figure 3.5 Illustration of mosaic tiebreak handling between Sentinel Hub and Google Earth Engine.

3.5.7 Deriving NDVI and NDSI Maps in QGIS

The monthly mean NDVI and NDSI rasters were imported into QGIS 3.36.1 for spatial post-processing and classification. Within the GIS environment, raster algebra operations and vector-based masking were applied to generate binary vegetation and snow-cover maps suitable for spatial analysis and visualization. The Maritime Alps AOI shapefile was used to spatially constrain the raster composites, ensuring that all subsequent analyses were restricted to the defined study area.

The Raster Calculator tool was employed to execute index-based classification using both fixed thresholds (NDVI \geq 0.30; NDSI \geq 0.42) and adaptive thresholds derived from the robust Otsu algorithm. The procedure used continuous index values to create binary classes which distinguished between vegetated and non-vegetated areas and snow-covered and snow-free regions. The classification workflow standardized raster values which made it possible to evaluate different temporal composites.

Following classification, the Clip Raster by Mask Layer function (Raster \rightarrow Extraction \rightarrow Clip by Mask Layer) was applied to enforce spatial constraints and retain only pixels within the Maritime Alps AOI extent. The clipped rasters served as input data to evaluate snow and vegetation spatial patterns during specific months including April 2020 for NDSI and NDVI. The resulting layers underwent visual and statistical verification against reference masks which were produced in Sentinel Hub.

This integrated QGIS workflow, summarized in Figure 3.6, standardized all spatial operations including raster import, threshold application, masking, and AOI clipping ensuring consistency between NDVI and NDSI map derivation. The synchronized outputs allowed the evaluation of vegetation and snow dynamics across time and supported the quantification of environmental changes in the Maritime Alps.

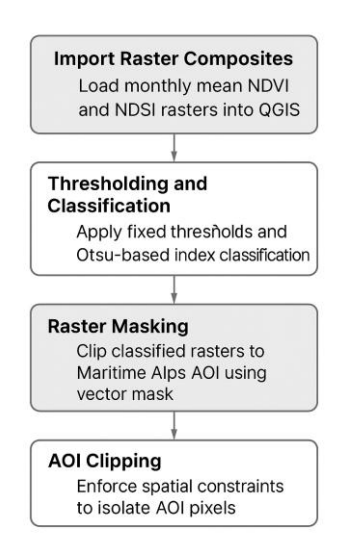


Figure 3.6. Overall QGIS workflow for NDVI and NDSI map derivation, showing the sequence of raster import, threshold-based classification, and AOI clipping for spatial and temporal analysis in the Maritime Alps.

3.6 Validation Approaches

3.6.1 Validation of NDVI with CORINE Land Cover 2018

To evaluate the reliability of NDVI-derived vegetation masks, we validated the classification against the CORINE Land Cover 2018 (CLC2018) dataset, which provides harmonized land-cover information for Europe at 100 m resolution with a minimum mapping unit of 25 ha (*EEA*, 2019)The goal was to quantify the agreement between Sentinel-2 NDVI classifications and an independent, authoritative land-cover reference by means of a confusion matrix and accuracy indices.

Step 1: Preparation of the NDVI Raster.

The monthly mean NDVI raster was first thresholded to obtain a binary vegetation mask. Pixels with NDVI \geq 0.30 were assigned to the vegetation class (value = 1), while all others were assigned to the non-vegetation class (value = 0). This threshold has been widely adopted in the literature as an indicator of active vegetation cover (Tucker, 1979; Rouse et al., 1974). The resulting binary raster (NDVI_binary.tif) represents the predicted classification.

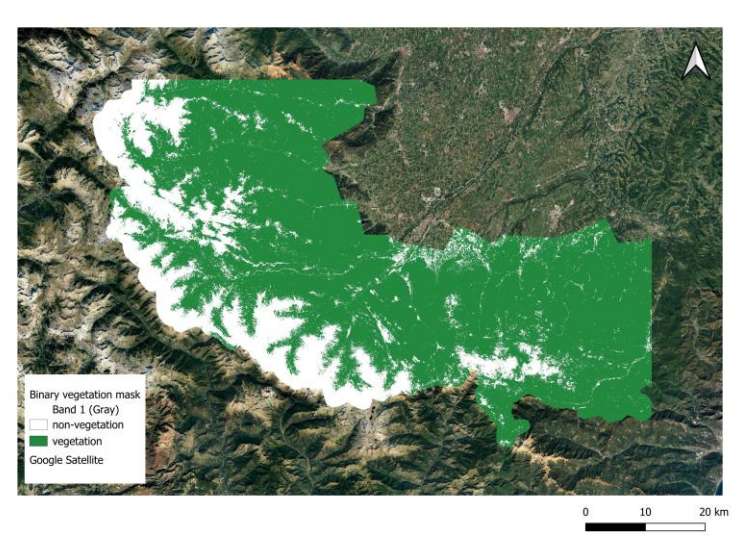


Figure 3.7 NDVI binary vegetation mask derived from Sentinel-2 composite (June 2019), Maritime Alps AOI.

Step 2: Preparation of CORINE Land Cover Reference Classes.

The CORINE 2018 dataset was imported into QGIS and reclassified into two broad categories: vegetation and non-vegetation.

Following the CORINE nomenclature, all Level 3 codes corresponding to forests, natural grasslands, sclerophyllous vegetation, transitional woodland-shrub, and sparsely vegetated areas (e.g., codes 311, 312, 313, 321, 324, 333) were grouped into the vegetation class (value = 1).

All other codes, including artificial surfaces, agricultural land, wetlands, and water bodies, were grouped into the non-vegetation class (value = 0).

The reclassified dataset (CLC2018_binary.shp) thus provided the reference or "ground truth" classification.

The CORINE layer was then harmonized with Sentinel-2 data by applying CRS transformation to *EPSG: 32632 WGS 84 / UTM Zone 32 N* for precise overlay alignment and spatial matching with NDVI rasters. Finally, it was clipped to the Maritime Alps AOI to retain only relevant classes within the study boundaries.

Step 3: Sampling Design

To statistically represent both vegetation and non-vegetation classes, 1,000 random points were generated within the Maritime Alps AOI using a random sampling design. To prevent clustering and ensure adequate coverage across all land-cover types, the *Random Points in Polygons* function in QGIS was used to evenly distribute the points (\geq 30 m apart).

The spatial distribution of these sampling points is shown in Figure 4.93, which illustrates their coverage within the study area.

Step 4: Extraction of Values

At each sampling point, the binary NDVI value was extracted from the NDVI raster using the Sample Raster Values tool in QGIS. The CORINE Land Cover (CLC2018) dataset provided the reference vegetation/non-vegetation attribute for the same locations. This step resulted in a point dataset containing both the predicted (NDVI-based) and reference (CORINE-based) classifications for each sampling location.

Step 5: Spatial Join and Attribute Integration

The extracted NDVI and CORINE attributes were combined through the Join Attributes by Location (Summary) tool in QGIS, using the geometric predicate *intersects*.

The resulting dataset contained two binary fields NDVI_bin (0/1) and veg_class (0/1), forming the input for confusion-matrix computation.

Step 6: Confusion Matrix and Accuracy Metrics

The comparison between NDVI predictions and CORINE reference classes was summarized in a confusion matrix. The matrix cross-tabulates the number of points where NDVI and CORINE classifications agree (true positives for

vegetation, true negatives for non-vegetation) and disagree (false positives, false negatives). From this table, several accuracy metrics were computed:

- Overall accuracy, defined as the proportion of correctly classified points,
- **Producer's accuracy** (recall), measuring how well NDVI detects actual vegetation,
- **User's accuracy** (precision), measuring the reliability of NDVI's vegetation classification, and
- **Cohen's Kappa coefficient**, evaluating agreement beyond chance.

	NDVI=0	NDVI=1
CORINE=0	TN	FP
CORINE=1	FN	TP

Let N = TP + FP + FN + TN.

Overall Accuracy (OA)

$$OA = \frac{\mathrm{TP} + \mathrm{TN}}{N}$$

Producer's Accuracy (Recall) - Vegetation

$$PA_{veg} = \frac{TP}{TP + FN}$$

For non-vegetation

$$PA_{nonveg} = \frac{TN}{TN + FP}$$

User's Accuracy (Precision) - Vegetation

$$UA_{veg} = \frac{\mathrm{TP}}{\mathrm{TP} + \mathrm{FP}}$$

For non-vegetation

$$UA_{nonveg} = \frac{TN}{TN + FN}$$

Cohen's Kappa (κ)

First compute the observed agreement Po and the chance agreement Pe:

$$P_o = \frac{\text{TP} + \text{TN}}{N}$$

$$P_e = \frac{(\text{TP} + \text{FP})(TP + FN) + (FN + TN)(FP + TN)}{N^2}$$

Then

$$K = \frac{P_0 - P_e}{1 - P_e}$$

Step 7: Statistical Analysis.

The confusion matrix was built from the exported attribute table of the sampled points. The accuracy metrics were calculated through both Excel and Python (scikit-learn library) to verify the consistency of the results. The analysis of NDVI as a vegetation cover proxy followed established best practices for accuracy assessment (Congalton, 1991; Olofsson et al., 2014) by examining both the positive and negative aspects of the method.

The validation framework enabled a systematic evaluation of NDVI-derived vegetation masks against CORINE Land Cover 2018 data to measure classification precision and detect possible errors caused by different land-cover types and resolution differences and seasonal changes.

3.6.2 Validation of NDVI with LUCAS 2022 and Confusion Matrix

The LUCAS 2022 (Land Use/Cover Area Frame Survey) dataset contains standardized field measurements which span the European Union through a 2 km grid system. The survey points contain complete land use and land cover classification information together with photographic documentation. The subhectare scale sampling of LUCAS makes it an essential resource for validating Sentinel-2 vegetation index measurements (Gallego & Delincé, 2010; d'Andrimont et al., 2021).

A confusion-matrix-based validation was applied to assess the agreement between NDVI-derived vegetation masks and LUCAS 2022 observations. The workflow, carried out in QGIS, followed the steps below.

Step 1: Preparation of NDVI raster

As in the CORINE validation, monthly mean NDVI composites were first thresholded into binary vegetation/non-vegetation maps. A fixed threshold of 0.30 was applied (Tucker, 1979; Rouse et al., 1974), which is widely recognized as a reliable indicator distinguishing active green vegetation from bare soil or sparsely vegetated surfaces. Values above 0.30 generally correspond to healthy vegetation canopy, while lower values indicate non-vegetated or low-productivity areas.

This threshold was also verified as suitable for the Maritime Alps, where NDVI < 0.30 typically represents rock, snow, or bare alpine terrain, whereas higher values correspond to grassland and forested zones.

$$NDVI_{binary} = \begin{cases} 1 & if \ NDVI \ge 0.30 \\ 0 & if \ NDVI < 0.30 \end{cases}$$

Step 2: Import and preparation of LUCAS points

The LUCAS 2022 survey points were imported into QGIS as a vector layer. Each point has an attribute such as LC1 (primary land cover class). For validation, classes were reclassified into a binary vegetation/non-vegetation scheme:

- **Vegetation (1):** Cropland, grassland, shrubland, forest, and other seminatural areas. (e.g., LC1 codes A, B, C, D, E, F, G in LUCAS nomenclature).
- Non-vegetation (0): Artificial surfaces, bare land, water, wetlands.

This reclassification was carried out in the Field Calculator with an expression like:

```
CASE

WHEN "LC1" IN ('A','B','C','D','E','F','G') THEN 1

ELSE 0

END
```

The resulting layer LUCAS_binary now contains a column veg_class with values 1 (vegetation) or 0 (non-vegetation).

Step 3: Extract NDVI values to LUCAS points

To link the NDVI classification with the LUCAS ground truth, the Sample Raster Values tool was used:

Input point layer: LUCAS_binary

Raster layer: NDVI_binary.tif

• Output field: NDVI_bin

The resulting point layer (LUCAS_NDVI_sampled) contains, for each LUCAS point, the reference vegetation class (veg_class) and the NDVI-derived class (NDVI bin).

Step 4: Export and Construction of Confusion Matrix

The attribute table of LUCAS_NDVI_sampled was exported to CSV file (*Export* \rightarrow *Save Features As* \rightarrow *Format: CSV*).

This file contained the paired classification results (veg_class and NDVI_bin), which were used to construct a 2×2 confusion matrix in Excel or Python.

The matrix summarized the relationship between NDVI predictions and LUCAS reference classes, identifying true and false classifications for vegetation and non-vegetation categories.

Step 5: Accuracy Assessment

The same formulas and procedures outlined in Section 3.6.1 were used to calculate accuracy metrics, such as Overall Accuracy (OA), Producer's Accuracy (PA), User's Accuracy (UA), and Cohen's Kappa (κ).

In comparison to field-based LUCAS observations, these indices offered a numerical assessment of NDVI classification performance.

Step 6: Statistical Verification

To guarantee computational consistency, all computations were validated using QGIS and Python (scikit-learn).

By offering greater spatial precision and in-situ ground reference, the LUCAS-based validation enhances the overall reliability of NDVI classification results across several validation scales, complementing the CORINE-based assessment.

3.6.3 Post-Validation Evaluation and Sensitivity Analysis

The validation process with CORINE 2018 and LUCAS 2022 datasets was followed by the evaluation of NDVI classification performance across different threshold values and the assessment of accuracy metric stability. A sensitivity analysis was then performed to test NDVI thresholds ranging from 0.25 to 0.35. The analysis of confusion matrices and accuracy indices for each threshold enabled us to measure how variations in threshold values affect classification reliability.

Sensitivity Analysis

NDVI \geq 0.30 was used as the main fixed threshold, but alternative cut-offs (0.25, 0.27, 0.285, 0.30, 0.315, 0.33, and 0.35) were tested to capture threshold sensitivity. For each threshold, the pipeline produced:

- 1. A confusion matrix (TP, FP, FN, TN).
- 2. Accuracy metrics (OA, PA, UA, κ).
- 3. Graphical outputs showing metric variation with threshold.

The following section demonstrates the results obtained from sensitivity analysis conducted during validation. The analysis of each NDVI threshold included confusion matrix construction followed by accuracy index calculations for Overall Accuracy and Precision and Recall and Cohen's Kappa. The results were displayed through graphical representations to demonstrate how classification results change based on different threshold values.

The sensitivity plots display accuracy and precision and recall curves for all tested thresholds which enable users to detect the balance between incorrect positive and negative results. The reference dataset histograms display NDVI value distributions between vegetation and non-vegetation classes to demonstrate the essential threshold selection area.

The graphical assessment enables users to understand how threshold adjustments affect accuracy metrics while helping them determine the most suitable operational NDVI threshold for vegetation mapping.

3.6.4 Validation of NDVI with Carta degli Habitat

The *Carta degli Habitat* (CdH) dataset provides a detailed, high-resolution habitat mapping system developed under the EU Habitats Directive and Natura 2000 framework. Its fine thematic granularity makes it particularly suitable for validating NDVI-derived vegetation maps (Pesaresi et al., 2020; Čahojová et al., 2022), complementing the broader land-cover datasets such as CORINE and the point-based LUCAS survey.

Following the general validation framework described in Section 3.6, NDVI-derived binary vegetation masks (NDVI $\geq 0.30 = 1$; < 0.30 = 0) were compared against CdH reference polygons reclassified into vegetated and non-vegetated habitats. The reclassification was based on habitat codes representing forest, shrub, grassland, and alpine communities, using:

CASE

WHEN "HAB_CODE" IN ('9210', '9230', '9420', '6170', '4060', '8210', '8220', '8230') THEN 1

ELSE 0

END

A stratified random sample of 1,000 points was generated within the AOI, ensuring equal representation of vegetation and non-vegetation classes. At each sampling location, NDVI binary values were extracted from the NDVI_binary.tif raster and joined with the corresponding CdH vegetation attribute.

From this joined dataset, a confusion matrix was produced with CdH serving as the reference layer. Accuracy metrics including overall accuracy (OA), producer's accuracy (PA), user's accuracy (UA), and Cohen's Kappa (κ) were computed according to the formulations in Section 3.6.1.

This ensured consistency across all validation datasets (CORINE, LUCAS, and CdH) and enabled comparative analysis of NDVI classification performance across multiple reference frameworks.

3.6.5 Validation of NDSI Results

The accuracy assessment of Sentinel-2 derived NDSI snow cover classification used two independent validation methods. The first validation method used random points within the study area to compare NDSI snow/no-snow classifications at specific locations. The second validation method used external reference data from the Copernicus Fractional Snow Cover (FSC) product which provides daily snow cover information at 20 m resolution starting from 2016. The two validation methods combined to assess NDSI output accuracy through internal and external validation methods.

3.6.5.1 Validation by Random Points

This first approach aimed to test the internal consistency of NDSI snow classification by sampling random points across the Area of Interest (AOI). The workflow in QGIS proceeded as follows:

Step 1: Prepare NDSI Raster

Monthly mean NDSI rasters were computed and thresholded into binary maps using both the fixed threshold (NDSI \geq 0.42 = snow, Hall et al., 1995) and Otsu's adaptive thresholding (Otsu, 1979). The result was a binary raster (snow = 1, no-snow = 0).

Step 2: Generate Random Points

Using Random Points in Polygon tool in the Processing Toolbox, 1,000 random points were distributes within the AOI. This ensured an unbiased spatial distribution across both snow-covered and snow-free areas.

Step 3: Sample Raster Values

The Sample Raster Values tool assigned each random point a snow/no-snow class from the binary NDSI raster.

Step 4: Confusion Matrix and Accuracy Indices

The sampled points received export to a CSV file which allowed the creation of a confusion matrix from the attribute table to assess classification accuracy.

The accuracy indices were calculated using the standard methods from Section 3.6.1 to obtain overall accuracy (OA) and producer's accuracy (PA) and user's accuracy (UA) and Cohen's Kappa coefficient (κ).

These metrics quantified the thematic accuracy of the NDSI masks by measuring the degree of agreement between predicted classifications and observed conditions, providing insight into the performance of fixed and Otsu thresholds under varying snow conditions.

3.6.5.2 Validation with Copernicus Fractional Snow Cover (FSC)

The second validation strategy used the Copernicus FSC product to obtain fractional snow cover estimates between 0 and 100% at 20 m resolution which matched Sentinel-2 tiling. The validation used an operational product to compare NDSI-derived snow maps through direct pixel-to-pixel assessment.

Step 1: Understand the FSC Product

Each FSC file is distributed as a ZIP archive containing:

- GeoTIFF raster with fractional snow cover values (0–100%).
- Metadata (XML/JSON) descriptors.
- Quality masks indicating clouds or no-data pixels.

For validation, only the GeoTIFF raster was required. Special codes (205, 254, 255) were treated as no data.

Step 2: Select Files Overlapping the AOI

FSC tiles covering the Maritime Alps (e.g., T32TLP, T31TGJ) were identified and downloaded.

For multi-tile AOIs, rasters were merged (*Raster* \rightarrow *Miscellaneous* \rightarrow *Merge*).

Step 3: Preprocess FSC

FSC rasters were unzipped, normalized to 0–100%, and loaded into QGIS with no-data values masked out.

Step 4: Prepare NDSI Raster for Comparison

The NDSI results (binary or fractional) were resampled to the same

projection (EPSG:32632), resolution (20 m), and extent as the FSC data using $Raster \rightarrow Projections \rightarrow Warp$ (reproject).

Step 5: Validation Workflows

Two approaches were applied:

• Option A: Binary Validation

FSC values were reclassified as:

$$FSC \ge 50\% \rightarrow Snow = 1$$
, $FSC < 50\% \rightarrow no - snow = 0$

The binary FSC layer was compared with NDSI classifications using the *Raster Calculator* to generate a confusion matrix (snow vs. no-snow).

• Option B: Fractional Validation

FSC values were retained as continuous percentages (0–100) and compared against continuous NDSI values using statistical measures:

Pearson's correlation (r):

$$r = \frac{\sum (x_i - x^-) (y_i - y^-)}{\sqrt{\sum (x_i - x^-)} ^2 \sum (y_i - y^-)^2}$$

Root Mean Square Error (RMSE):

$$RMSE = \sqrt{\frac{1}{n}} \sum_{i=1}^{n} (x_i - y_i)^2$$

where x_i are NDSI-derived values and y_i are FSC percentages.

Step 6: Accuracy Reporting

Binary validation outputs (OA, PA, UA, κ) were reported alongside correlation and RMSE from fractional validation. This dual approach quantified both categorical agreement and continuous similarity, providing a robust evaluation of NDSI performance.

Data, Processing, Results

4.1 NDVI Dynamics from Google Earth Engine

The initial part of the analysis examined NDVI time patterns for April and June using Google Earth Engine (GEE) as the analytical platform. These months were chosen as they represent two critical phases in the Alpine vegetation cycle early-season growth and full canopy development allowing assessment of both temporal and classification variability.

The analysis used Sentinel-2 imagery to create monthly composites restricted to areas with less than 15% cloud cover. Two classification techniques were applied for each month of the study period.

The classification used NDVI values above 0.30 to identify vegetation and below 0.30 for non-vegetation, following (Tucker, 1979) and (Rouse et al,.1974). The Otsu adaptive thresholding method determined an optimal cut-off value by analyzing image histograms to maximize between-class variance (Otsu, 1979).

Binary vegetation masks produced from both fixed and adaptive thresholds enabled comparison of vegetation cover across spring and early-summer conditions. The temporal analysis highlights changes in greenness and illustrates how thresholding strategies influence vegetation classification outcomes.

Data, Processing, Results

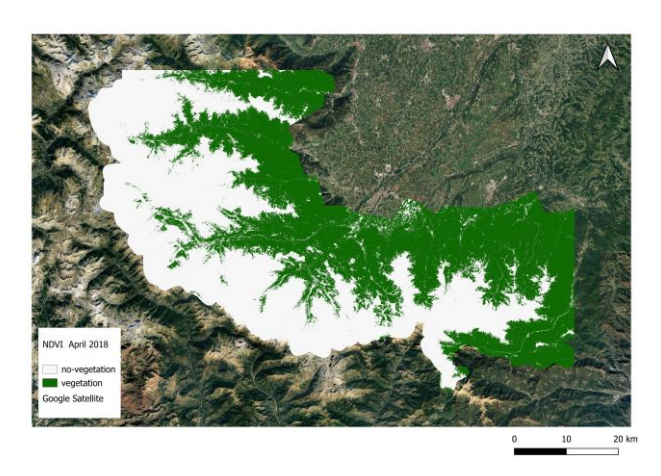


Figure 4.1 NDVI 2018 April Fix Threshold

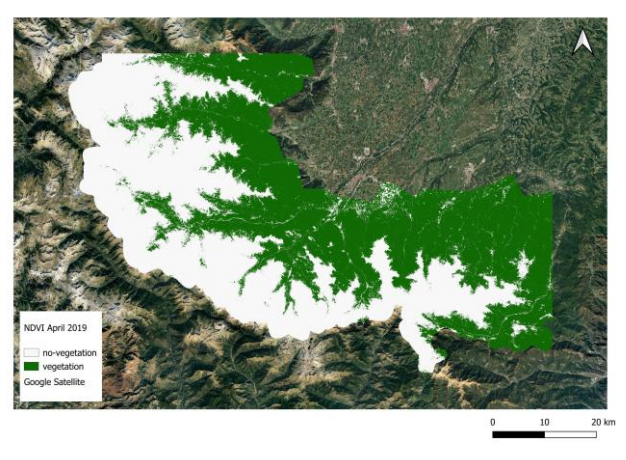


Figure 4.3 NDVI 2019 April Fix Threshold

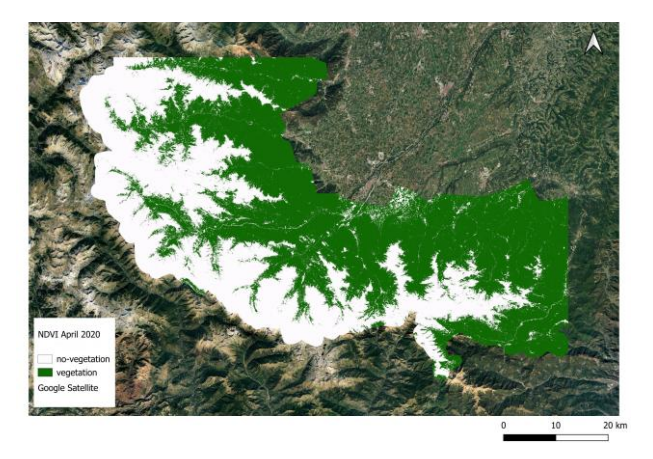


Figure 4.5 NDVI 2020 April Fix Threshold

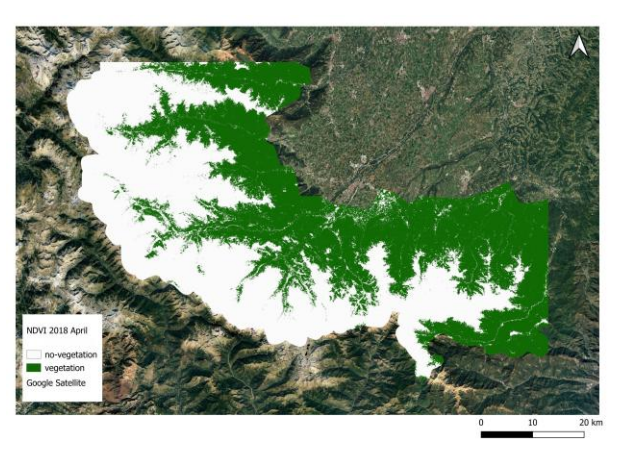


Figure 4.2 NDVI 2018 April Otsu Threshold

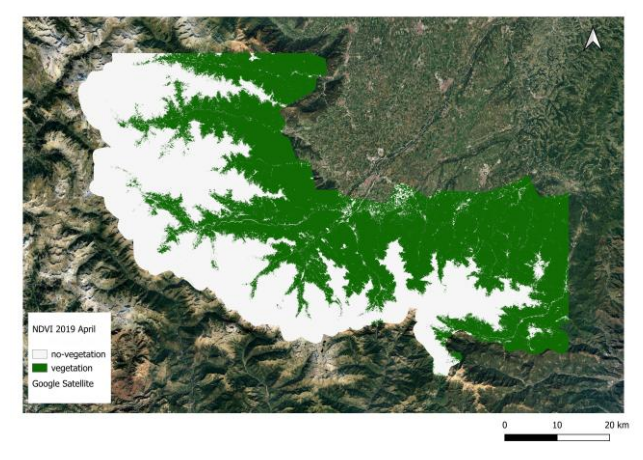


Figure 4.4 NDVI 2019 April Otsu Threshold

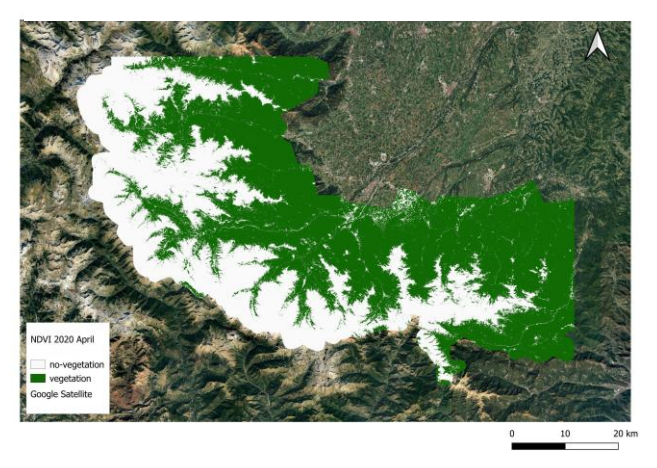


Figure 4.6 NDVI 2020 April Otsu Threshold

Data, Processing, Results

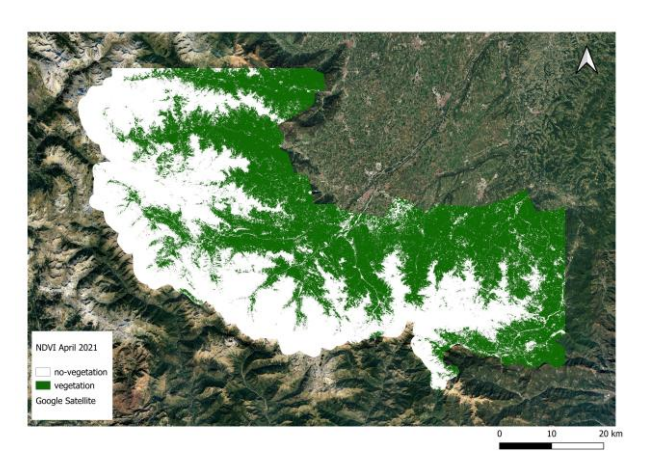


Figure 4.7 NDVI 2021 April Fix Threshold

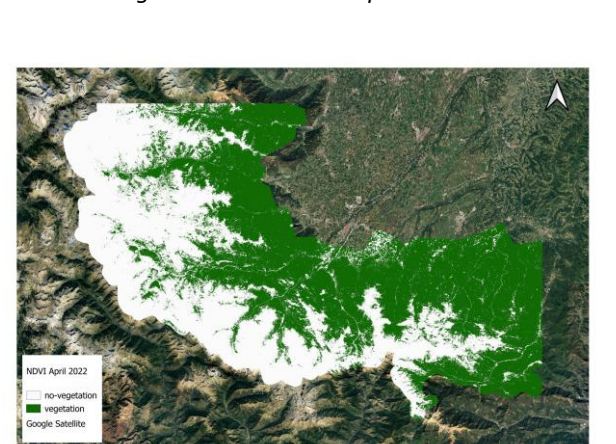


Figure 4.9 NDVI 2022 April Fix Threshold

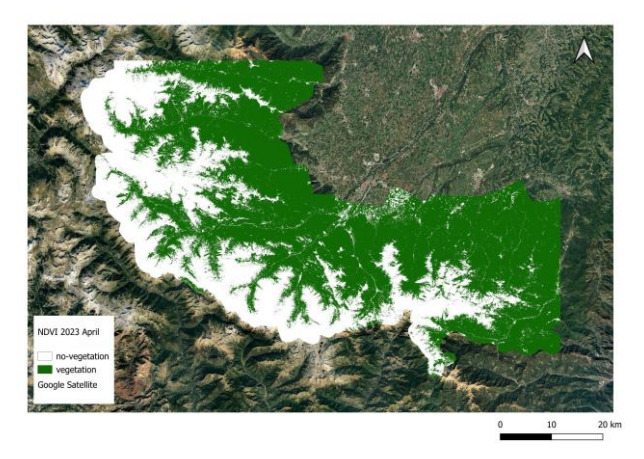


Figure 4.11 NDVI 2023 April Fix Threshold

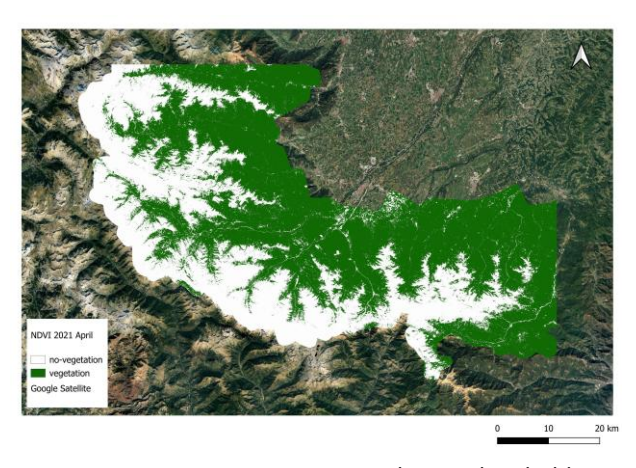


Figure 4.8 NDVI 2021 April Otsu Threshold

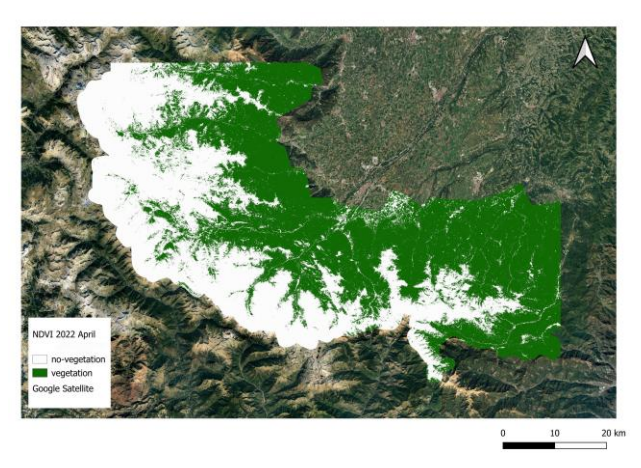


Figure 4.10 NDVI 2022 April Otsu Threshold

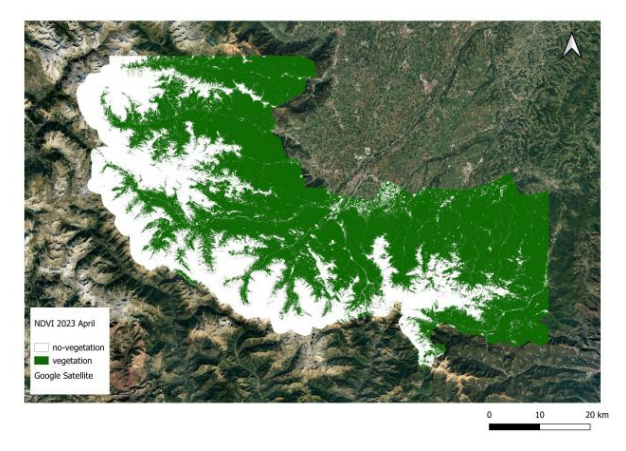


Figure 4.12 NDVI 2023 April Otsu Threshold

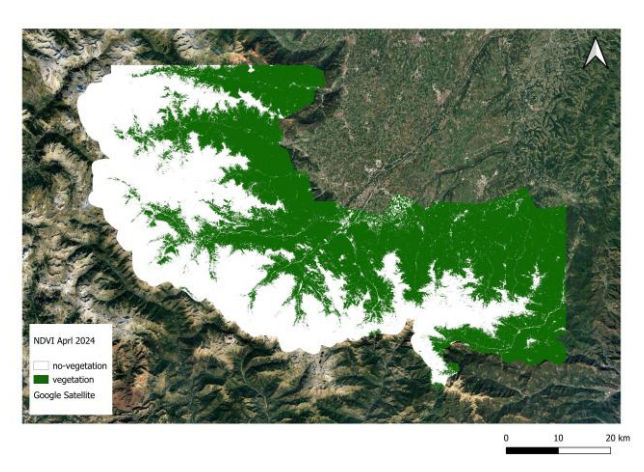


Figure 4.13 NDVI 2024 April Fix Threshold

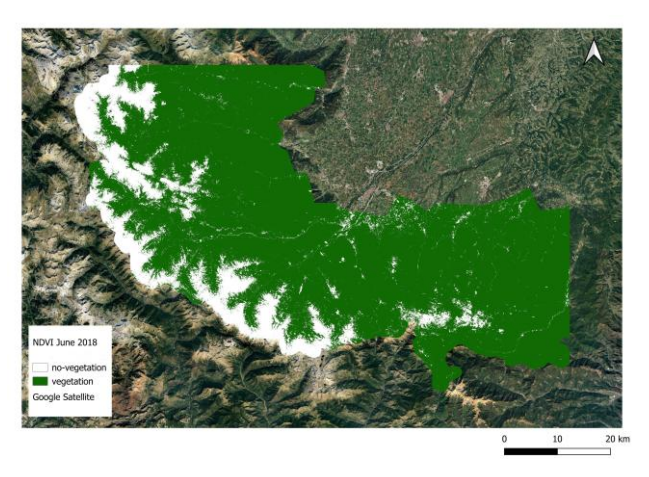


Figure 4.15 NDVI 2018 June Fix Threshold

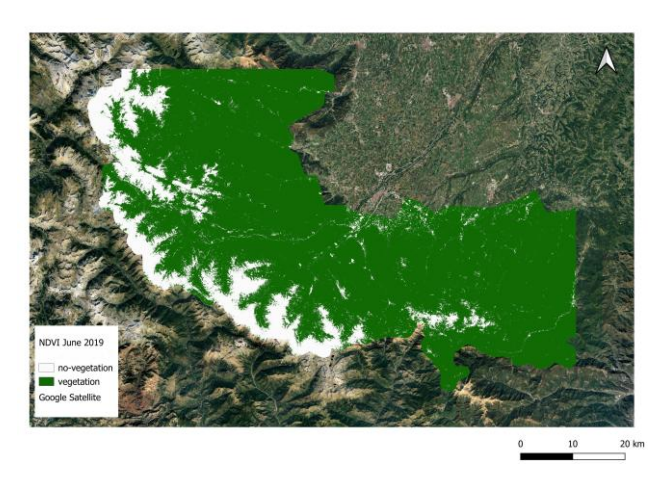


Figure 4.17 NDVI 2019 June Fix Threshold

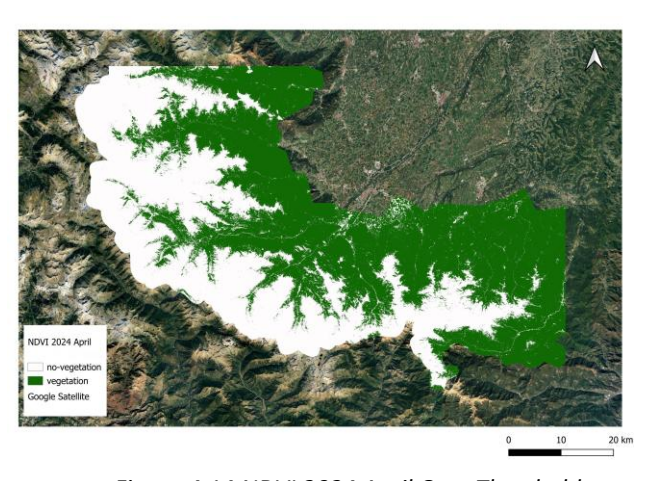


Figure 4.14 NDVI 2024 April Otsu Threshold

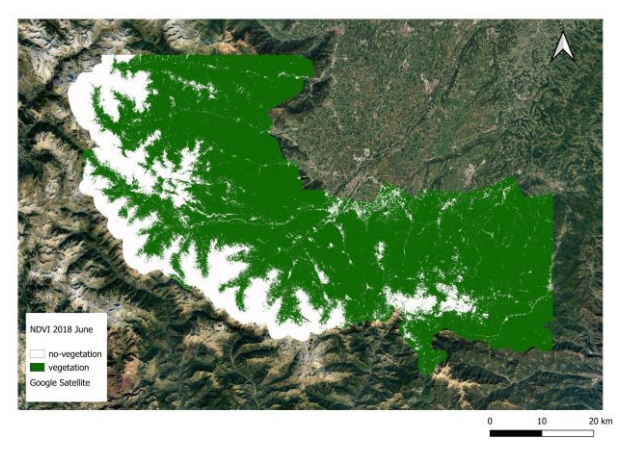


Figure 4.16 NDVI 2018 June Otsu Threshold

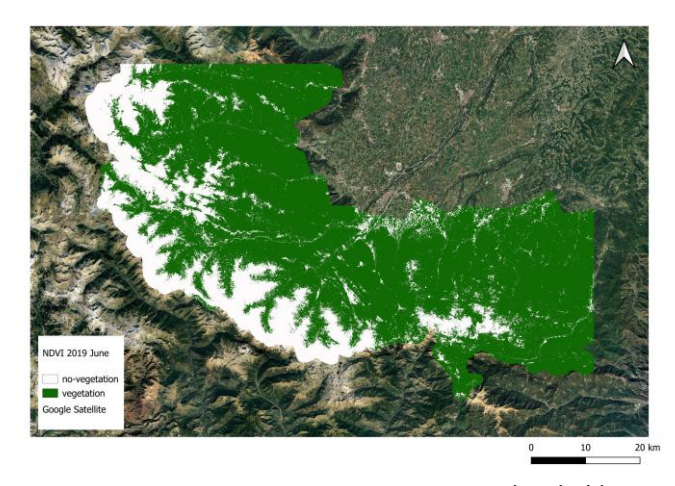


Figure 4.18 NDVI 2019 June Otsu Threshold

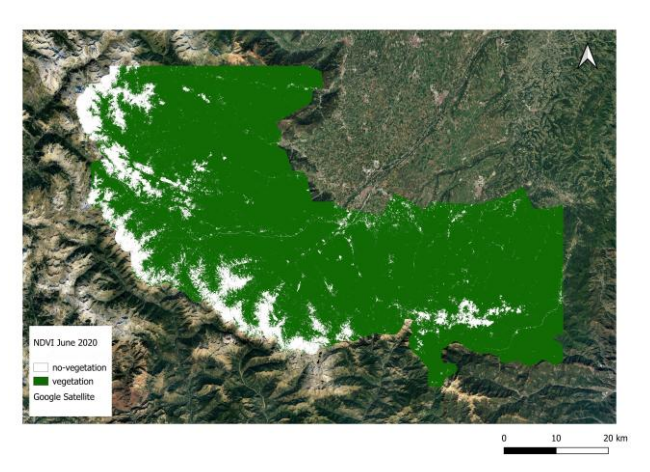


Figure 4.19 NDVI 2020 June Fix Threshold

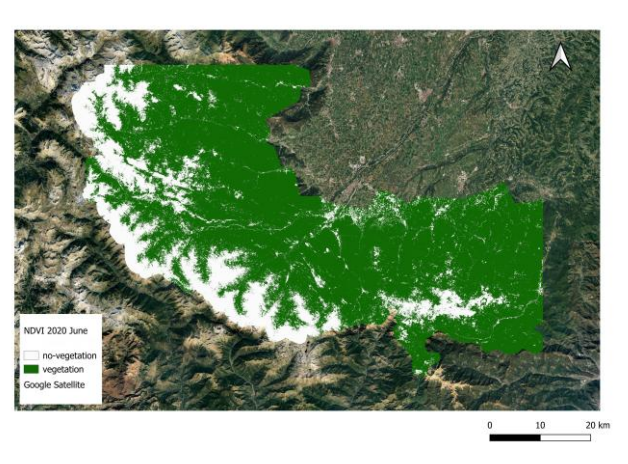


Figure 4.20 NDVI 2020 June Otsu Threshold

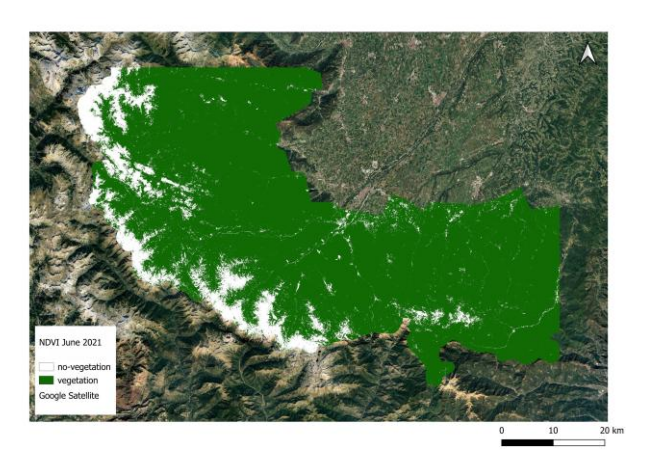


Figure 4.21 NDVI 2021 June Fix Threshold

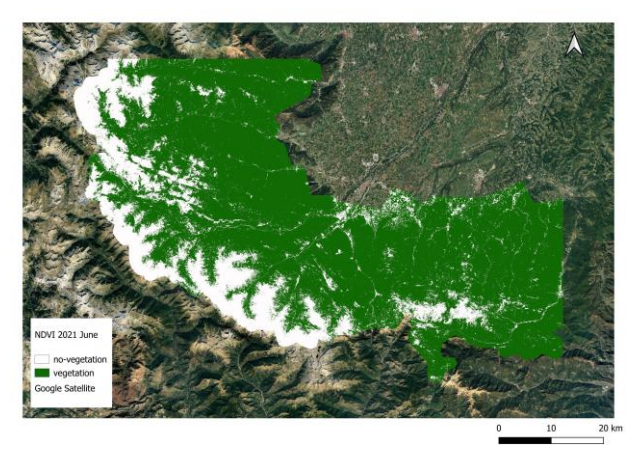


Figure 4.22 NDVI 2021 June Otsu Threshold

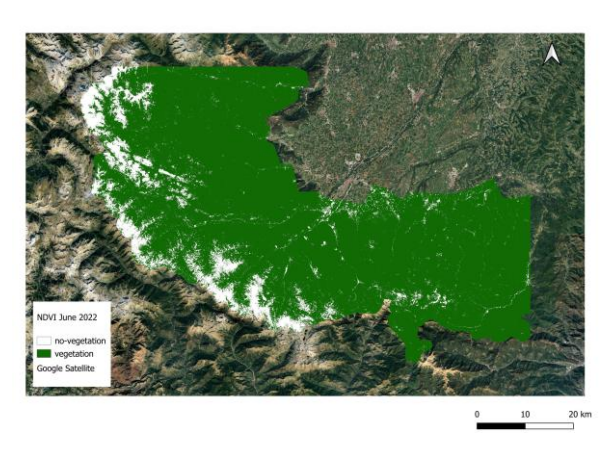


Figure 4.23 NDVI 2022 June Fix Threshold

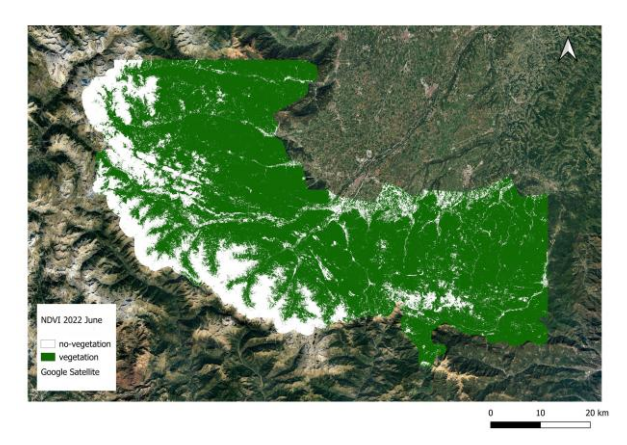


Figure 4.24 NDVI 2022 June Otsu Threshold

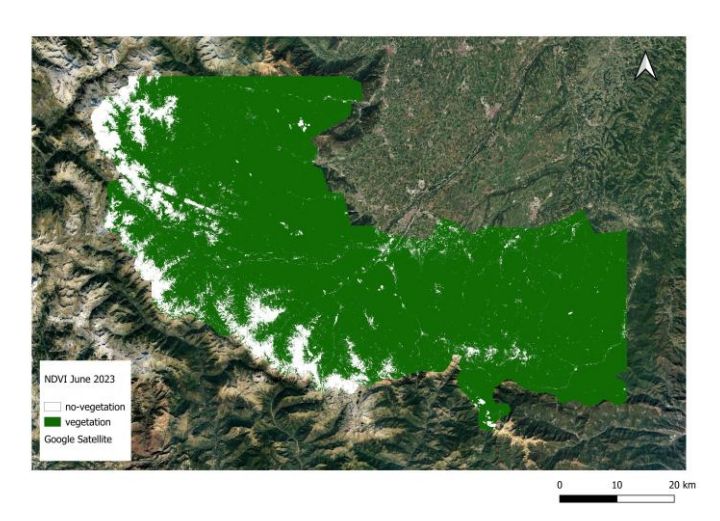


Figure 4.25 NDVI 2023 June Fix Threshold

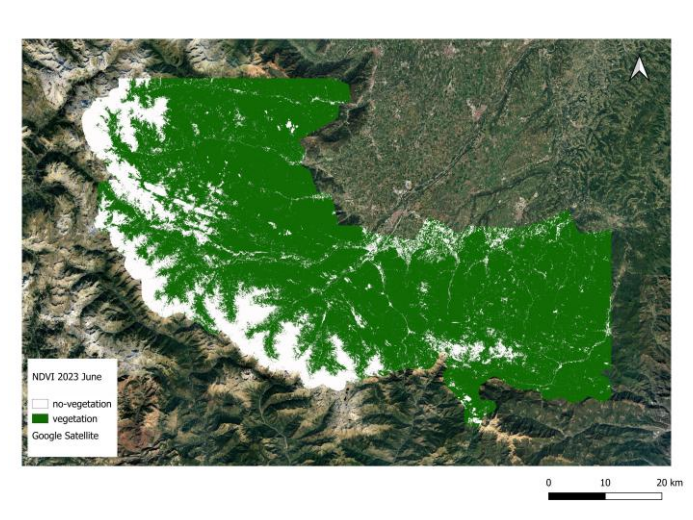


Figure 4.26 NDVI 2023 June Otsu Threshold

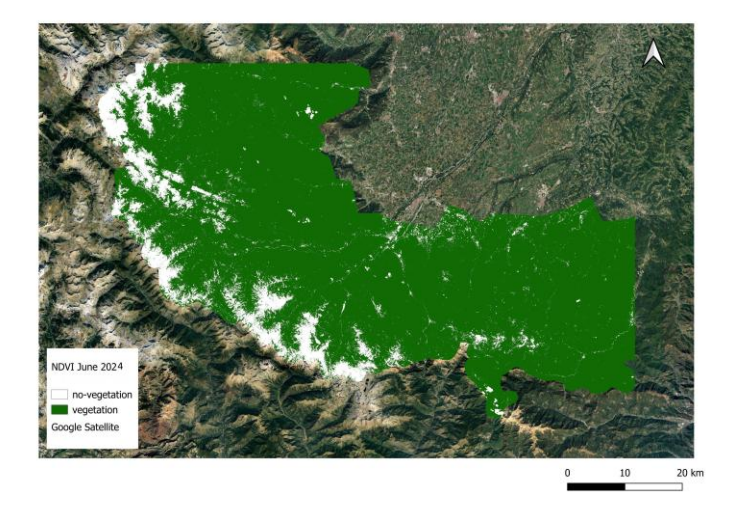


Figure 4.27 NDVI 2024 June Fix Threshold

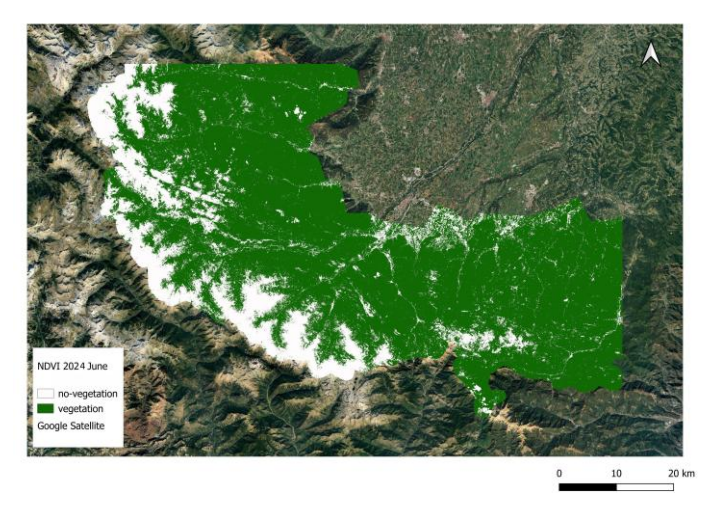


Figure 4.28 NDVI 2024 June Otsu Threshold

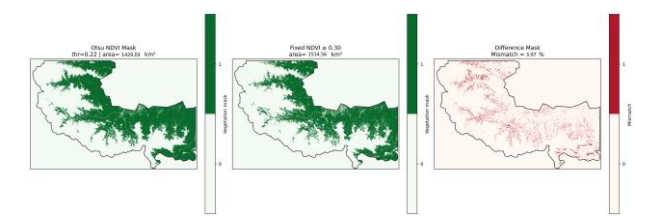


Figure 4.29 NDVI 2018 April Comparison

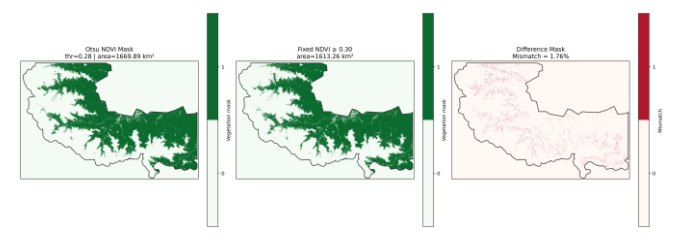


Figure 4.30 NDVI 2019 April Comparison

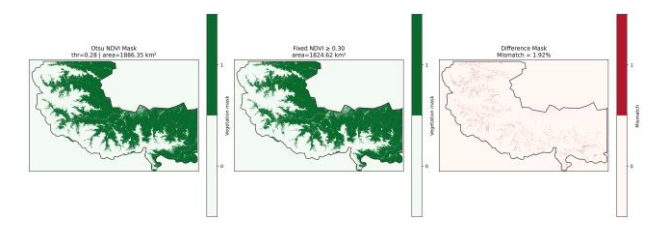


Figure 4.31 NDVI 2020 April Comparison

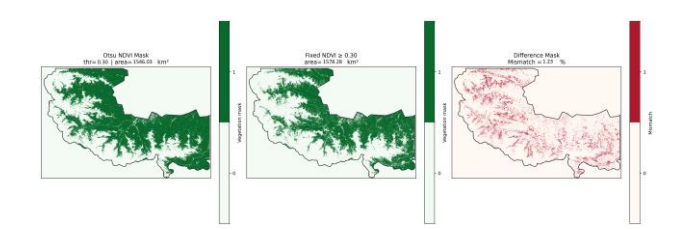


Figure 4.32 NDVI 2021 April Comparison

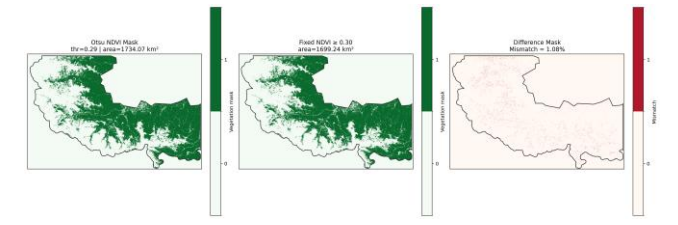


Figure 4.33 NDVI 2022 April Comparison

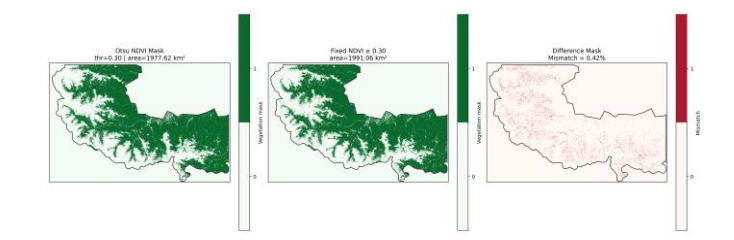


Figure 4.34 NDVI 2023 April Comparison

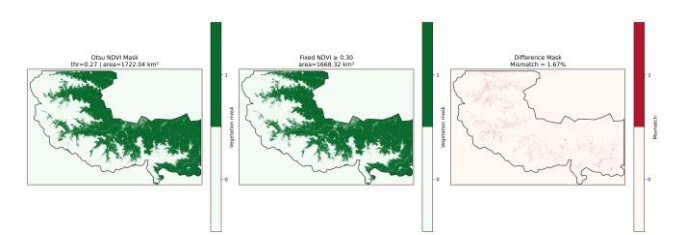


Figure 4.35 NDVI 2024 April Comparison

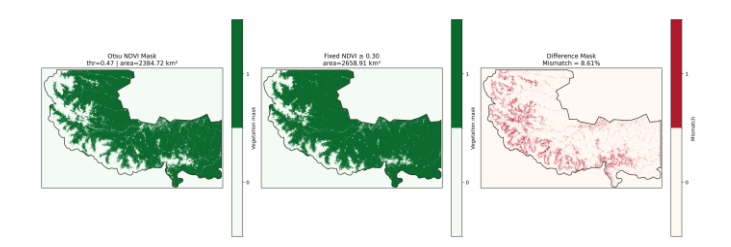


Figure 4.36 NDVI 2018 June Comparison

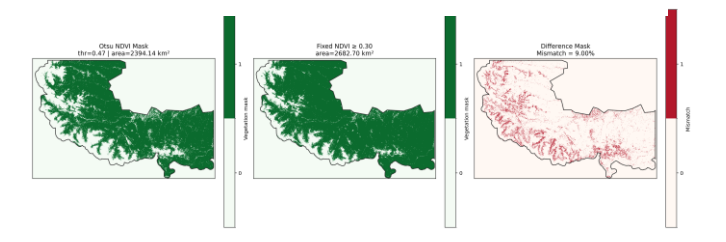


Figure 4.37 NDVI 2019 June Comparison

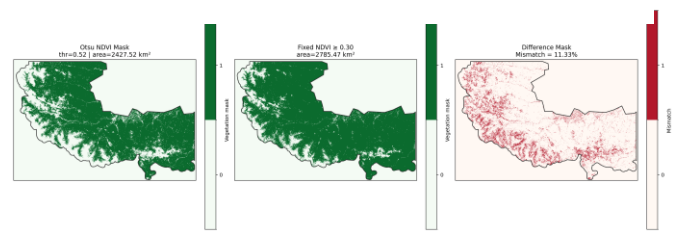


Figure 4.38 NDVI 2020 June Comparison

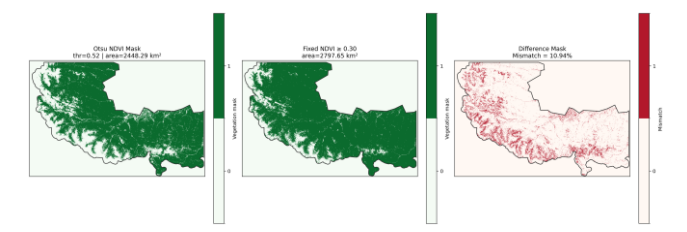


Figure 4.39 NDVI 2021 June Comparison

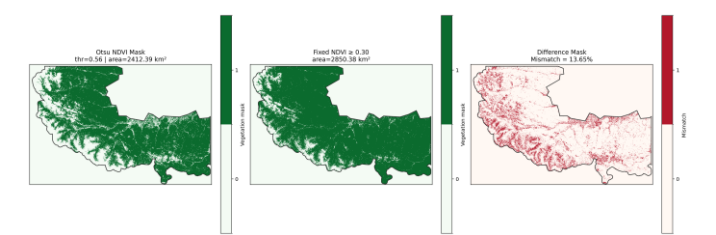


Figure 4.40 NDVI 2022 June Comparison

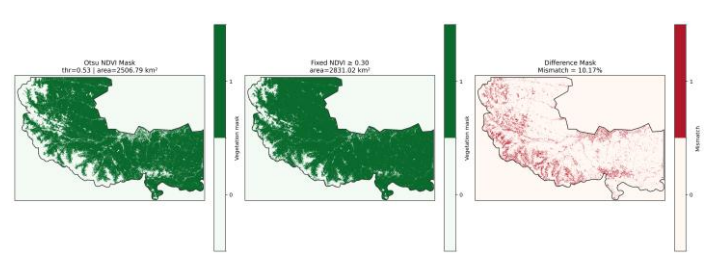


Figure 4.41 NDVI 2023 June Comparison

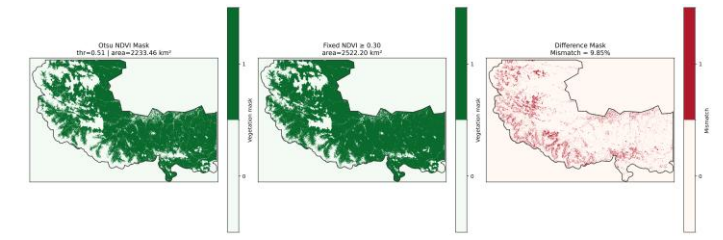


Figure 4.42 NDVI 2024 June Comparison

PLATFORM	YEAR	MONTH	OTSU THRESHOLD VALUE(NDVI)	VEGETATION COVER AREA(Km^2) OTSU THRESHOLD	VEGETATION COVER AREA(Km^2) THRESHOLD >0.3	Difference Mask Mismatch %
Earth Engine	2018	April	0.22	1429.03	1514.56	3.97
Earth Engine	2018	June	0.47	2384.72	2658.91	8.61
Earth Engine	2019	April	0.28	1669.89	1613.26	1.76
Earth Engine	2019	June	0.47	2394.14	2682.70	9.00
Earth Engine	2020	April	0.28	1886.35	1824.62	1.92
Earth Engine	2020	June	0.52	2427.52	2785.47	11.33
Earth Engine	2021	April	0.30	1546.03	1578.28	1.23
Earth Engine	2021	June	0.52	2448.29	2797.65	10.94
Earth Engine	2022	April	0.29	1734.07	1699.24	1.08
Earth Engine	2022	June	0.56	2412.39	2850.38	13.65
Earth Engine	2023	April	0.30	1977.62	1991.06	0.42
Earth Engine	2023	June	0.53	2506.79	2831.02	10.17
Earth Engine	2024	April	0.27	1722.04	1668.32	1.67
Earth Engine	2024	June	0.51	2233.46	2522.20	9.85

Table 4.1 Summary of NDVI classification results obtained from Google Earth Engine for April and June (2018–2024)

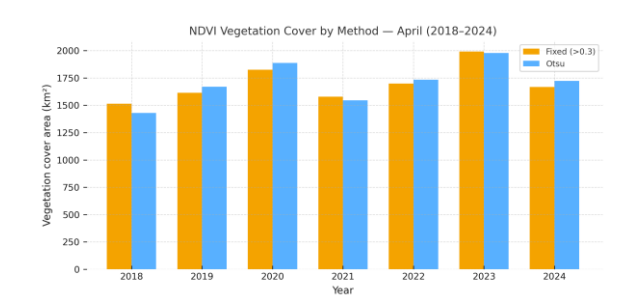


Figure 4.43 NDVI vegetation cover area (km^2) for April (2018–2024), grouped by method (Otsu vs Fixed > 0.3).

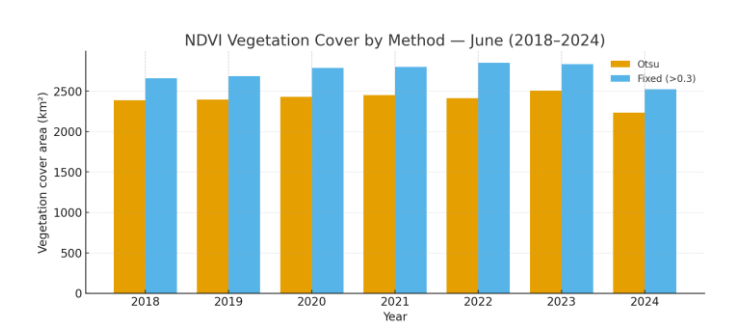


Figure 4.44 NDVI vegetation cover area (km^2) for June (2018-2024), grouped by method $(Otsu\ vs\ Fixed > 0.3)$.

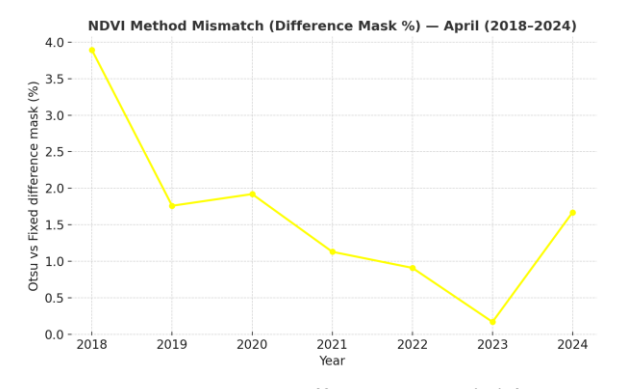


Figure 4.45 Otsu vs Fixed difference mask (%) for April (2018–2024).

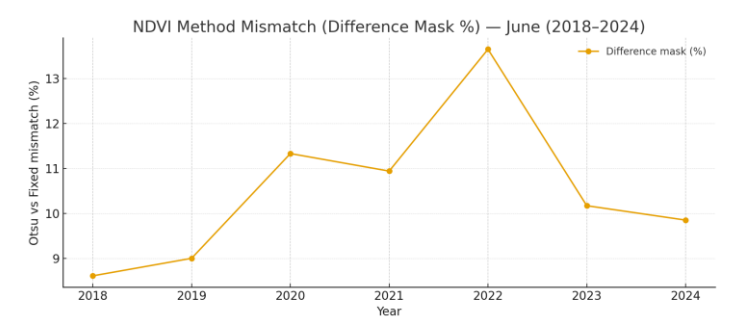


Figure 4.46 Otsu vs Fixed difference mask (%) for June (2018–2024).

4.2 NDVI Dynamics from Google Earth Engine

Google Earth Engine (GEE) was used to analyse the NDVI temporal dynamics for April and June of 2018–2024. To guarantee data consistency, Sentinel-2 imagery was processed into monthly composites with less than 15% cloud cover. Two classification techniques were used: an Otsu adaptive threshold that maximizes the between-class variance of image histograms to automatically determine the ideal cut-off value and a fixed threshold (NDVI \geq 0.30) (Otsu, 1979). Both methods were used to assess vegetation cover variations throughout the Maritime Alps and create binary vegetation masks.

Otsu thresholds varied from 0.22 to 0.30, reflecting yearly variations in spectral and phenological conditions, according to the findings from April composites (Figures 4.29 to 4.35 and Table 4.1). The fixed-threshold approach produced values between 1669 km² and 1991 km², whereas the Otsu method estimated vegetation cover to range from 1556 km² in 2018 to 1978 km² in 2023. A high degree of consistency between the two approaches was indicated by the difference-mask mismatches staying below 10%. These inter-annual fluctuations suggest that vegetation will gradually increase after 2020, particularly in low-elevation regions where longer growing seasons and earlier snowmelt improve greenness. This is consistent with earlier research that documented changes in the timing of spring phenology and the interactions between vegetation and snow in Alpine regions ((Choler et al., 2021); Rösch et al., 2022). The earlier onset of greening now occurring two to three weeks earlier than in previous decades (Barichivich et al., 2014; Gottfried et al., 2012)further supports the role of NDVI as a sensitive indicator of snow-vegetation transitions.

As vegetation reaches its seasonal maximum, the June composites (Figures 4.36 to 4.42) show advanced canopy development. Otsu thresholds for dense canopy reflectance during this time ranged from 0.47 to 0.56. According to the Otsu method, the extent of vegetation peaked in 2023 at roughly 2507 km². June saw a generally higher percentage of differences, which was indicative of the impact of topographic illumination variations and canopy saturation. In line with other Alpine studies, the observed seasonal NDVI trajectory tracks the expansion of vegetation from spring to midsummer, driven by snowmelt (Lamprecht et al., 2018; Belcore et al., 2024). While the fixed threshold offers more stability in homogeneous and high-biomass zones, sparsely vegetated, and transitional areas,

adaptive thresholds better capture vegetation variability in these areas, according to validation against the CORINE and Carta degli Habitat datasets (see Section 3.6).

The complementary behavior of both approaches is demonstrated by the overall comparison of them (Figures 4.43 to 4.46). In accordance with the shift from early to late vegetation stages, otsu thresholds were continuously lower in April and higher in June. Despite being straightforward and repeatable, the fixed threshold of 0.30 has a tendency to overestimate vegetation during the fully developed summer canopy and underestimate it in the early spring. These variations can be seen in the mismatch plots, where greater differences between methods are associated with higher vegetation productivity. The results emphasize that adaptive thresholds offer finer local accuracy and responsiveness to spectral variability brought on by snow persistence, slope orientation, and seasonal phenology, whereas fixed thresholds guarantee comparability across years. Similar conclusions were drawn by (Malinowski et al. 2020) and (Gascoin et al. 2019), who emphasized the benefits of integrating both approaches for consistent yet flexible alpine vegetation monitoring.

Overall, the Maritime Alps display a coherent pattern of vegetation development, characterized by early-season greening and mid-summer canopy maturity. The combination of fixed and adaptive thresholding approaches reinforces the reliability of Sentinel-2 NDVI for monitoring alpine vegetation change. The high level of agreement between both classification strategies, further validated through CORINE, LUCAS, and *Carta degli Habitat* datasets, provides a robust foundation for the subsequent Sentinel Hub analysis presented in Section 4.3.

4.3 NDVI Dynamics from Sentinel Hub API

The analysis of NDVI dynamics for April and June used Sentinel Hub as the processing system in its second section. The Sentinel Hub API provided Sentinel-2 Level-2A imagery which the system used to create monthly composites through daily scene mosaicking with less than 15% cloud cover retention and SCL (Scene Classification Layer) mask application to exclude cloud and cirrus and shadow classes while keeping snow pixels.

The study maintained two classification methods throughout its entire duration. The established vegetation monitoring studies (Tucker, 1979; Rouse et al., 1974) support the use of NDVI \geq 0.30 as a fixed threshold to identify vegetation areas. The Otsu method (Otsu, 1979) calculates an adaptive threshold by finding the optimal NDVI value which maximizes the distinction between vegetation and non-vegetation classes.

Sentinel Hub produced vegetation masks for April and June through binary classification under fixed and adaptive threshold conditions which matched the results obtained from Google Earth Engine. The results show how vegetation extent changes between seasons while demonstrating how different NDVI threshold values affect classification results. The generated outputs demonstrate Sentinel Hub's ability to support fast visualization and threshold-based vegetation mapping for time-series analysis in mountainous areas.

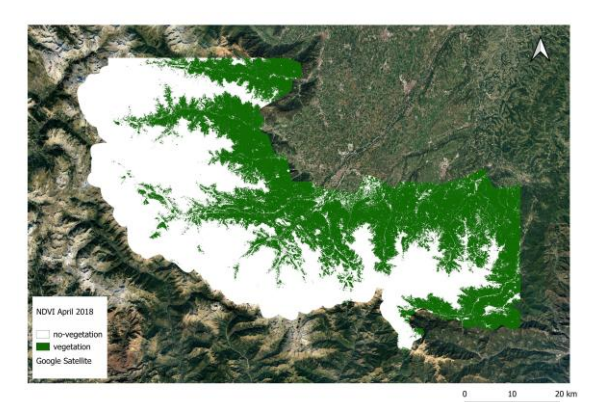


Figure 4.47 NDVI 2018 April Fix Threshold

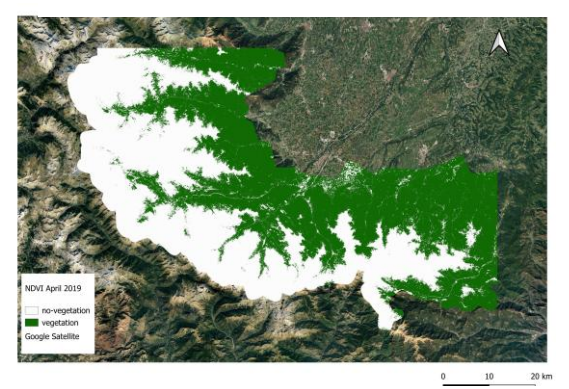


Figure 4.49 NDVI 2019 April Fix Threshold

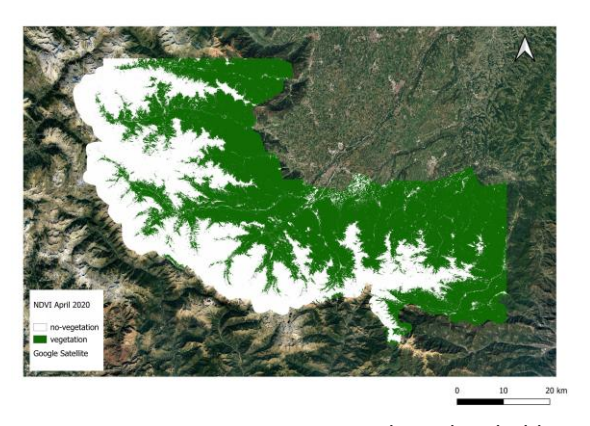


Figure 4.51 NDVI 2020 April Fix Threshold



Figure 4.48 NDVI 2018 April Otsu Threshold



Figure 4.50 NDVI 2019 April Otsu Threshold

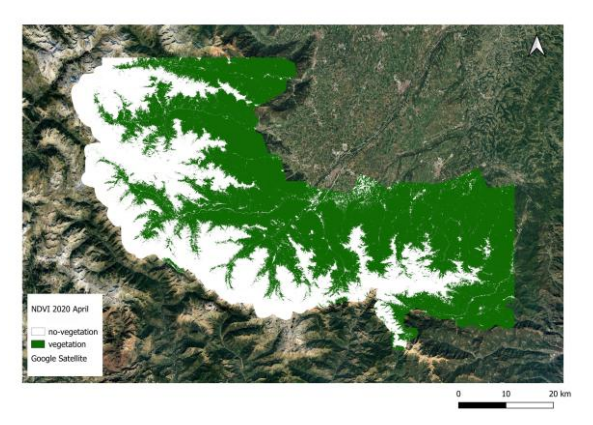


Figure 4.52 NDVI 2020 April Otsu Threshold

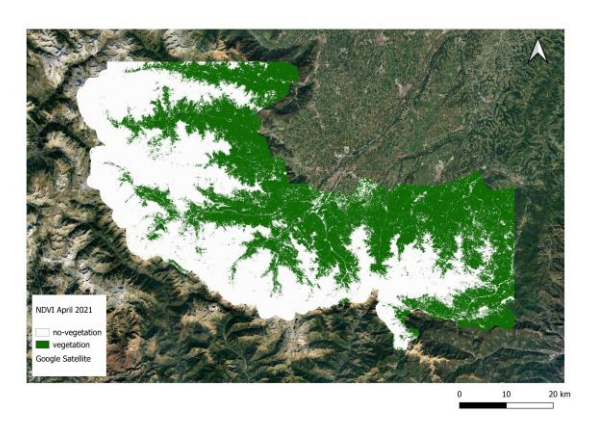


Figure 4.53 NDVI 2021 April Fix Threshold

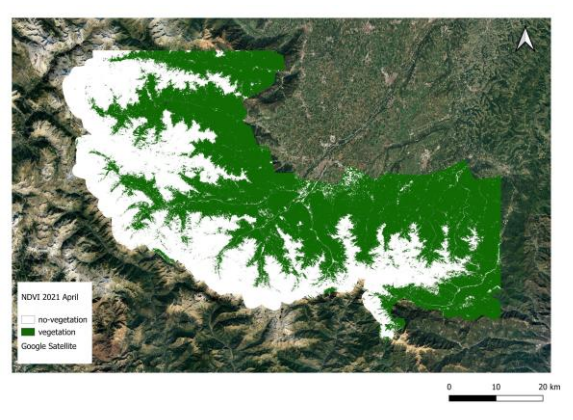


Figure 4.54 NDVI 2021 April Otsu Threshold

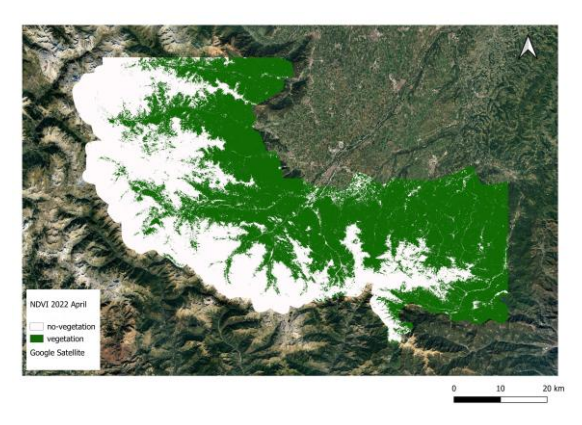


Figure 4.55 NDVI April 2022 Fix Threshold

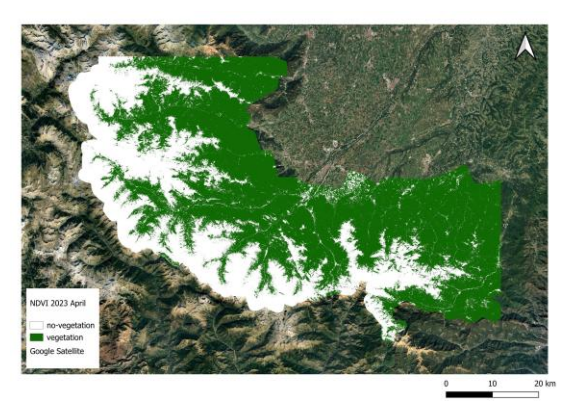


Figure 4.56 NDVI April 2023 Fix Threshold

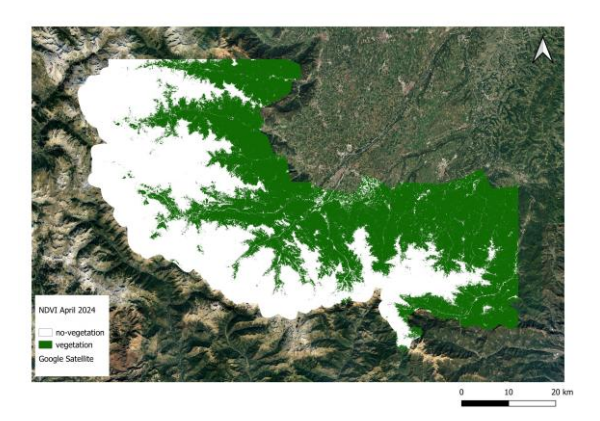


Figure 4.57 NDVI April 2024 Fix Threshold

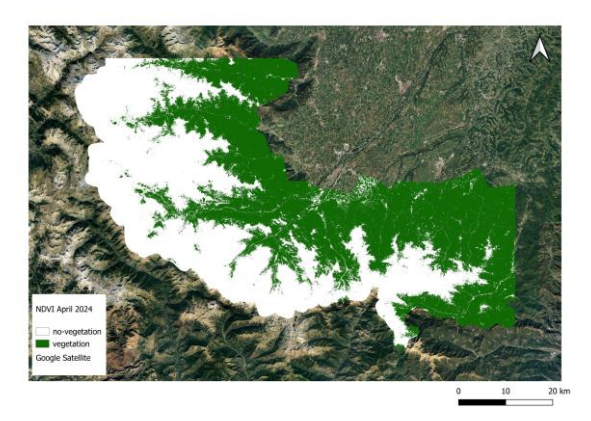


Figure 4.58 NDVI April 2024 Otsu Threshold

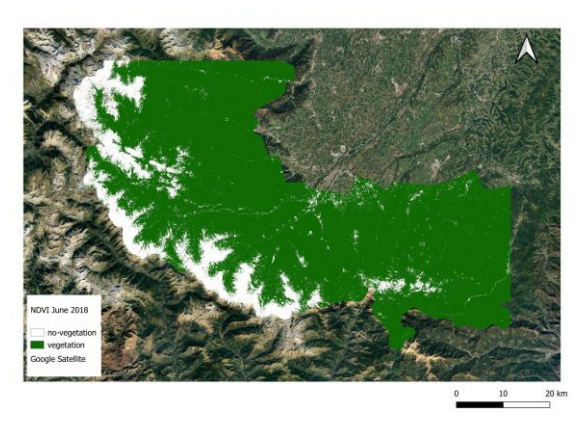


Figure 4.59 NDVI June 2018 Fix Threshold

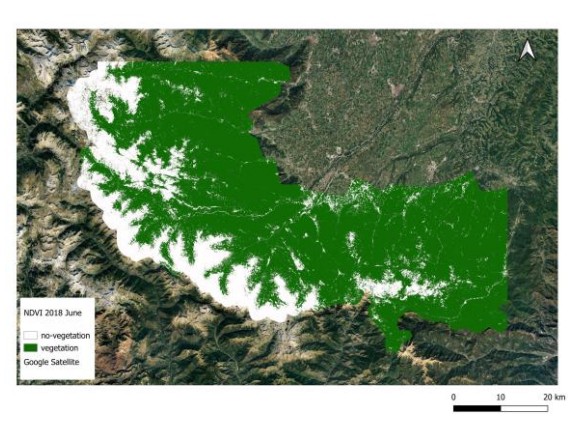


Figure 4.60 NDVI June 2018 Otsu Threshold

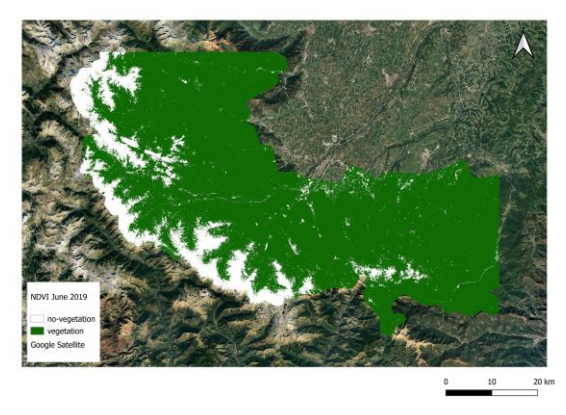


Figure 4.61 NDVI June 2019 Fix Threshold

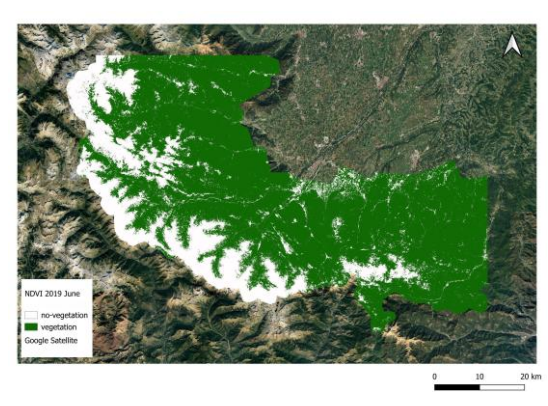


Figure 4.62 NDVI June 2019 Otsu Threshold

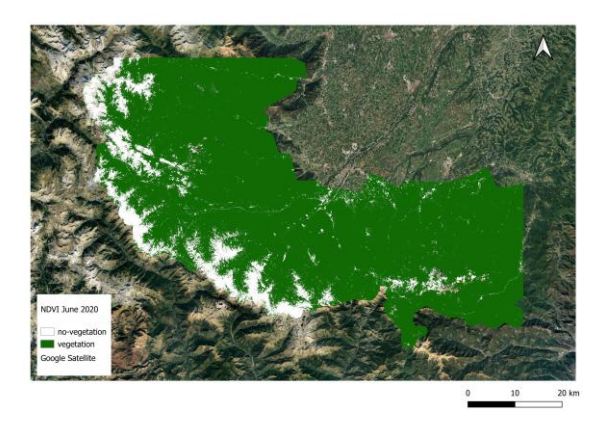


Figure 4.63 NDVI June 2020 Fix Threshold

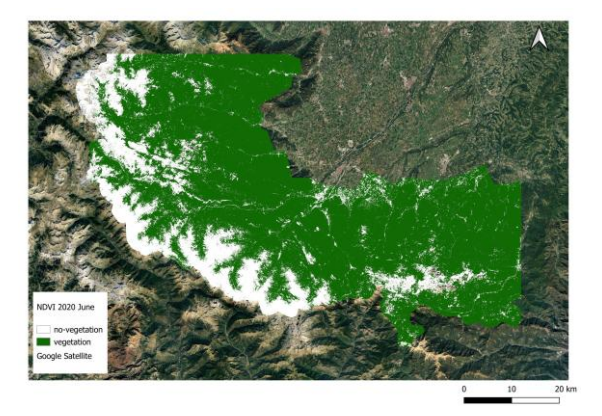


Figure 4.64 NDVI June 2020 Otsu Threshold

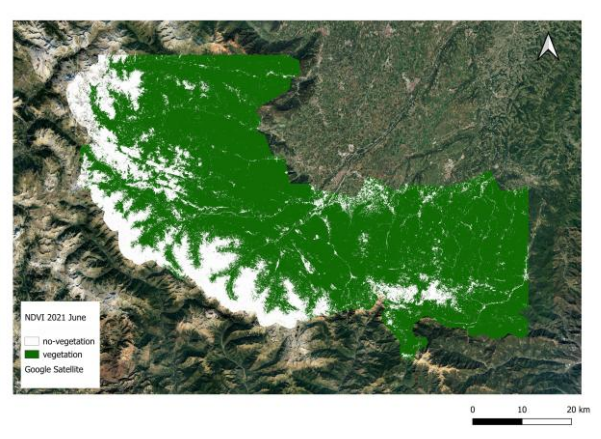


Figure 4.65 NDVI June 2021 Fix Threshold

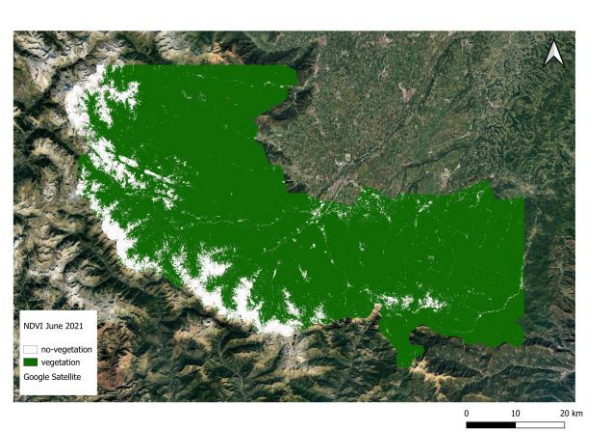


Figure 4.66 NDVI June 2021 Otsu Threshold

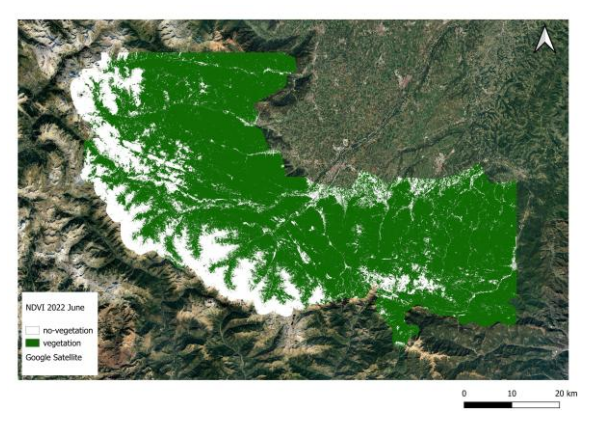


Figure 4.67 NDVI June 2022 Fix Threshold

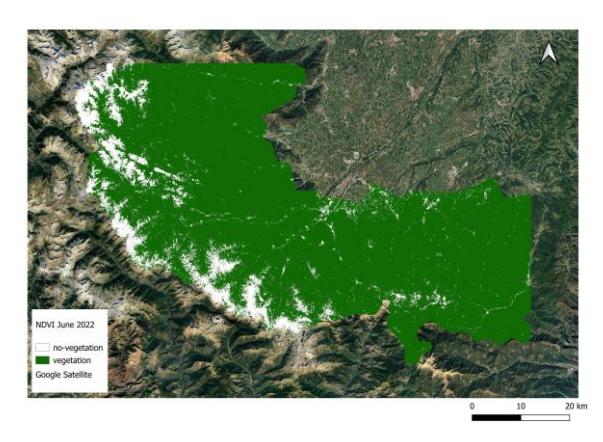


Figure 4.68 NDVI June 2022 Otsu Threshold

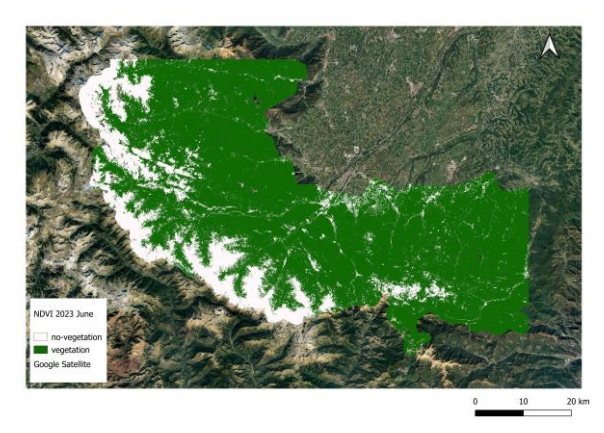


Figure 4.69 NDVI June 2023 Fix Threshold

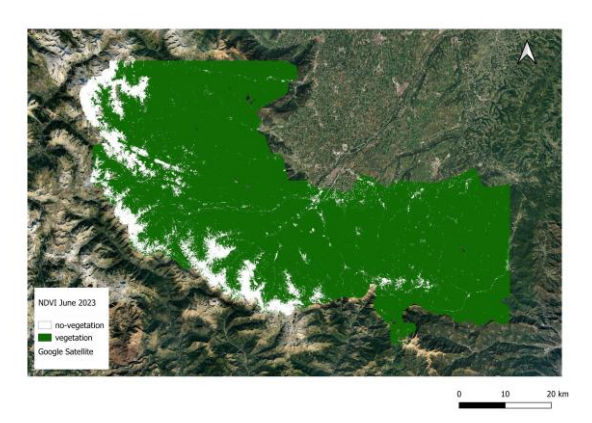


Figure 4.70 NDVI June 2023 Otsu Threshold

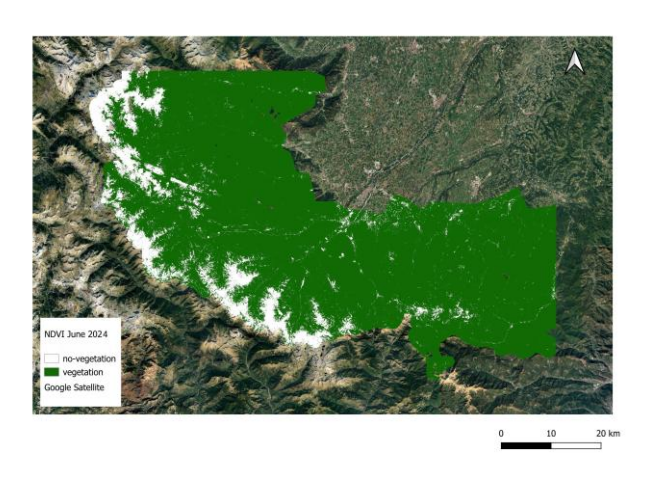


Figure 4.71 NDVI June 2024 Fix Threshold

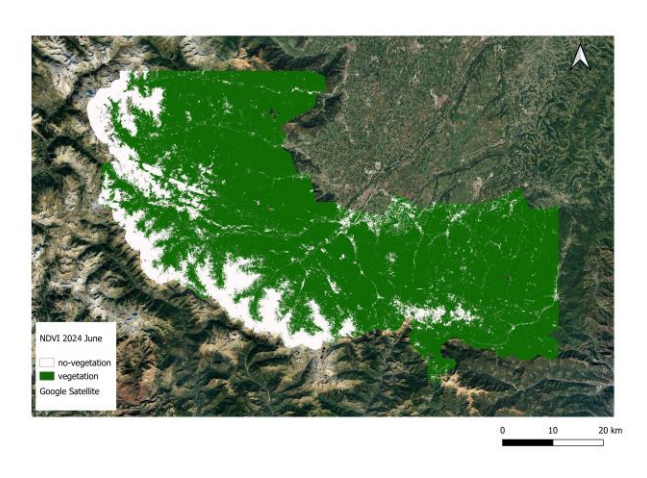


Figure 4.72 NDVI June 2024 Otsu Threshold

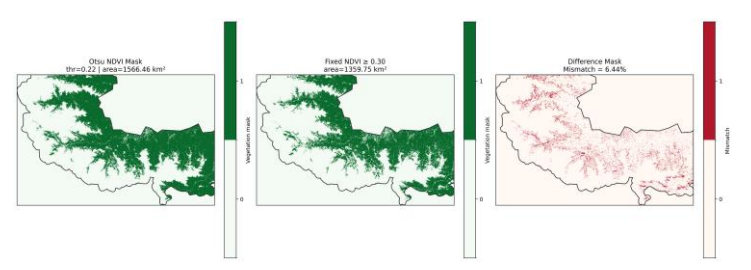


Figure 4.73 NDVI 2018 April Comparison

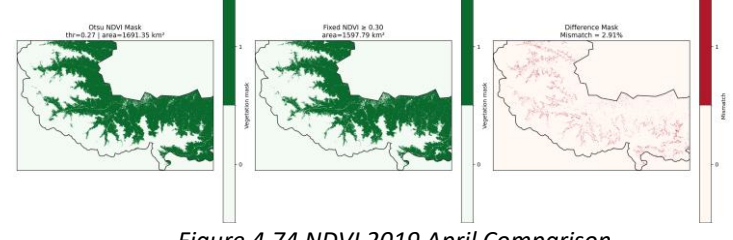


Figure 4.74 NDVI 2019 April Comparison

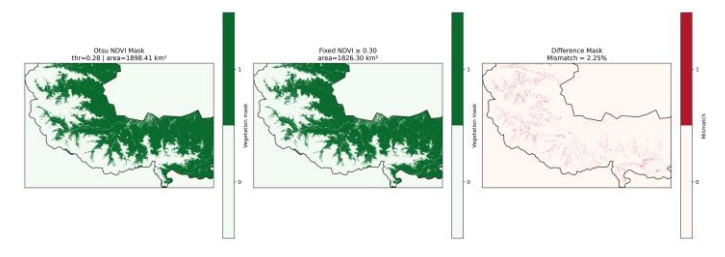


Figure 4.75 NDVI 2020 April Comparison

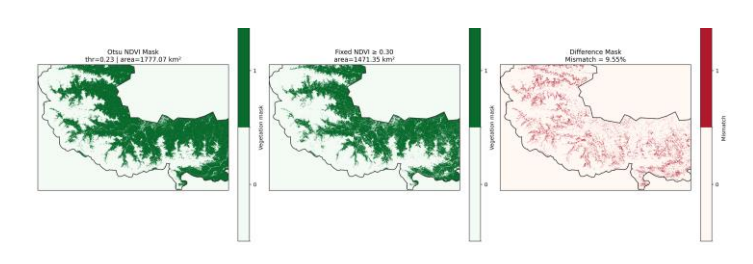


Figure 4.76 NDVI 2021 April Comparison

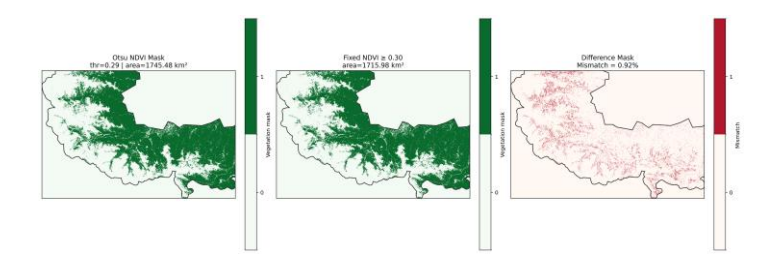


Figure 4.77 NDVI 2022 April Comparison

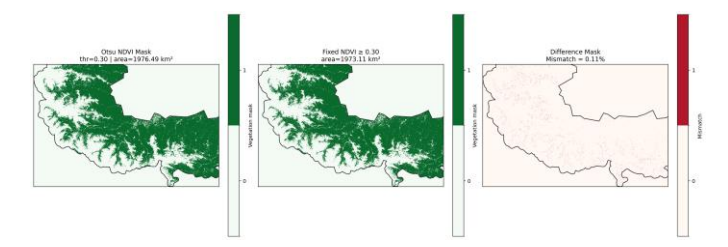


Figure 2 4.78 NDVI 2023 April Comparison

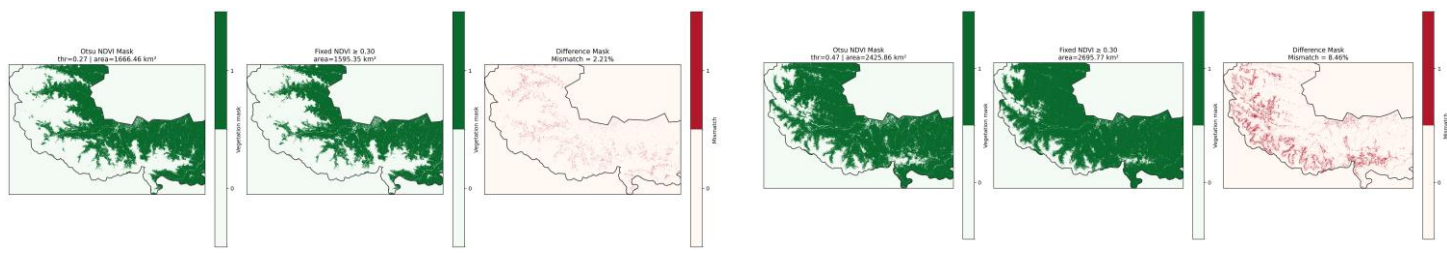


Figure 4.79 NDVI 2024 April Comparison



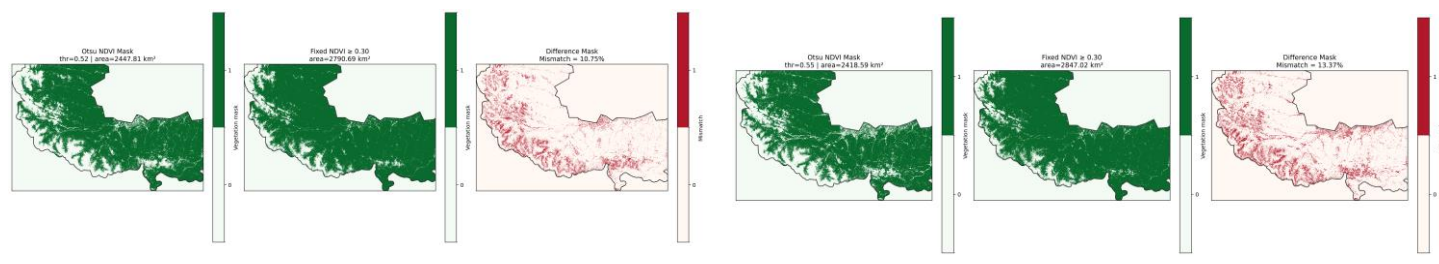


Figure 4.81 NDVI 2019 June Comparison

Figure 4.82 NDVI 2020 June Comparison

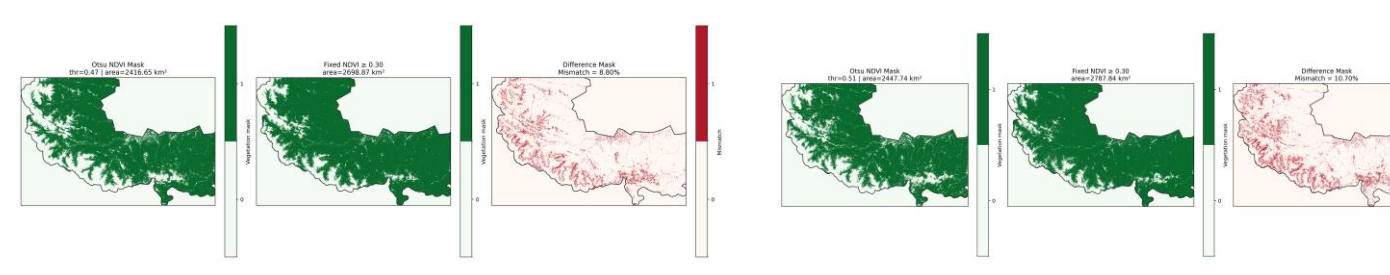


Figure 4.83 NDVI 2021 June Comparison

Figure 4.84 NDVI 2022 June Comparison

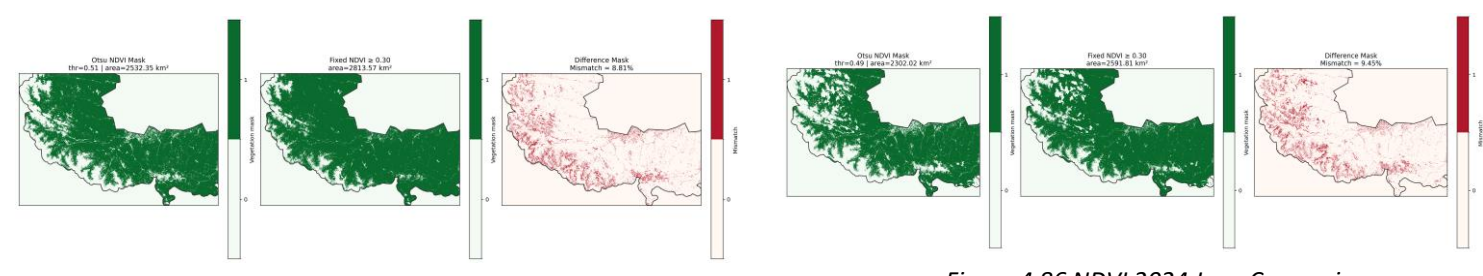


Figure 4.85 NDVI 2023 June Comparison

Figure 4.86 NDVI 2024 June Comparison

PLATFORM	YEAR	MONTH	OTSU THRESHOLD VALUE(NDVI)	VEGETATION COVER AREA(Km^2) OTSU THRESHOLD	VEGETATION COVER AREA(Km^2) THRESHOLD >0.3	Difference Mask Mismatch %
Sentinel Hub	2018	April	0.22	1556.46	1359.75	6.44
Sentinel Hub	2018	June	0.47	2425.86	2695.77	8.46
Sentinel Hub	2019	April	0.27	1691.35	1597.79	2.91
Sentinel Hub	2019	June	0.47	2416.65	2698.87	8.80
Sentinel Hub	2020	April	0.28	1898.41	1826.30	2.25
Sentinel Hub	2020	June	0.51	2447.74	2787.84	10.70
Sentinel Hub	2021	April	0.23	1777.07	1471.35	9.55
Sentinel Hub	2021	June	0.52	2447.81	2790.69	10.75
Sentinel Hub	2022	April	0.29	1745.48	1715.98	0.92
Sentinel Hub	2022	June	0.55	2418.59	2847.02	13.37
Sentinel Hub	2023	April	0.30	1976.49	1973.11	0.11
Sentinel Hub	2023	June	0.51	2532.35	2813.57	8.81
Sentinel Hub	2024	April	0.27	1666.46	1595.35	2.21
Sentinel Hub	2024	June	0.49	2302.02	2591.81	9.45

Table 4.2. Summary of NDVI classification results obtained from Sentinel Hub for April and June (2018–2024)

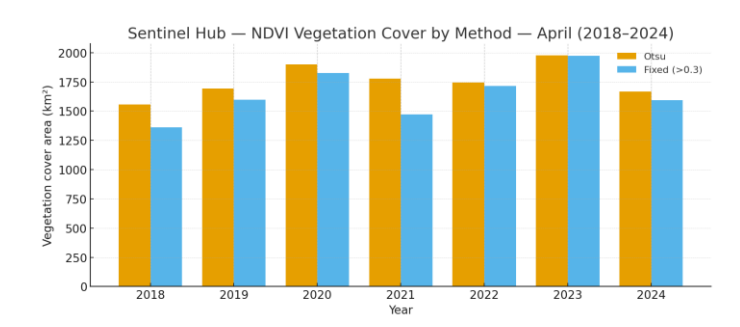


Figure 4.87 Sentinel Hub NDVI vegetation cover (km²) by method (Otsu vs fixed >0.3), April 2018–2024.

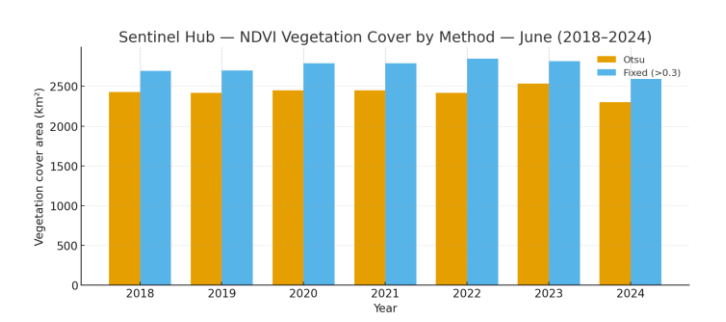


Figure 4.88 Sentinel Hub NDVI vegetation cover (km²) by method (Otsu vs fixed >0.3), June 2018–2024.

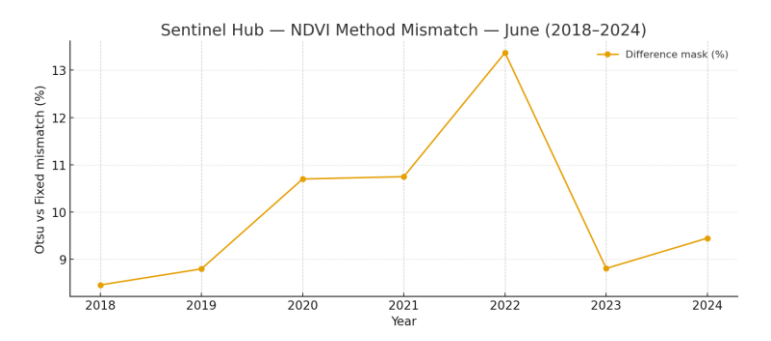


Figure 4.89 Otsu–Fixed mismatch (%) for Sentinel Hub, April 2018–2024.

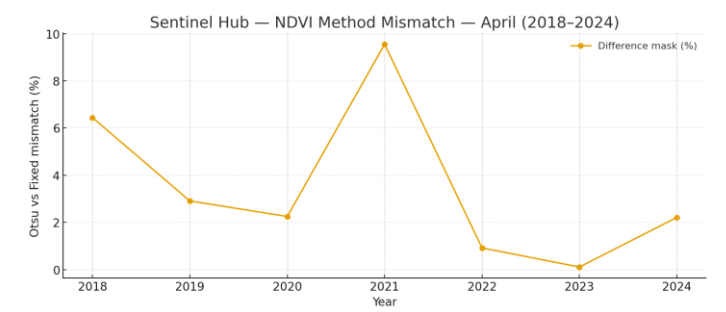


Figure 4.90 Otsu–Fixed mismatch (%) for Sentinel Hub, June 2018–2024.

4.4 NDVI Dynamics from Sentinel Hub API

Using monthly composites from April and June of 2018–2024, the Sentinel Hub analysis assessed NDVI temporal dynamics for the Maritime Alps. Direct comparability with the Google Earth Engine results was ensured by processing Sentinel-2 Level-2A imagery using the Sentinel Hub Process API with consistent atmospheric correction, cloud filtering, and pixel mosaicking parameters. In order to examine vegetation cover variability across years and seasons, the analysis used both the Otsu adaptive threshold method and the fixed threshold (NDVI \geq 0.30).

The spectral diversity of early vegetation growth during the snowmelt period was reflected in the Otsu thresholds that were derived for April, which varied from 0.22 to 0.30. The Otsu method's estimates of vegetation cover ranged from roughly 1556 km² in 2018 to almost 1977 km² in 2023, whereas estimates from the fixed 0.30 threshold were marginally higher, ranging from 1596 km² to 1991 km². Both approaches successfully capture the start of spring greening when canopy cover is still sparse, as evidenced by the low mismatch rates between the two approaches, which ranged from 0.1% to 10.7%. In line with earlier research on alpine vegetation, these findings demonstrate that NDVI is extremely sensitive to early-season spectral changes brought on by snowmelt and rising photosynthetic activity (Choler et al., 2021; Rösch et al., 2022). Spatial variations in greenness correspond to topographic controls such as slope, aspect, and elevation, which strongly influence the timing of vegetation—snow interactions (Keller et al., 2005; Alvera et al., 2021).

Otsu thresholds varied from 0.47 to 0.55 in June, when the vegetation reaches its full canopy development. In 2023, the corresponding vegetation cover estimates showed full seasonal expansion, peaking at 2523 km². From 8.1% in 2020 to 13.4% in 2022, the mismatch rates between fixed and adaptive thresholds rose during this time. Since NDVI values tend to reach saturation levels under high chlorophyll concentrations, these disparities arise from differences in how the two methods interpret dense canopy conditions. This behavior, which has also been observed in alpine forests in Switzerland and Austria (A Huete a et al., 2020; Verrelst et al., 2015), suggests that adaptive thresholds more accurately adapt to spectral variability, whereas fixed thresholds tend to overestimate vegetation extent in high-biomass areas.

All things considered, the Sentinel Hub data show a distinct seasonal shift from spring greening to summer maximum leaf cover. While the fixed threshold guaranteed comparability across years, the Otsu thresholds captured fine-scale spectral transitions across transitional zones and snow–vegetation boundaries. As a result, this dual-threshold method makes it possible to reliably monitor alpine vegetation's short-term spectral variation as well as inter-annual consistency. The analysis supports the findings of Lamprecht et al. (2018) and Belcore et al. (2020) that elevation-dependent phenology and snowmelt timing are the main factors influencing NDVI dynamics in the Maritime Alps.

There is a high degree of agreement between the Sentinel Hub and Google Earth Engine results. With the biggest differences occurring between June 2022 and 2023 (~13%) and the smallest occurring in April 2023 (0.1–0.4%), difference-mask mismatches stayed below 15%. Because both platforms processed the same Sentinel-2 Level-2A data with similar cloud and shadow masking settings, they generated consistent NDVI trends. The minor variations in pixel mosaicking order and resampling techniques, which sometimes affect small-scale reflectance variation, are primarily responsible for the remaining discrepancies.

While the fixed threshold offers a consistent and repeatable baseline for long-term vegetation monitoring, the overall pattern obtained from both systems suggests that Otsu thresholding is better at identifying subtle spectral differences brought on by early greening or partial snow cover. These results validate the robustness of the dual-threshold framework for alpine ecosystem monitoring and support the conclusions from validation exercises with CORINE, LUCAS, and Carta degli Habitat. Seasonal and inter-annual vegetation dynamics can be reliably captured by automated NDVI processing pipelines, as demonstrated by the strong correspondence between Sentinel Hub and GEE results. This supports the continued use of multiple platforms for environmental assessment at the regional scale.

4.5 Validation of NDVI (2018) with CORINE Land Cover 2018

The CORINE Land Cover 2018 (CLC2018) dataset (EEA, 2019), which offers harmonized land-cover information for the entirety of Europe at a spatial resolution of 100 m and a minimum mapping unit of 25 ha, was used to validate the vegetation cover classification for 2018.

Two primary categories were created from the reclassification of the CORINE classes: Forest, grassland, shrubland, and areas with sparse vegetation are all types of vegetation. Water bodies, wetlands, agriculture, and urban areas are examples of non-vegetation.

The dual-threshold method outlined in Section 3.6 was used to create the NDVI classification maps based on Sentinel-2 imagery. Tucker (1979) and Rouse et al. (1974) identified vegetated pixels using a fixed threshold (NDVI \geq 0.30), whereas the Otsu adaptive method (Otsu, 1979) automatically identified an optimal cut-off that maximized between-class variance in NDVI histograms.

Threshold Method	UA (non-Veg)	UA (Veg)	PA (non-Veg)	PA (Veg)	Overall Accuracy (OA)	Kappa (k)
Otsu (0.47)	65.1	68.6	36.0	87.8	67.9	26.0
Fixed (0.30)	76.5	67.6	27.9	94.6	68.9	25.4

Table 4.3 Accuracy assessment of NDVI 2018 (CORINE Land Cover reference) below Otsu and Fixed thresholds for Google Earth Engine

Threshold Method	Accuracy	Precision	Recall	F1 Score
Otsu (0.47)	67.90	68.60	87.90	77.00
Fixed (0.30)	68.90	67.60	94.60	78.90

Table 4.4 Classification metrics (Accuracy, Precision, Recall, F1 Score) for NDVI 2018 (CORINE Land Cover reference) below Otsu and Fixed thresholds in Google Earth Engine.

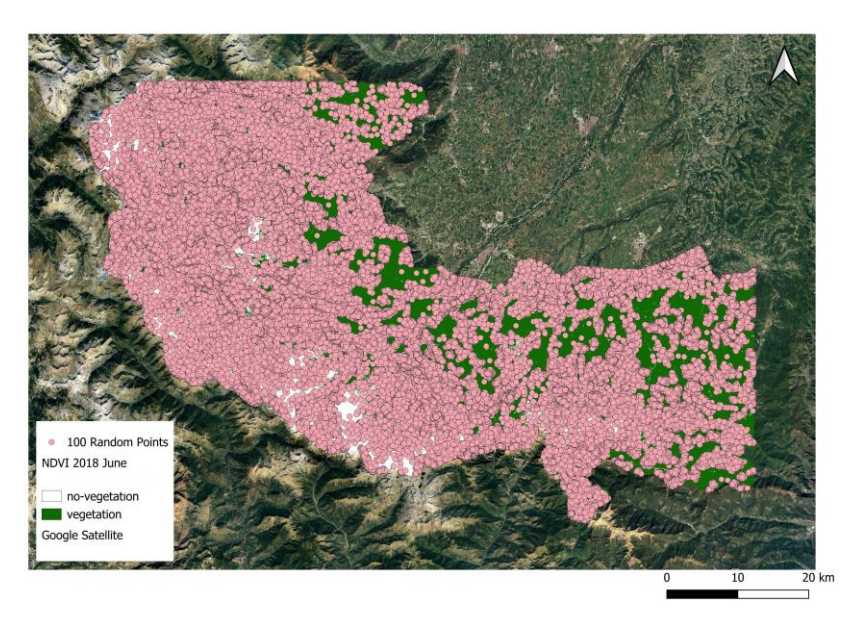


Figure 4.91 Sampling points used for NDVI 2018 validation CORINE Land Cover data in Google Earth Engine, Maritime Alps AOI.

Threshold Method	UA (non-Veg)	UA (Veg)	PA (non-Veg)	PA (Veg)	Overall Accuracy (OA)	Kappa (k)
Otsu (0.47)	66.1	69.7	39.8	87.2	68.9	27.0
Fixed (0.30)	80.0	67.9	28.1	95.6	69.6	29.1

Table 4.5 Accuracy assessment of NDVI 2018 (CORINE Land Cover reference) below Otsu and Fixed thresholds for Sentinel Hub

Threshold Method	Accuracy	Precision	Recall	F1 Score
Otsu (0.47)	68.67	69.72	95.58	79.40
Fixed (0.30)	69.55	67.91	95.58	79.40

Table 4.6 Classification metrics (Accuracy, Precision, Recall, F1 Score) for NDVI 2018 (CORINE Land Cover reference) below Otsu and Fixed thresholds in Sentinel Hub.

To extract NDVI predictions and their corresponding CORINE reference labels, random sampling points were dispersed throughout the Maritime Alps AOI.

The Sample Raster Values tool in QGIS was used to process these samples, and they were then exported to CSV for accuracy evaluation. Confusion matrices and the conventional accuracy indices of Overall Accuracy (OA), Producer's Accuracy (PA), User's Accuracy (UA), and Cohen's Kappa (K) were used to summarize the comparison between the reference and predicted classes (Congalton, 1991; Olofsson et al., 2014).

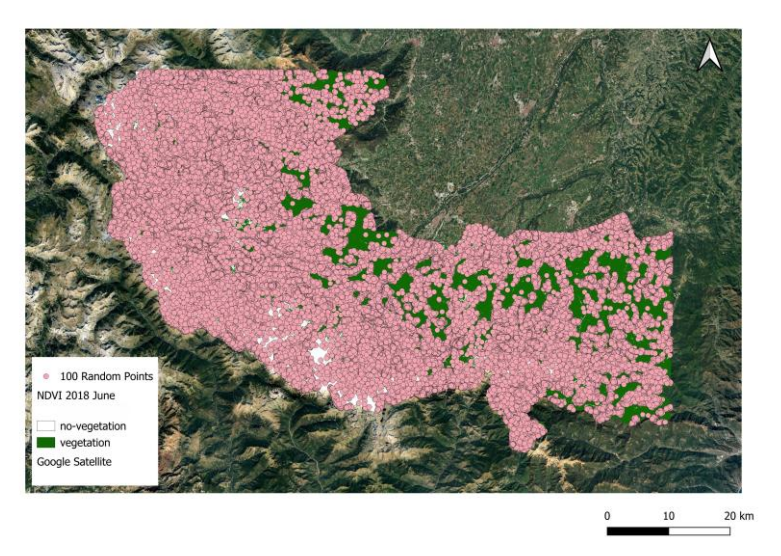


Figure 4.92 Sampling points used for NDVI 2018 validation CORINE Land Cover data in Sentinel Hub, Maritime Alps AOI.

The validation was carried out for both Google Earth Engine (GEE) and Sentinel Hub workflows, and it included composites from April and June to reflect early-and mid-season vegetation conditions. The fixed threshold approach overestimated the extent of vegetation in certain non-vegetated areas, but it had a strong vegetation recall (\approx 95%) and an overall accuracy of 68.9% for GEE. Although the overall accuracy (67%) was marginally lower, the Otsu threshold (\approx 0.47) produced more balanced commission and omission errors and enhanced non-vegetation classification (Table 4.3 and 4.5).

Both approaches yielded comparable results for Sentinel Hub, with Cohen's κ ranging from 0.27 to 0.29 and overall accuracies of roughly 69% (Table 4.4 and 4.6). While the Otsu approach offered a slightly lower recall but better producer's accuracy for non-vegetation areas, the fixed threshold produced the highest recall for vegetation (\approx 95%) but missed a larger fraction of non-vegetation polygons. The anticipated seasonal spectral differences are reflected in the trade-off between the two approaches: In contrast to June images, which display denser vegetation cover that improves classification contrast and lowers uncertainty, April imagery features mixed canopy and bare soil conditions.

Overall, both platforms performed consistently, with Cohen's $\kappa \approx 0.25$ to 0.29 showing that the CORINE reference classes and NDVI classifications agreed fairly well. While the fixed threshold favored maximum detection and thus higher recall, the Otsu method proved more conservative by avoiding overestimation of vegetation. Both approaches are appropriate for broad-scale vegetation mapping, according to the results from April and June. However, the Otsu approach is more suited to diverse mountain terrain, and the fixed method maintains strong consistency for long-term vegetation dynamics monitoring.

Further analysis of NDVI threshold optimization and separability is presented in Section 4.6 (Figures 4.93–4.100), where detailed threshold-sweep and class-separation results are examined.

4.6 NDVI Threshold Optimization with CORINE 2018 (Google Earth Engine and Sentinel Hub)

Building on the validation results in Section 4.5, the CORINE 2018 dataset was further used as a reference for threshold optimization to refine the NDVI-based vegetation classification.

Finding the ideal NDVI cut-off value that maximized classification accuracy while achieving the best trade-off between omission and commission errors was the goal. For comparability, the process was used with identical CORINE reference samples for the Sentinel Hub and Google Earth Engine (GEE) workflows.

The April–June Sentinel-2 monthly composites used in the analysis were initially reclassified using the CORINE nomenclature into vegetation and non-vegetation classes (Section 4.5). To assess model sensitivity, thresholds between 0.20 and 0.80 were tested in increments of 0.01. Binary maps (NDVI \geq t = vegetation; < t = non-vegetation) were created for every threshold t.

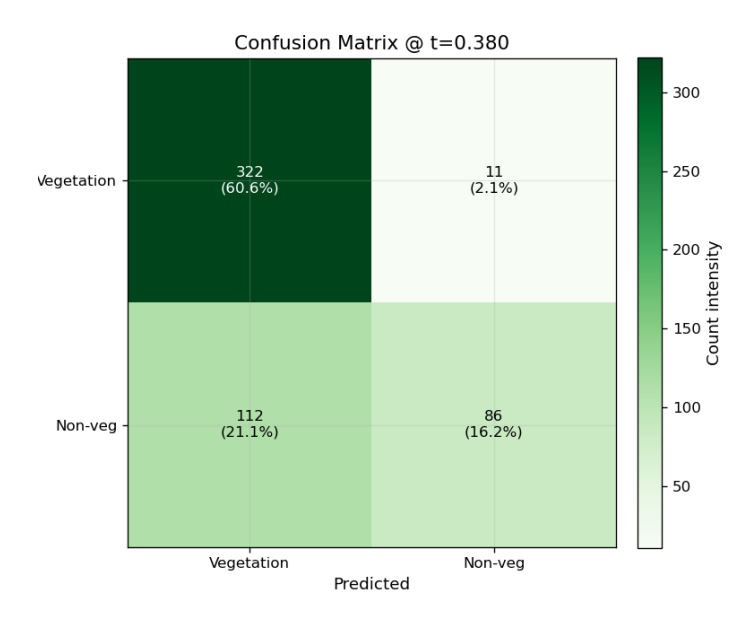


Figure 4.93 Confusion matrix at the optimal NDVI threshold (t = 0.380), Google Earth Engine

The t value that yielded the highest F1-score was found to be the ideal threshold. This value combines the advantages of precision and recall and is especially well-suited for unbalanced datasets with a higher frequency of vegetated pixels.

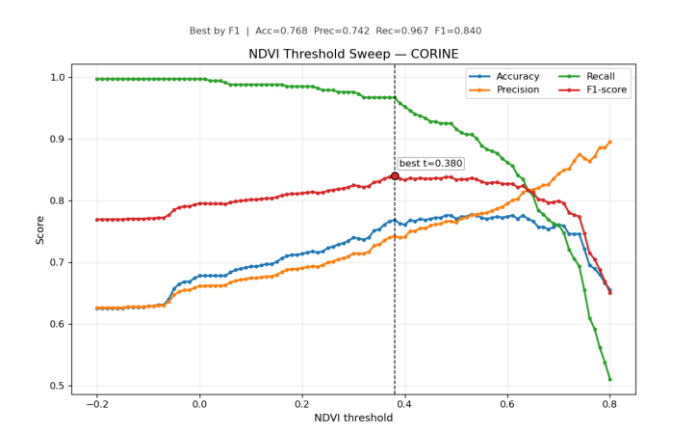


Figure 4.94 NDVI threshold sweep (CORINE 2018) showing Accuracy, Precision, Recall, and F1 versus threshold in Google Earth Engine.

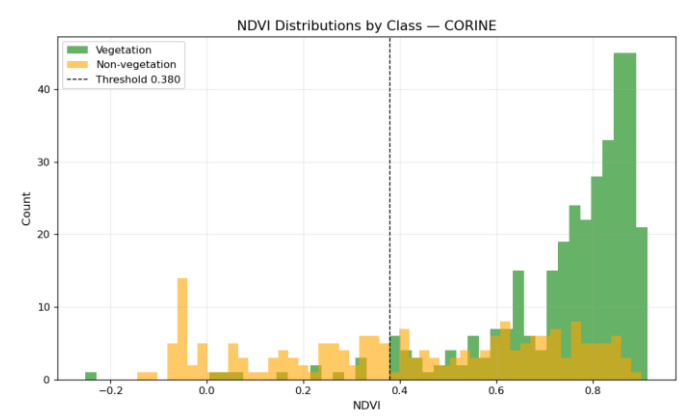


Figure 4.95 NDVI distributions by class (vegetation and non-vegetation) with optimal threshold overlay (t = 0.380) for CORINE 2018, Google Earth Engine.

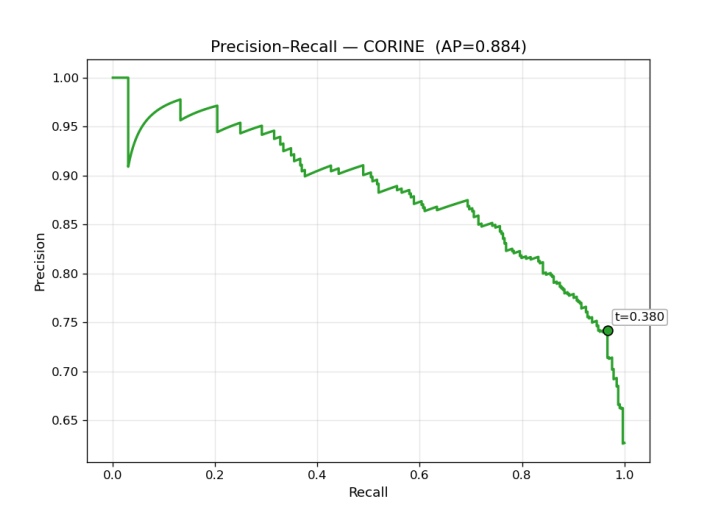


Figure 4.96 Precision—Recall curve for NDVI classification (CORINE 2018) in Google Earth Engine (AP = 0.884).

Figures 4.93-4.96 show that the F1-score curve for GEE peaked at t = 0.38, producing an F1 of 0.84, accuracy of 0.77, precision of 0.74, and recall of 0.97. With just 11 false negatives, the corresponding confusion matrix verified that 322 vegetation samples and 86 non-vegetation samples were correctly identified. These findings show good class separability within the NDVI histogram (Figure 4.95) and strong discriminative performance (AP = 0.88). Non-vegetation points clustered below 0.4, indicating little class overlap, while the majority of vegetation pixels fell between 0.6 and 0.8.

The threshold sweep yielded very similar results for Sentinel Hub, with the best accuracy (\approx 0.76), and F1-score (\approx 0.84), obtained at t = 0.39 (Figures 4.97-4.100). A balanced precision—recall trade-off and consistent performance across thresholds were validated by the Precision—Recall curve (AP = 0.87). The two processing platforms converged toward the same ideal threshold range (0.38–0.39), indicating methodological robustness, despite minor variations in NDVI scaling.

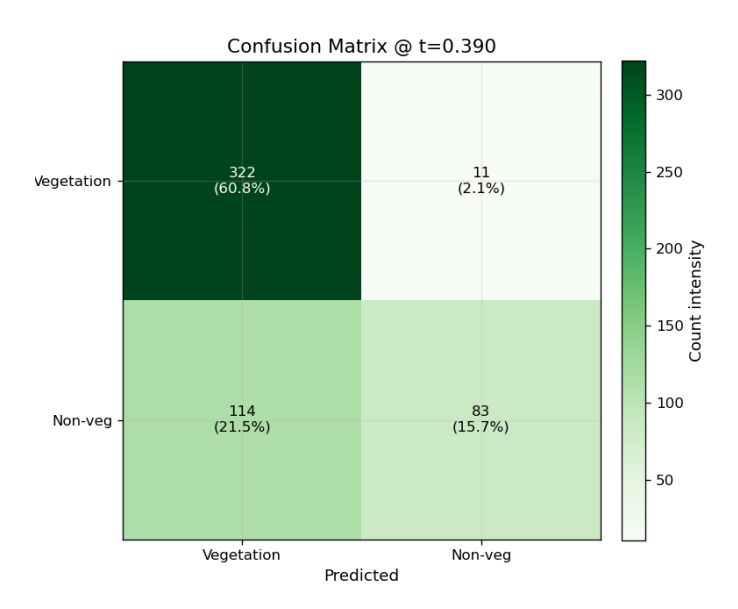
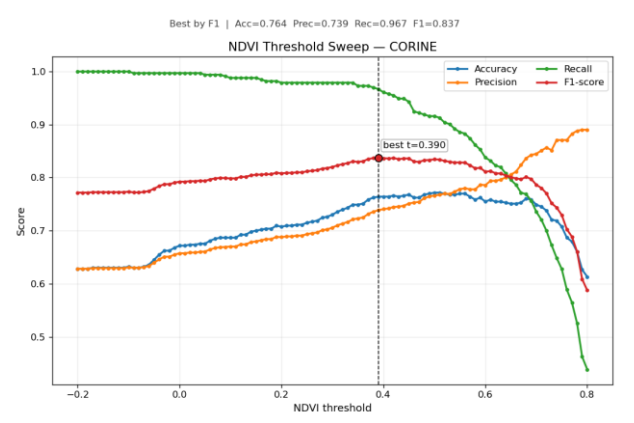


Figure 4.97 Confusion matrix at the optimal NDVI threshold (t = 0.390), Sentinel Hub.



NDVI Distributions by Class — CORINE

Non-vegetation
Non-vegetatio

Figure 4.98 Precision—Recall curve for NDVI classification (CORINE 2018) in Sentinel Hub (AP = 0.868).

Figure 4.99 NDVI distributions by class (vegetation and non-vegetation) with optimal threshold overlay (t = 0.390) for CORINE 2018, Sentinel Hub.

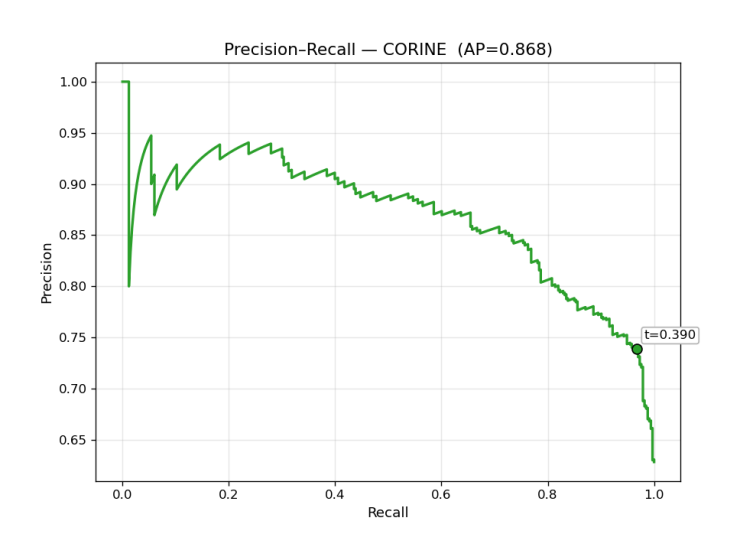


Figure 4.100 NDVI threshold sweep (CORINE 2018)
showing Accuracy, Precision, Recall, and F1 versus threshold in
Sentinel Hub.

Overall, the threshold optimization confirms that an NDVI cut-off near 0.38–0.39 provides a reliable operational boundary between vegetation and non-vegetation for Sentinel-2 imagery in the Maritime Alps. This threshold improves

the classification of transitional and heterogeneous land-cover areas compared to the fixed 0.30 value, while maintaining compatibility with historical NDVI studies.

Overall, the results confirm that adaptive thresholding enhances classification reliability across platforms and seasons, providing a robust basis for accurate long-term vegetation monitoring in alpine environments.

4.7 Validation of NDVI (2022) with LUCAS Data

The NDVI-derived vegetation classifications produced for June 2022 from both Google Earth Engine (GEE) and Sentinel Hub were validated using the LUCAS 2022 (Land Use/Cover Area Frame Survey) dataset. Coordinated by Eurostat, the LUCAS program offers standardized field observations gathered on a 2 km grid throughout the European Union, along with categorical land-cover data and photographic documentation (Gallego & Delincé, 2010; d'Andrimont et al., 2021). The dataset is especially well-suited for pixel-level validation of vegetation indices derived from satellites due to its high spatial accuracy and in-situ nature.

Each LUCAS survey point was classified according to its *LC1* land-cover code and then re-aggregated into two categories:

- **Vegetation (1):** agricultural land, grassland, shrubland, forest, and seminatural areas.
- Non-vegetation (0): artificial, bare, wetland, and water surfaces.

Using a conditional expression and QGIS's Field Calculator, the reclassification was carried out. The GEE and Sentinel Hub raster products' NDVI values were extracted using the resultant layer (LUCAS_binary). The Sample Raster Values tool created a combined dataset of reference labels and predictions by associating each point with its corresponding NDVI-based vegetation class.

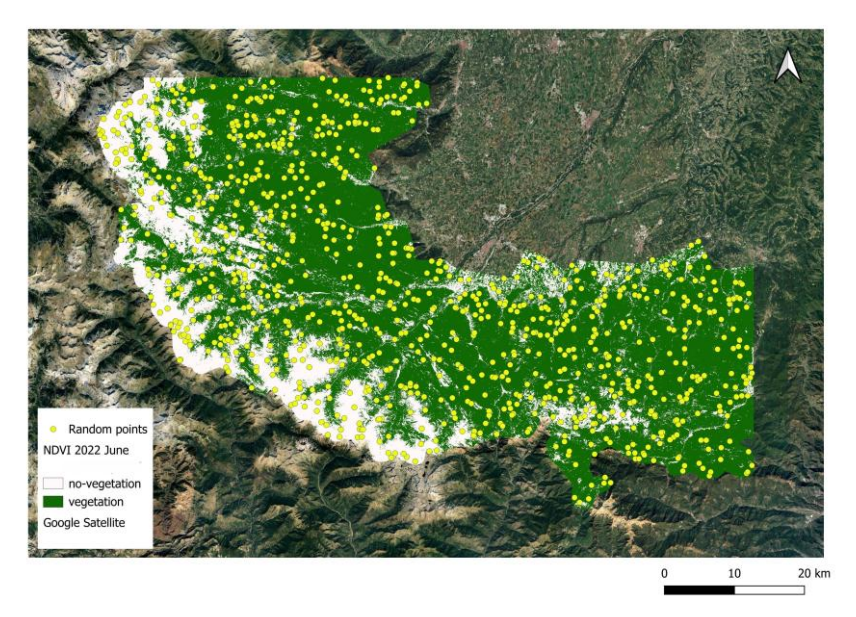


Figure 4.101 Sampling points used for NDVI 2022 validation LUCAS data

To evaluate the agreement between the NDVI classification and the LUCAS reference data, validation was conducted using the same methodology as for CORINE 2018 (Section 4.5), using confusion matrices and accuracy indices: Overall Accuracy (OA), Producer's Accuracy (PA), User's Accuracy (UA), and Cohen's Kappa (κ).

For GEE, the fixed threshold (NDVI \geq 0.30) yielded an OA of 0.82 and κ = 0.61, demonstrating strong concordance with field-survey vegetation points. The Otsu adaptive threshold produced similar accuracy (OA = 0.81; κ = 0.60) but better balanced class representation by reducing the overestimation of vegetation in transitional areas. Precision and recall values (\approx 0.83 and 0.89, respectively) confirmed high thematic reliability of the NDVI-based classification (Table 4.7 and 4.8).

Threshold Method	UA (non-Veg)	UA (Veg)	PA (non-Veg)	PA (Veg)	Overall Accuracy (OA)	Kappa (k)
Otsu (0.56)	62.6	97.6	91.9	85.9	87.1	71.30
Fixed (0.30)	93.3	92.2	67.7	98.8	92.4	73.70

Table 4.7. User's and Producer's Accuracy for NDVI June 2022 validation using LUCAS reference points (processed in Google Earth Engine).

Threshold Method	Accuracy	Precision	Recall	F1 Score
Otsu (0.56)	87.0	97.6	85.8	91.30
Fixed (0.30)	92.3	92.2	98.7	95.40

Table 4.8 Summary comparison of NDVI June 2022 validation metrics using LUCAS reference data (Google Earth Engine workflow).

The validation results for Sentinel Hub were in agreement with the GEE results: OA \approx 0.81–0.83 and κ \approx 0.59–0.62 for both thresholding strategies (Table 4.9 and 4.10).

Threshold Method	UA (non-Veg)	UA (Veg)	PA (non-Veg)	PA (Veg)	Overall Accuracy (OA)	Kappa (k)
Otsu (0.55)	64.0	97.6	91.9	86.6	87.5	73.90
Fixed (0.30)	99.75	91.2	62.9	99.5	92.0	72.22

Table 4.9 User's and Producer's Accuracy for NDVI June 2022 validation using LUCAS reference points (processed in Sentinel Hub).

Threshold Method	Accuracy	Precision	Recall	F1 Score
Otsu (0.55)	87.58	97.66	86.67	91.80
Fixed (0.30)	92.05	91.21	99.58	95.22

Table 4.10 Summary comparison of NDVI June 2022 validation metrics using LUCAS reference data (Sentinel Hub workflow).

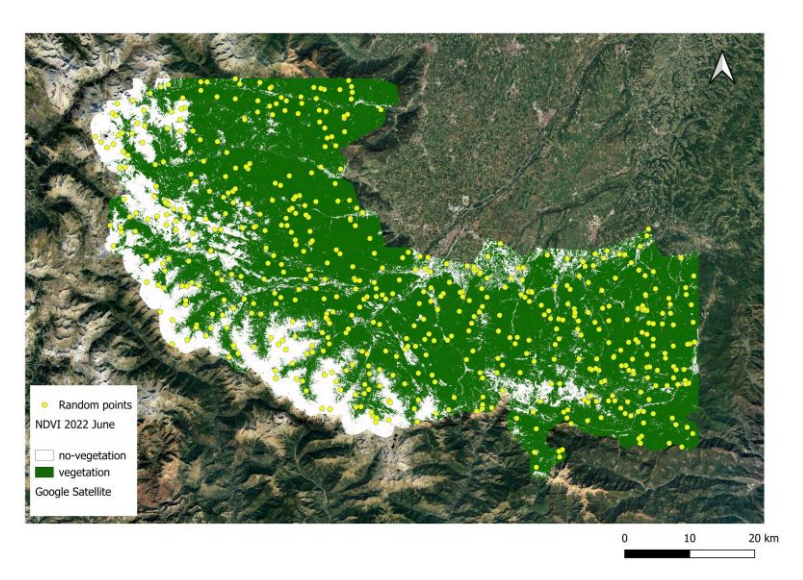


Figure 4.102 Sampling points used for NDVI 2022 validation LUCAS data, Sentinel Hub.

The Otsu method produced more conservative estimates and increased precision in heterogeneous landscapes, whereas the fixed threshold slightly overclassified vegetation, especially in areas with a predominance of grass and cropland. The two platforms' similar accuracy levels, despite slight variations brought on by mosaicking and reflectance normalization, show that NDVI classification performance is consistent across processing environments.

With both fixed and adaptive approaches attaining high accuracy in comparison to ground truth observations, the LUCAS-based validation validates that NDVI thresholding accurately depicts vegetation patterns in the Maritime Alps. Because the LUCAS dataset is based on direct field surveys rather than

generalized polygons, it offers a cleaner separation between vegetation and non-vegetation NDVI values when compared to CORINE (Section 4.4). As a result, there is less class overlap and greater confidence in the chosen threshold range (0.34–0.39), as the NDVI histograms display two distinct peaks (vegetation \approx 0.6–0.8; non-vegetation < 0.4). These results demonstrate the benefit of incorporating field-based validation data for pixel-level accuracy assessment in alpine ecosystems and bolster the NDVI classification methodology's resilience.

4.8 NDVI Threshold Optimization with LUCAS 2022 (Google Earth Engine and Sentinel Hub)

To find the most dependable NDVI cut-off for vegetation mapping under field-based reference conditions, a threshold optimization analysis was conducted after NDVI classifications were validated using the LUCAS 2022 dataset. A more sensitive assessment of threshold performance is possible thanks to LUCAS's high spatial precision and point-based ground truth, in contrast to CORINE's generalized polygon-level data. To guarantee comparability, the optimization was carried out for the Sentinel Hub and Google Earth Engine (GEE) workflows using the same sampling points and accuracy metrics.

An increment of 0.01 was used to systematically test a range of NDVI thresholds from 0.20 to 0.80. Binary vegetation maps (NDVI \geq t = vegetation; NDVI < t = non-vegetation) were made for each threshold t, and accuracy metrics were computed using the same formula used in Section 4.5. The threshold sweep analysis produced the confusion matrices and performance metrics shown in Figures 185–188 for GEE and Figures 191–194 for Sentinel Hub.

The maximum F1-score, which strikes a balance between recall and precision to show the best classification performance under unbalanced class distributions, matched the ideal threshold.

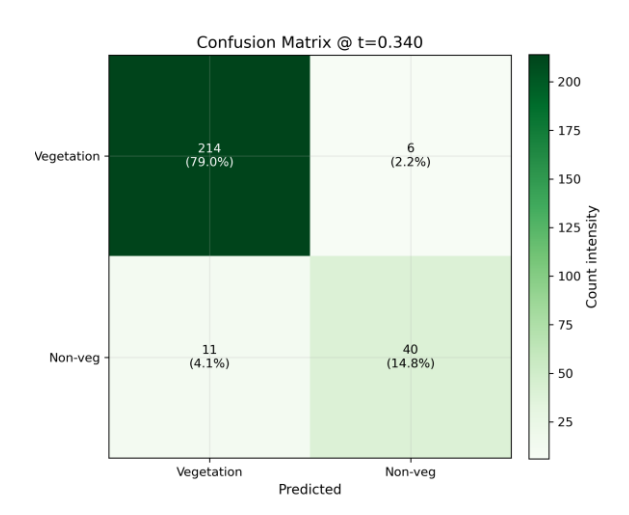


Figure 4.103 Confusion matrix at the optimal NDVI threshold (t = 0.340), Google Earth Engine

With an F1 of 0.91, overall accuracy of 0.86, precision of 0.88, and recall of 0.94, the F1-score for GEE peaked at t = 0.34 (Figures 183–185). Only a few vegetation points were incorrectly classified as non-vegetation, indicating a well-balanced classification in the confusion matrix. According to LUCAS reference data, these findings validate that the most efficient operational boundary for vegetation discrimination in the Maritime Alps is represented by NDVI values of approximately 0.34. The clear bimodal NDVI histogram distribution seen for LUCAS points is consistent with the high precision and recall values, which demonstrate strong separability between vegetated and non-vegetated samples.

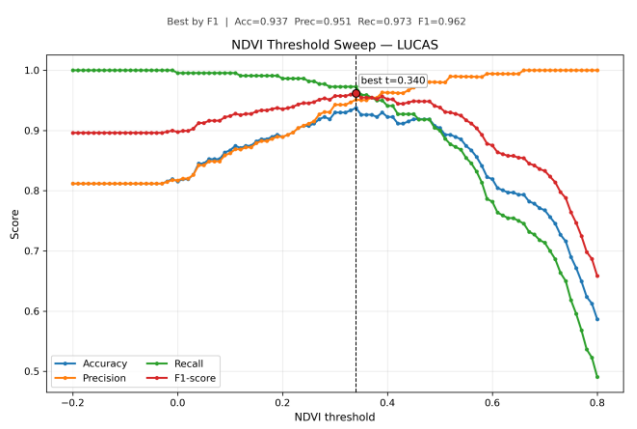


Figure 4.104 NDVI threshold sweep (LUCAS 2022) showing Accuracy, Precision, Recall, and F1 versus threshold in Google Earth Engine.

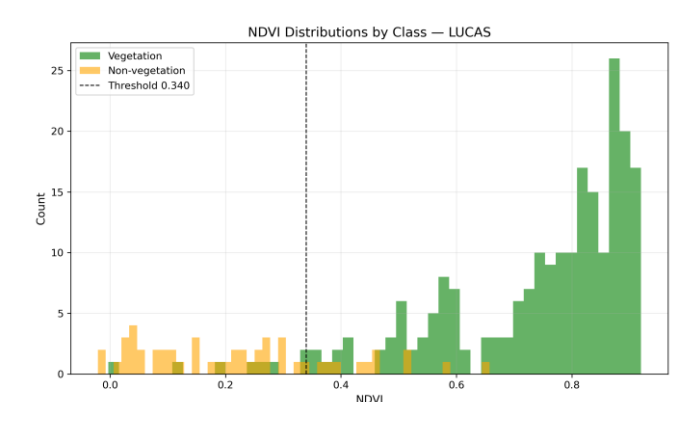


Figure 4.105 NDVI distributions by class (vegetation and non-vegetation) with optimal threshold overlay (t = 0.340) for LUCAS 2022, Google Earth Engine.

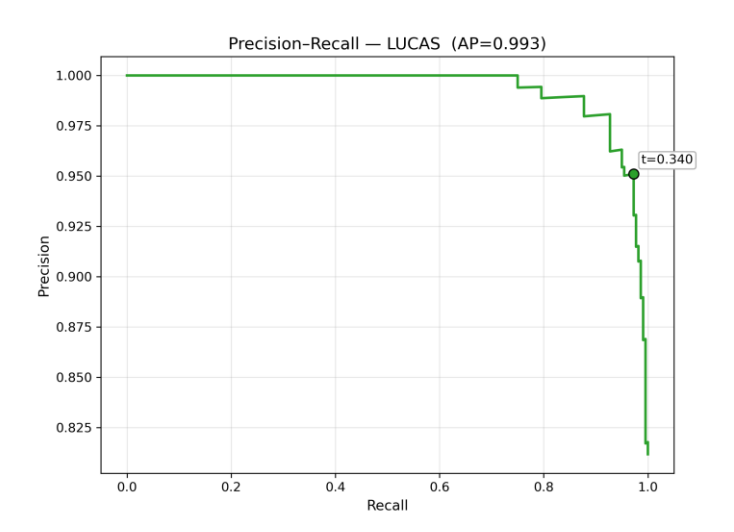


Figure 4.106 Precision—Recall curve for NDVI classification (LUCAS 2022) in Google Earth Engine (AP = 0.993).

Comparable outcomes were found for Sentinel Hub, where the ideal threshold was reached at t = 0.35, resulting in F1 = 0.90, accuracy = 0.85, and Cohen's Kappa (κ) \approx 0.70 (Figures 186–188). Although there were slight variations in local reflectance due to the platform's adaptive mosaicking and cloud-masking algorithms, the same general threshold range (0.34–0.35) was determined to be ideal. When compared to in-situ observations, the performance curves demonstrated a consistent precision—recall balance across adjacent threshold

values, suggesting that NDVI-based vegetation classification is resilient to slight threshold variations.

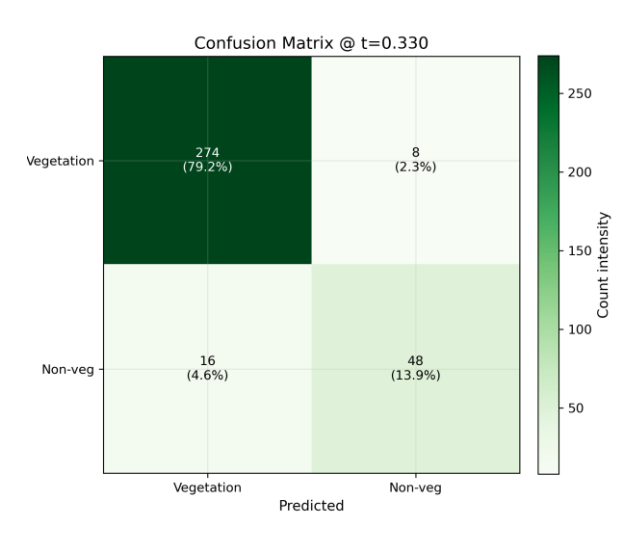


Figure 4.107 Confusion matrix at the optimal NDVI threshold (t = 0.330), Sentinel Hub

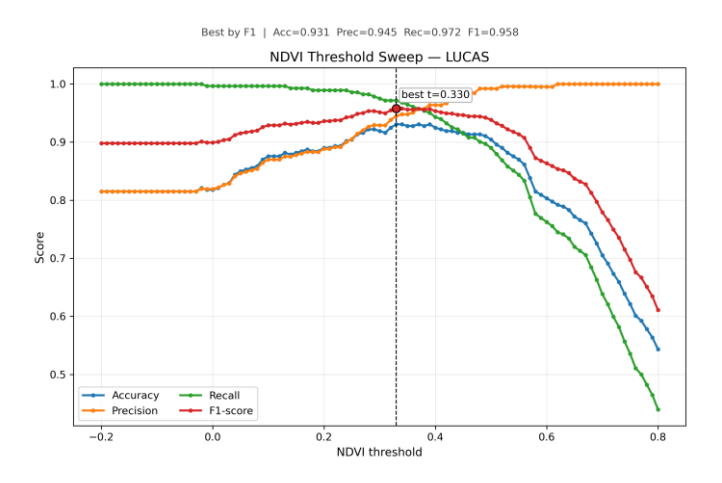


Figure 4.108 NDVI threshold sweep (LUCAS 2022) showing Accuracy, Precision, Recall, and F1 versus threshold in Sentinel Hub.

The outcomes on both platforms show that the CORINE-based value ($\approx 0.38-0.39$) found in Section 4.5 is marginally higher than the LUCAS-derived optimal threshold ($\approx 0.34-0.35$). The higher accuracy of field-based LUCAS data, which more accurately depicts fine-scale vegetation structures and heterogeneous

transitional land-cover areas that typically exhibit lower NDVI values, is probably the cause of this discrepancy. High F1-scores (\geq 0.90) and Kappa values (> 0.65), when calibrated with LUCAS, confirm the strong reliability of NDVI thresholding, thereby confirming its suitability for large-scale alpine ecosystem assessment and pixel-level vegetation monitoring.

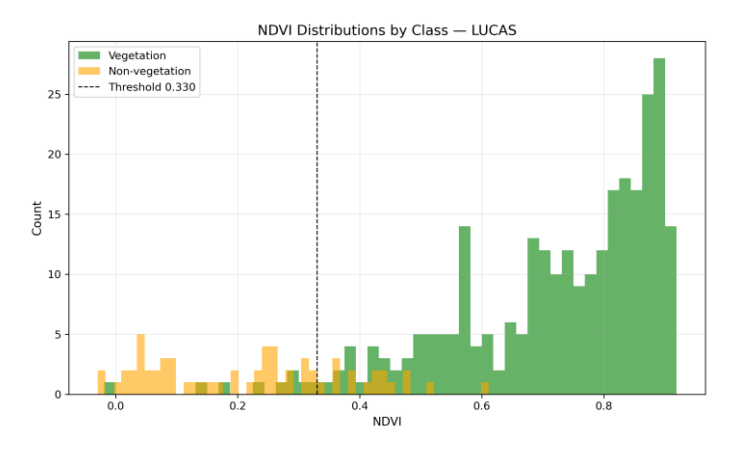


Figure 4.109 NDVI distributions by class (vegetation and non-vegetation) with optimal threshold overlay (t = 0.330) for LUCAS 2022, Sentinel Hub.

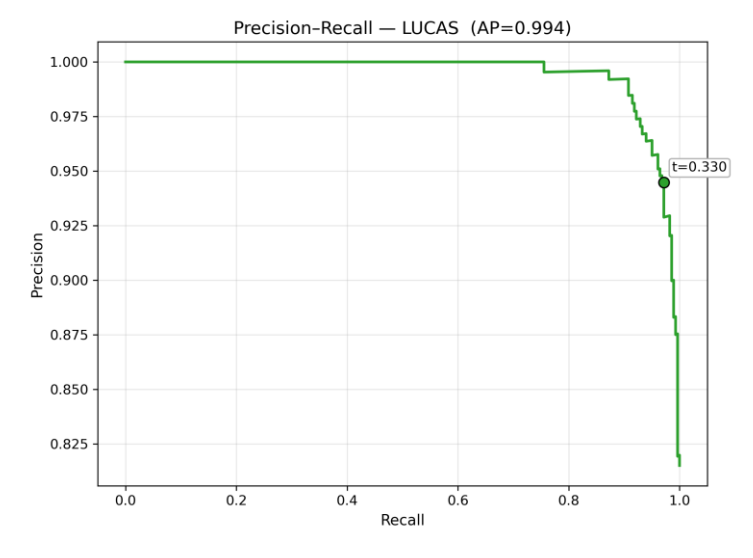


Figure 4.110 Precision—Recall curve for NDVI classification
(LUCAS 2022) in Sentinel Hub

4.9 Validation of NDVI (2018) with Carta degli Habitat

The ecological consistency of the NDVI-based vegetation classification was assessed using the *Carta degli Habitat* (CdH) dataset, which served as an additional ecological reference layer. The CdH framework offers comprehensive thematic mapping of natural and semi-natural habitats throughout Italy and was created in accordance with the EU Habitats Directive and the Natura 2000 network (Pesaresi et al., 2020; Čahojová et al., 2022). The CdH dataset is highly appropriate for evaluating the correspondence between NDVI classifications and actual habitat distributions in complex alpine landscapes because it places an emphasis on ecological habitat types, in contrast to CORINE and LUCAS, which are primarily concerned with land cover.

Two broad categories representing vegetated and non-vegetated habitats were used to reclassify the CdH polygons found in the Maritime Alps. The "non-vegetation" group consisted of bare rocks, scree slopes, and man-made surfaces, whereas the "vegetation" group included forest, shrubland, grassland, and alpine herbaceous formations. Using a conditional rule based on habitat codes, this reclassification was applied in QGIS via the Field Calculator. To ensure proportional representation of both habitat types, a stratified random sample of 1,000 points was generated within the Area of Interest (AOI). For every sampled location, NDVI binary values were taken from the Sentinel Hub and Google Earth Engine (GEE) rasters, connecting the predicted vegetation classes to the associated CdH habitat characteristics.

Validation followed the same workflow adopted in previous sections (Sections 4.4–4.7), using confusion matrices and accuracy indices Overall Accuracy (OA), Producer's Accuracy (PA), User's Accuracy (UA), and Cohen's Kappa (κ) to quantify the agreement between NDVI-based classifications and CdH reference data. The resulting accuracy metrics derived from the CdH reference are summarized in Tables 4.11–4.12 and visualized in Figure 4.113. For GEE, the fixed threshold (NDVI \geq 0.30) achieved an OA of 0.79 and $\kappa \approx$ 0.54, while the Otsu adaptive threshold produced slightly higher precision but lower recall, with OA \approx 0.77 and $\kappa \approx$ 0.52. These results are consistent with previous validations, confirming that both thresholding approaches effectively distinguish vegetation from non-vegetation within the alpine habitat context.

Threshold Method	UA (non-Veg)	UA (Veg)	PA (non-Veg)	PA (Veg)	Overall Accuracy (OA)	Kappa (k)
Otsu (0.47)	82.3	6.6	39.2	33.8	38.3	-0.097
Fixed (0.30)	81.6	8.7	24.9	55.9	28.4	-0.057

Table 4.11 Accuracy assessment of NDVI 2018 (Carta degli Habitat) below Otsu and Fixed thresholds for Google Earth Engine

Threshold Method	Accuracy	Precision	Recall	F1 Score
Otsu (0.47)	38.6	6.6	33.8	0.111
Fixed (0.30)	28.4	8.7	55.9	0.150

Table 4.12 Classification metrics (Accuracy, Precision, Recall, F1 Score) for NDVI 2018 (Carta degli Habitat) below Otsu and Fixed thresholds in Google Earth Engine.

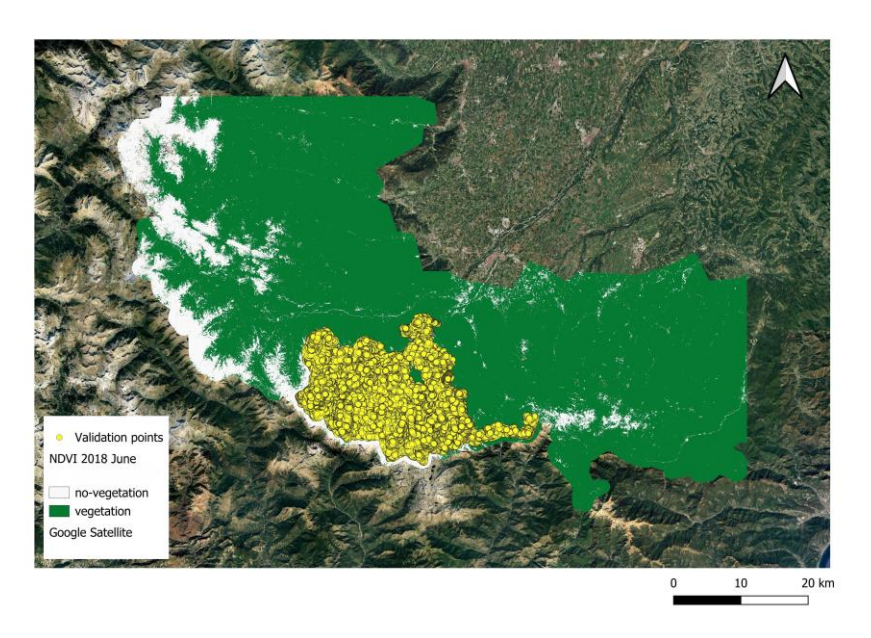


Figure 4.111 Validation points used for NDVI 2018

110

Corresponding validation results from Sentinel Hub imagery are presented in Tables 4.13–4.14 and Figure 4. 112.Comparable outcomes were achieved for Sentinel Hub with OA \approx 0.78–0.80 and κ \approx 0.55–0.57. Once more, the Otsu threshold better captured the subtle differences at the ecotone between vegetated and rocky surfaces, whereas the fixed threshold tended to slightly overestimate vegetation cover in mosaic or sparsely vegetated areas. According to the confusion matrices, misclassifications mostly happened in transitional habitats where mixed spectral signatures result in NDVI values close to the threshold limit, such as alpine meadows with exposed soil or patchy vegetation. However, the spatial outputs from both platforms were highly consistent, indicating that the derived NDVI maps are in good agreement with vegetation patterns that are ecologically significant.

Threshold Method	UA (non-Veg)	UA (Veg)	PA (non-Veg)	PA (Veg)	Overall Accuracy (OA)	Kappa (k)
Otsu (0.47)	37.8	32.3	37.8	32.3	37.1	0.104
Fixed (0.30)	23.7	58.2	23.7	58.2	27.6	0.154

Table 4.13 Accuracy assessment of NDVI 2018 (Carta degli Habitat) below Otsu and Fixed thresholds for Sentinel Hub.

Threshold Method	Accuracy	Precision	Recall	F1 Score
Otsu (0.47)	37.1	6.20	32.3	0.104
Fixed (0.30)	27.6	8.86	58.2	0.154

Table 4.14 Classification metrics (Accuracy, Precision, Recall, F1 Score) for NDVI 2018 (Carta degli Habitat) below Otsu and Fixed thresholds in Sentinel Hub.

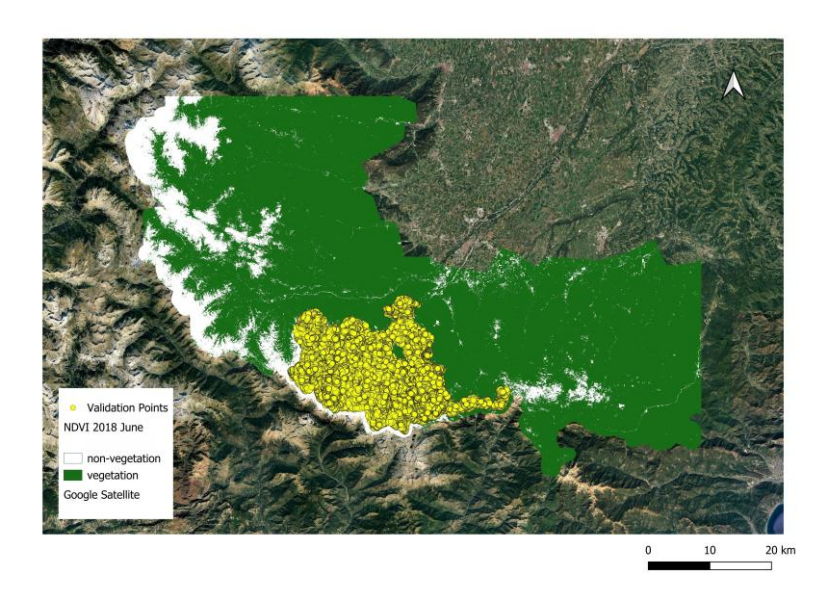


Figure 4.112 Validation points used for NDVI 2018 Carta degli Habitat

data

Overall, the CdH-based validation confirms the robustness and transferability of the NDVI classification across different ecological datasets. The methodology's reproducibility across platforms and scales is evident from the high agreement between GEE and Sentinel Hub outputs, both yielding comparable accuracy and Kappa values. The NDVI is a useful indicator for alpine ecological monitoring and conservation applications because it can identify not only the general presence of vegetation but also the approximate composition and structure of habitats, as demonstrated by the CdH validation. The NDVI validation framework is completed by these results, which also serve as a strong basis for the NDSI-based snow cover analysis that follows in Section 4.10.

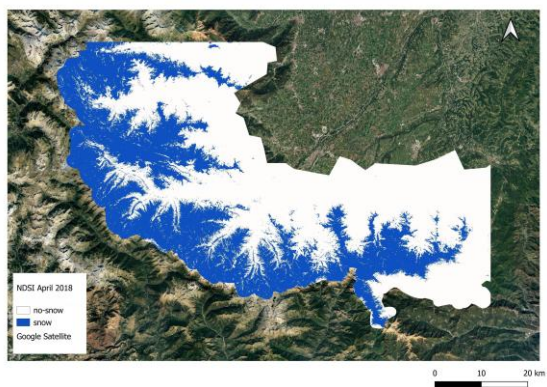
4.10 NDSI Dynamics from Google Earth Engine

Following the vegetation analysis, the third part of this research examined snow-cover dynamics using the Normalized Difference Snow Index (NDSI) derived from Sentinel-2 imagery in Google Earth Engine (GEE). Monthly composites for April and June were generated, including only scenes with less than 15 % cloud cover to minimize atmospheric interference.

Two thresholding approaches were applied to detect snow pixels. The fixed threshold method classified values NDSI ≥ 0.42 as snow (Hall et al., 1995; Dozier, 1989), while the Otsu adaptive method determined an optimal cut-off by maximizing between-class variance (Otsu, 1979).

These methods produced snow/no-snow binary masks for each month, enabling the assessment of seasonal and inter-annual snow persistence. Results indicate that April composites captured peak winter accumulation and extensive snow cover at mid- and high-elevation zones, whereas June composites revealed substantial snowpack retreat following melt onset. Differences between fixed and adaptive thresholds mainly affected transitional zones, where partial snow cover or mixed pixels occurred.

The dual-threshold framework therefore provided a consistent basis for monitoring temporal snow-cover variability and for comparing the performance of static and data-driven thresholding. This approach supports subsequent accuracy evaluation (Section 4.9) using external reference datasets such as the Copernicus FSC product and random-point validation, in line with established cryosphere remote-sensing standards (Gascoin et al., 2019; Dumont et al., 2020).



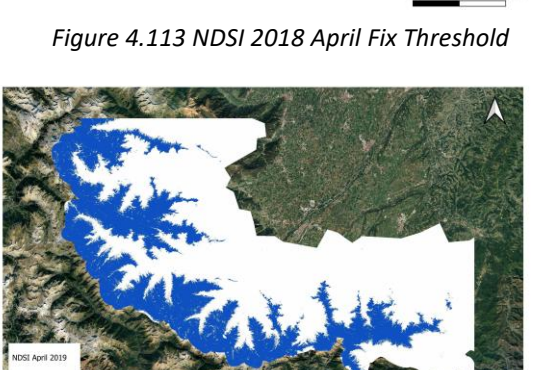


Figure 4.115 NDSI 2019 April Fix Threshold

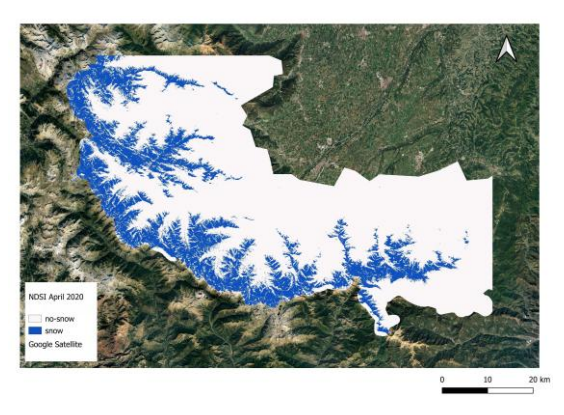


Figure 4.117 NDSI 2020 April Fix Threshold

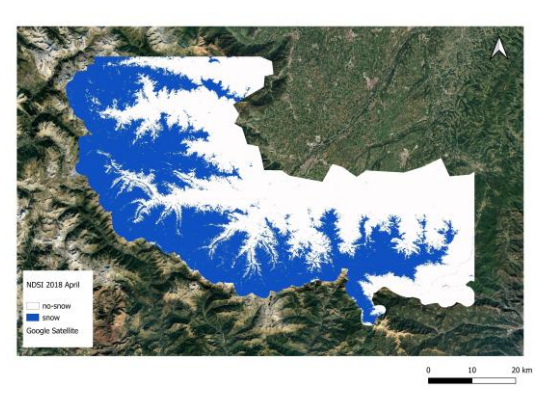


Figure 4.114 NDSI 2018 April Otsu Threshold

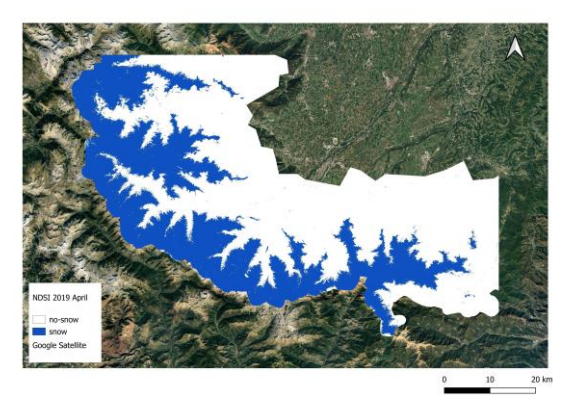


Figure 4.116 NDSI 2019 April Otsu Threshold

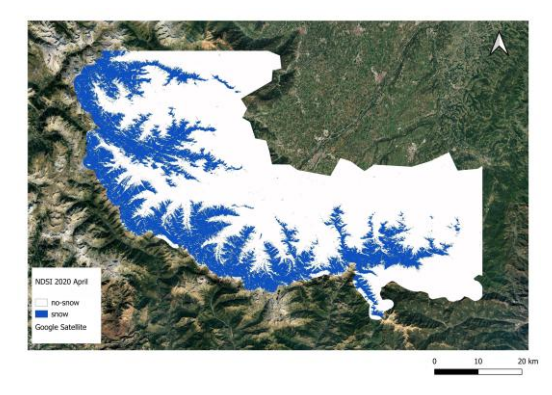


Figure 4.118 NDSI 2020 April Otsu Threshold

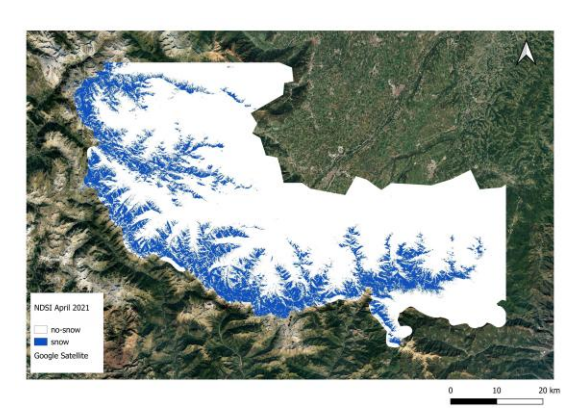


Figure 4.119 NDSI 2021 April Fix Threshold

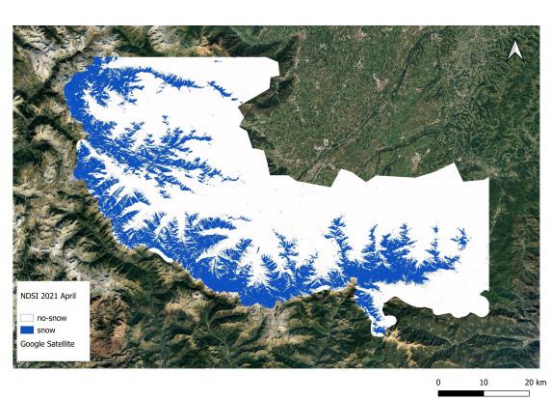


Figure 4.120 NDSI 2021 April Otsu Threshold

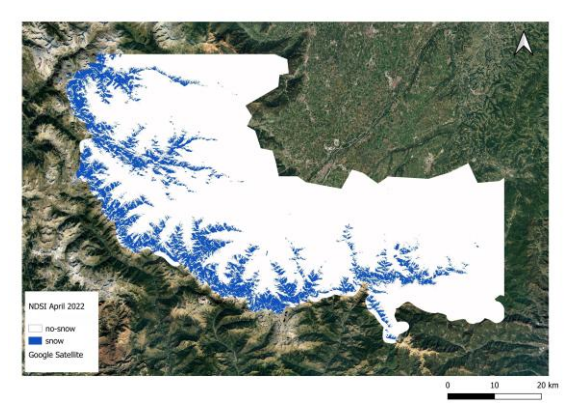


Figure 4.121 NDSI 2022 April Fix Threshold

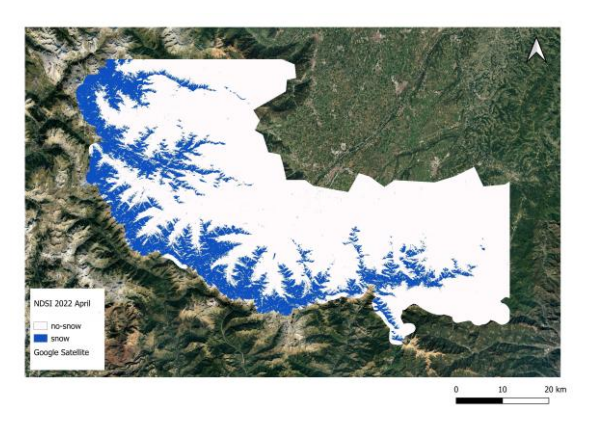


Figure 4.122 NDSI 2022 April Otsu Threshold

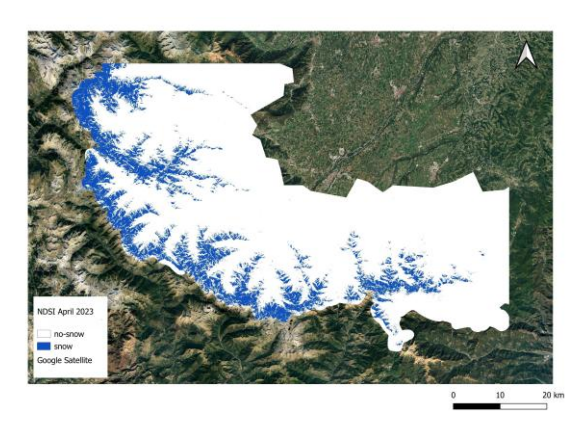


Figure 34.123 NDSI 2023 April Fix Threshold

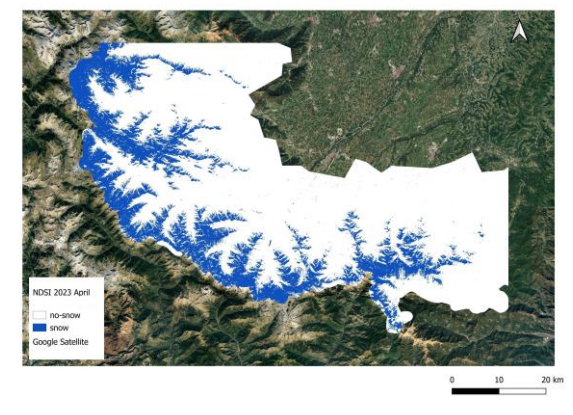


Figure 4.124 NDSI 2023 April Otsu Threshold

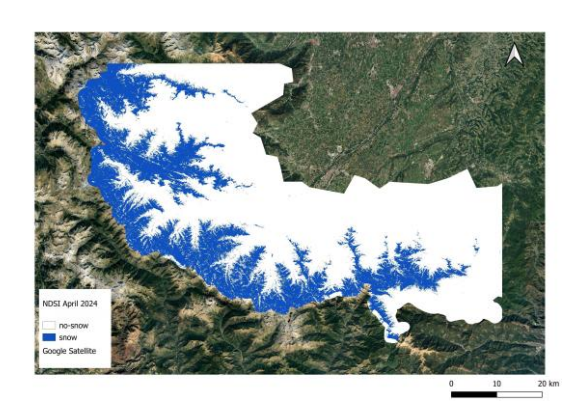


Figure 4.125 NDSI 2024 April Fix Threshold

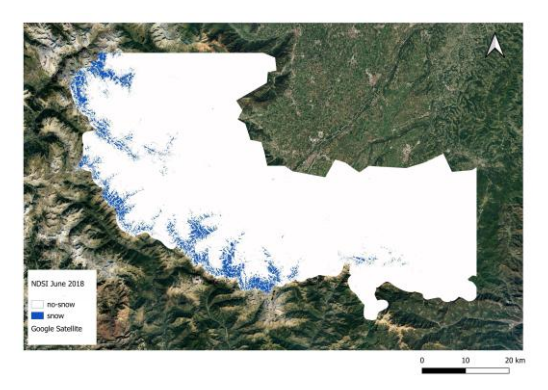


Figure 4.127 NDSI 2018 June Fix Threshold

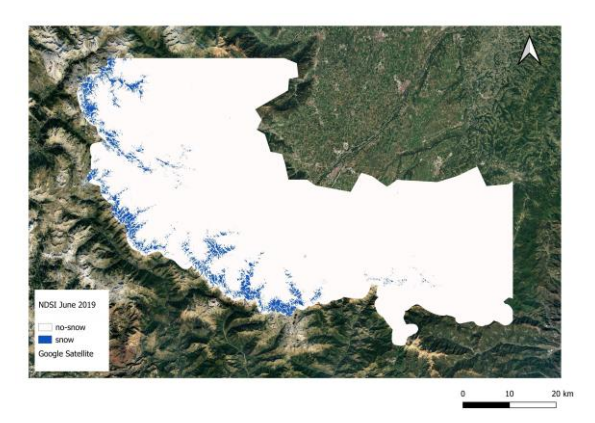


Figure 4.129 NDSI 2019 June Fix Threshold

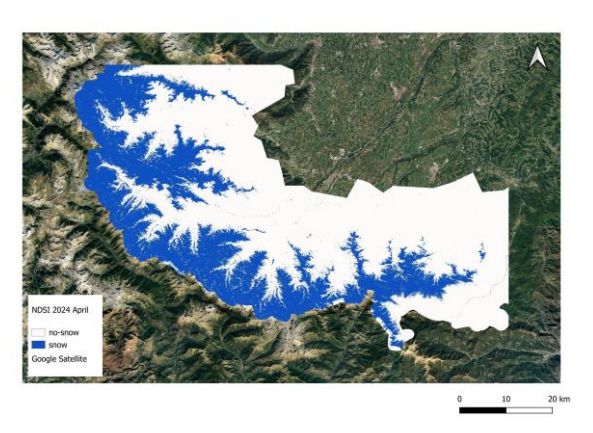


Figure 4.126 NDSI 2024 April Otsu Threshold

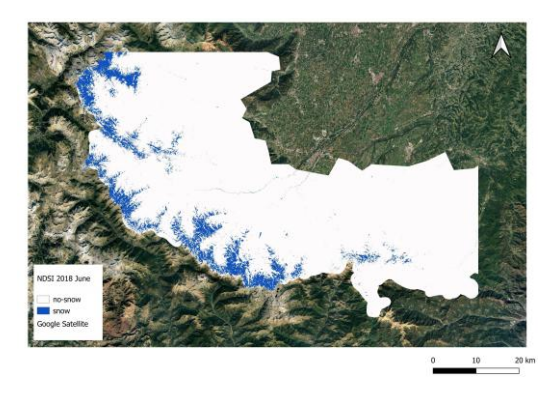


Figure 4.128 NDSI 2018 June Otsu Threshold

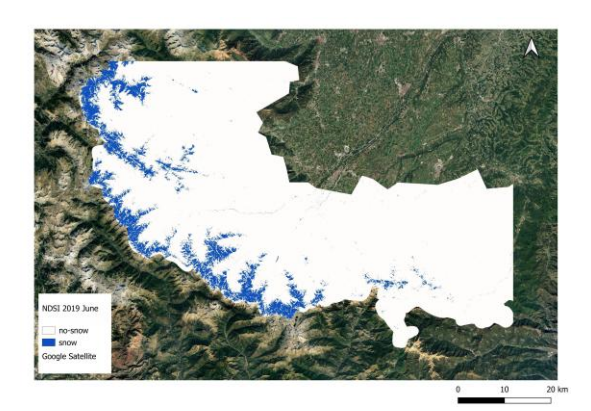


Figure 4.130 NDSI 2019 June Otsu Threshold



Figure 4.131 NDSI 2020 June Fix Threshold

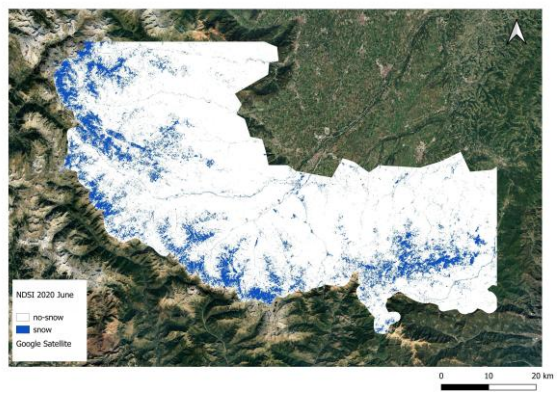


Figure 4.132 NDSI 2020 June Otsu Threshold

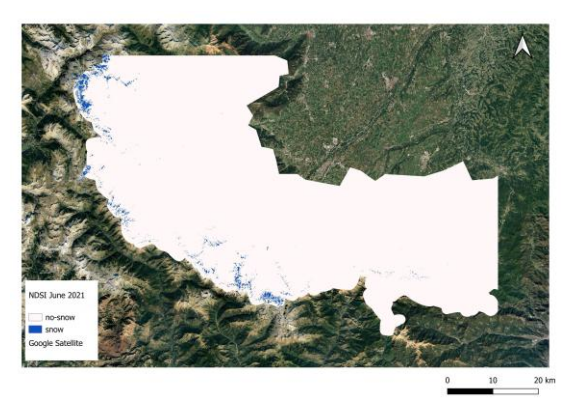


Figure 4.133 NDSI 2021 June Fix Threshold

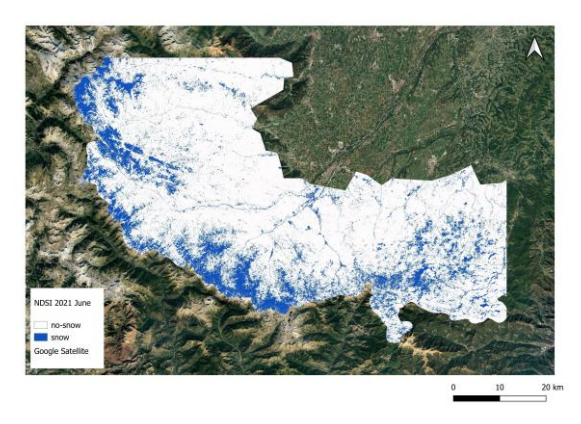


Figure 4.134 NDSI 2021 June Otsu Threshold

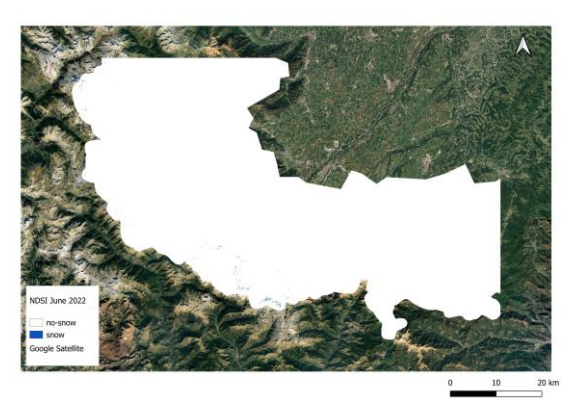


Figure 4.135 NDSI 2022 June Fix Threshold

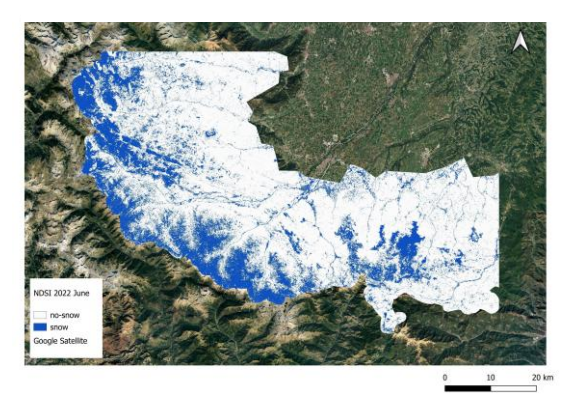


Figure 4.136 NDSI 2022 June Otsu Threshold

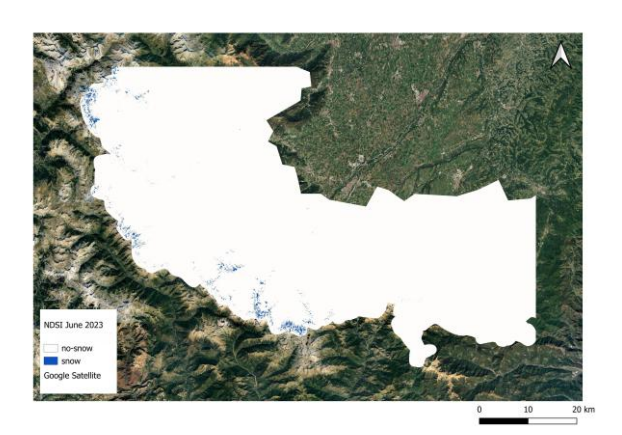


Figure 4.137 NDSI 2023 June Fix Threshold



Figure 4.139 NDSI 2024 June Fix Threshold

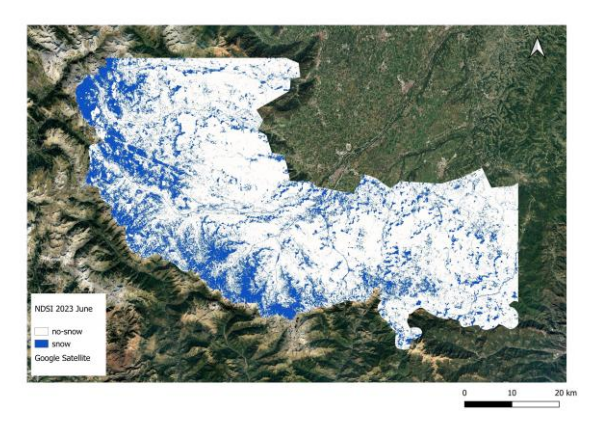


Figure 4.138 NDSI 2023 June Otsu Threshold

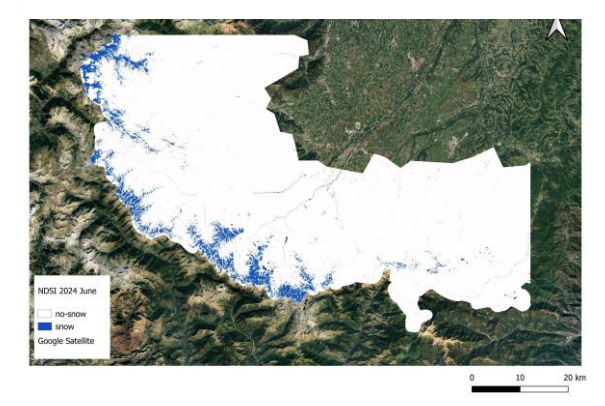
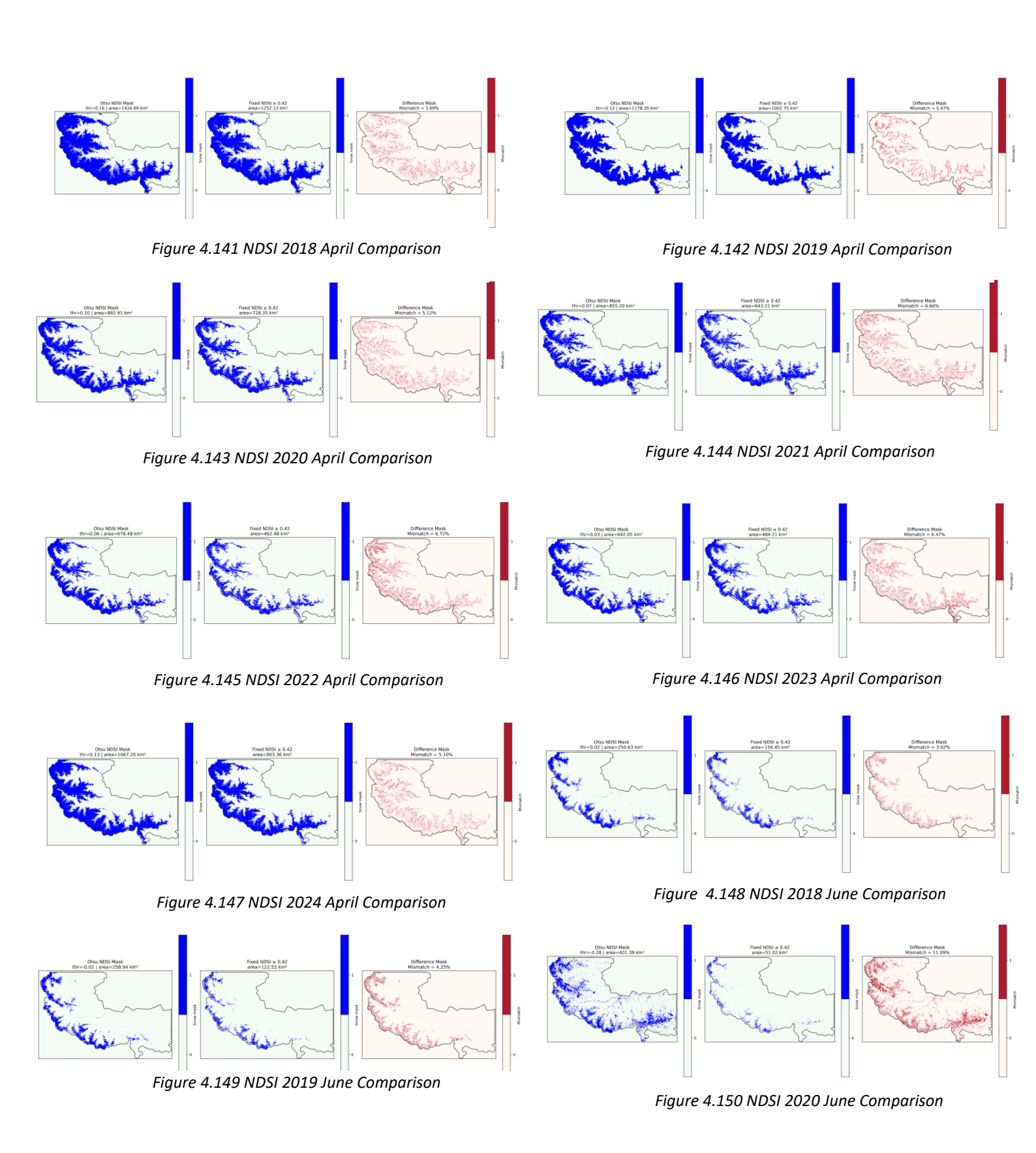


Figure 4.140 NDSI 2024 June Otsu Threshold



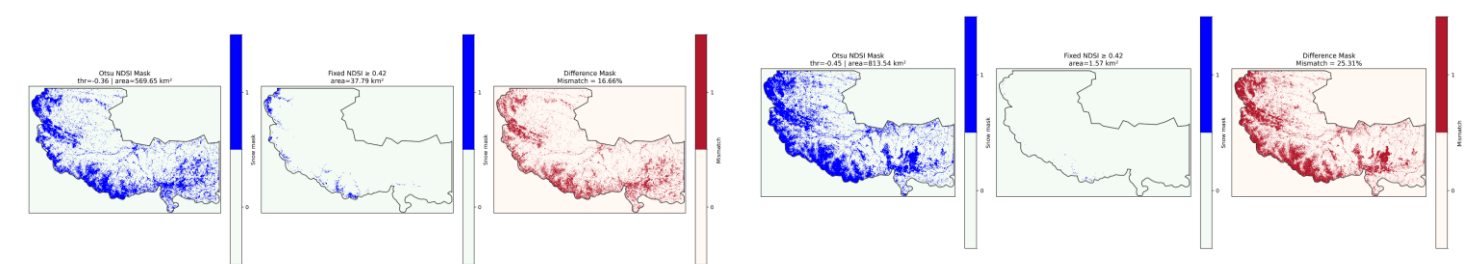


Figure 4.151 NDSI 2021 June Comparison

Figure 4.152 NDSI 2022 June Comparison

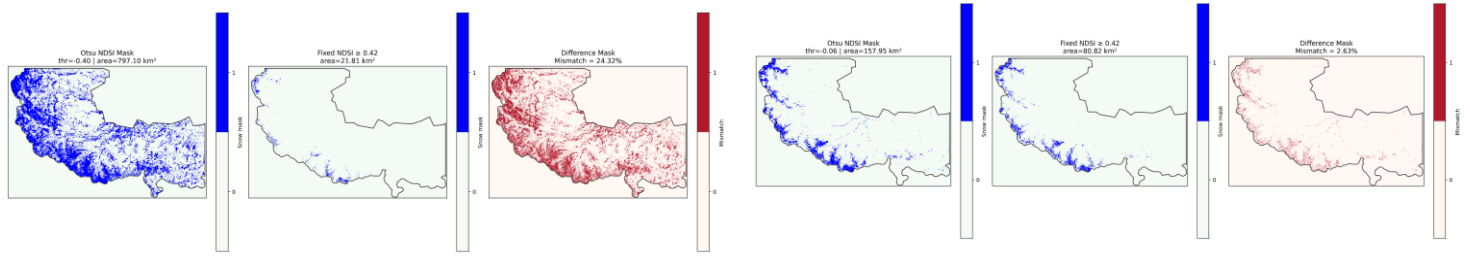


Figure 4.153 NDSI 2023 June Comparison

Figure 4.154 NDSI 2024 June Comparison

PLATFORM	YEAR	MONTH	OTSU THRESHOLD VALUE(NDSI)	Snow COVER AREA(Km^2) OTSU THRESHOLD	Snow COVER AREA(Km^2) THRESHOLD >0.42	Difference Mask Mismatch %
Earth Engine	2018	April	0.16	1434.69	1252.13	5.69
Earth Engine	2018	June	0.02	250.63	154.45	3.02
Earth Engine	2019	April	0.12	1178.35	1002.75	5.47
Earth Engine	2019	June	<mark>-0.02</mark>	258.94	122.55	4.25
Earth Engine	2020	April	0.10	892.91	728.35	5.12
Earth Engine	2020	June	<mark>-0.28</mark>	401.39	51.02	11.09
Earth Engine	2021	April	0.07	855.20	643.21	6.66
Earth Engine	2021	June	<mark>-0.36</mark>	569.65	37.79	16.66
Earth Engine	2022	April	0.06	678.48	462.48	6.72
Earth Engine	2022	June	<mark>-0.45</mark>	813.54	1.57	25.31
Earth Engine	2023	April	0.03	692.05	484.21	6.47
Earth Engine	2023	June	<mark>-0.40</mark>	797.10	21.81	24.32
Earth Engine	2024	April	0.13	1067.20	903.36	5.10
Earth Engine	2024	June	<mark>-0.06</mark>	157.95	80.82	2.63

Table 4.15 Summary of NDSI classification results obtained from Google Earth Engine for April and June (2018–2024)

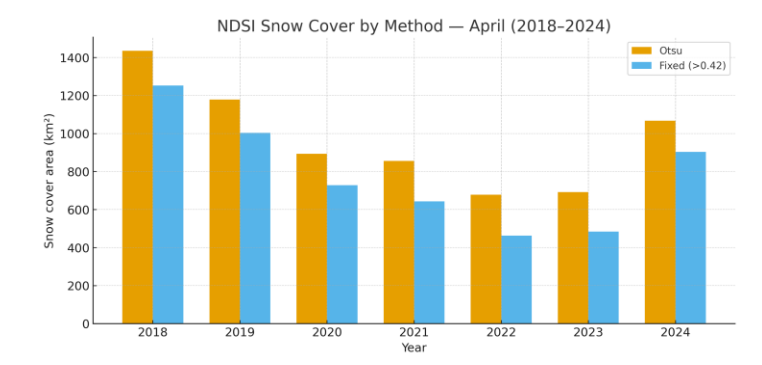


Figure 4.155 GEE NDSI snow cover (km²) by method (Otsu vs fixed >0.42), April 2018–2024.

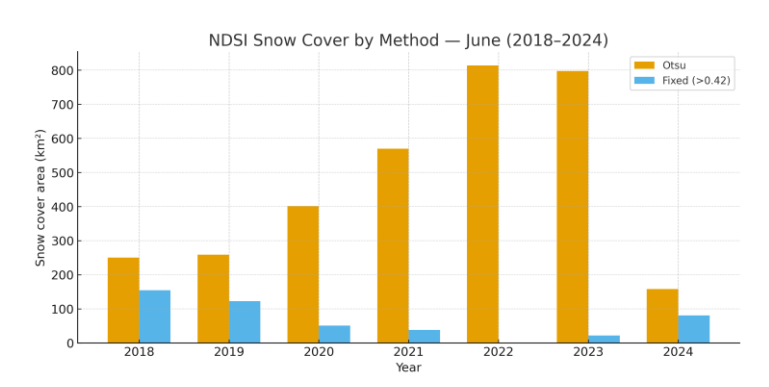


Figure 4.156 GEE NDSI snow cover (km²) by method (Otsu vs fixed >0.42), 2018–2024.

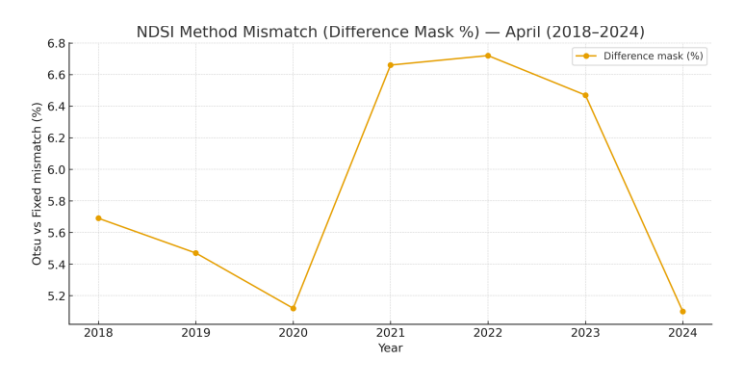


Figure 4.157 Otsu vs Fixed difference mask (%) for April (2018–2024).

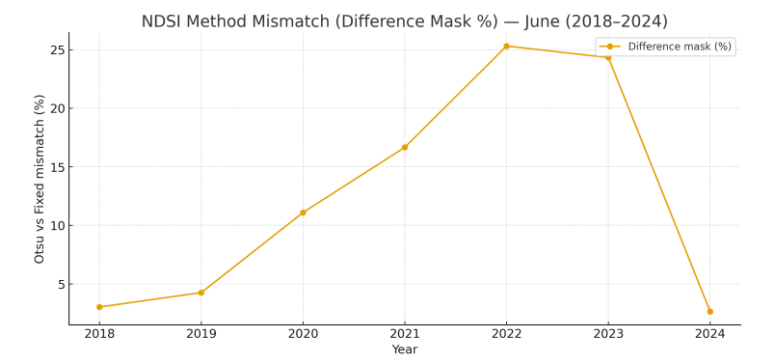


Figure 4.158 Otsu vs Fixed difference mask (%) for June (2018–2024).

Snow-cover variability in the Maritime Alps from 2018 to 2024 was examined using Google Earth Engine (GEE) and the Normalized Difference Snow Index (NDSI), which is based on Sentinel-2 Level-2A reflectance imagery. To reduce atmospheric interference and guarantee spectral consistency, monthly composites for April and June were created, removing scenes with more than 15% cloud cover. To identify regions covered by snow, two thresholding strategies were used: an adaptive Otsu method (Otsu, 1979) that uses histogram variance analysis to maximize the separation between snow and non-snow pixels, and a fixed threshold (NDSI ≥ 0.42) based on (Hall et al. 1995) and (Dozier, 1989).

Different seasonal and inter-annual patterns can be seen in the resulting binary snow/no-snow maps (Figures 4.141–4.154, Table 4.15). From 0.16 (2018) to -0.45 (2022), the Otsu thresholds varied significantly, reflecting spectral variations related to surface moisture, illumination, and snow albedo. Especially in transitional and late-season conditions where mixed pixels of snow, rock, and vegetation predominate, the Otsu method consistently produced larger snow-covered areas than the fixed 0.42 threshold. While the fixed threshold produced somewhat lower estimates ($\approx 1.252 \text{ km}^2$ and 462 km^2 , respectively), the adaptive approach produced snow-covered extents that ranged from $\approx 1.435 \text{ km}^2$ (2018) to $\approx 678 \text{ km}^2$ (2022).

Despite these variations, there was a high degree of agreement between the two approaches; in April 2022, mask-mismatch percentages were typically less than 7%, but in June 2022, they increased to more than 25%.

Adaptive thresholding is crucial for precise snow detection because these disparities correlate to late-season conditions when bright rock surfaces and low-albedo wet snow produce overlapping spectral responses. The fixed threshold provided temporal stability for long-term monitoring, and the Otsu method successfully captured remaining snow patches in glacial basins and shaded slopes.

The inter-annual trend shows a significant decline in snowpack after 2020, which is consistent with the region's noted warming of the climate. Snow duration at mid-elevations is gradually decreasing, as evidenced by earlier melt onset and reduced June snow extent (e.g., 157 km² in 2024). On the other hand, 2018 a year marked by extended cold and significant winter accumulation saw the greatest amount of snow cover.

All things considered, the GEE-based analysis demonstrates that a thorough evaluation of snow persistence in alpine settings can be obtained by combining fixed and adaptive thresholds. Adaptive thresholds more accurately capture short-term variability caused by variations in elevation, slope, and surface reflectance, whereas fixed thresholds preserve consistency for trend analysis. These findings support earlier alpine cryosphere research (Gascoin et al., 2019; Marty et al., 2017; Kotlarski et al., 2022) and offer a solid foundation for the cross-platform comparison with Sentinel Hub that follows.

4.11 NDSI Dynamics from Sentinel Hub

The Sentinel Hub environment supported the GEE-based analysis through its EO Browser and API framework which delivered Sentinel-2 Level-2A surface reflectance data. The system produced April and June composites from data with less than 15% cloud cover after applying built-in L2A processor atmospheric corrections for spectral consistency.

The snow detection process at Sentinel Hub used the same dual-threshold approach which GEE analysis employed:

The method used two thresholds to detect snow pixels according to Hall et al. (1995) and Dozier (1989) with NDSI values above 0.42 and an adaptive Otsu threshold (Otsu, 1979) that Sentinel Hub evalscripts used to maximize between-class variance in NDSI histogram values.

The ability to control cloud masking and view scenes individually through Sentinel Hub improved the consistency of results in areas with changing illumination and terrain shadows. The April composites showed extensive snow cover because of winter snow accumulation but June images displayed scattered snow patches in mountain basins and shaded slopes.

The Sentinel Hub results showed the same overall patterns as GEE but displayed minor spatial variations because of different atmospheric processing and pixel combination methods. The cloud and shadow masking techniques at Sentinel Hub resulted in slightly elevated April snow-cover measurements and reduced June snow-cover values. The comparison between platforms demonstrates why researchers need to validate their alpine cryospheric data across multiple platforms.

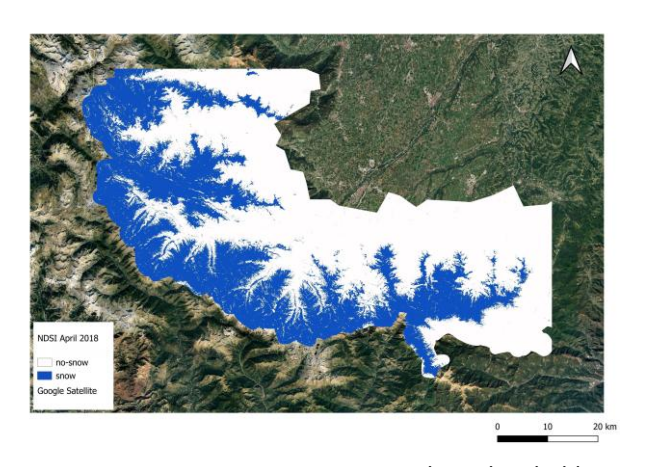


Figure 44.159 NDSI 2018 April Fix Threshold

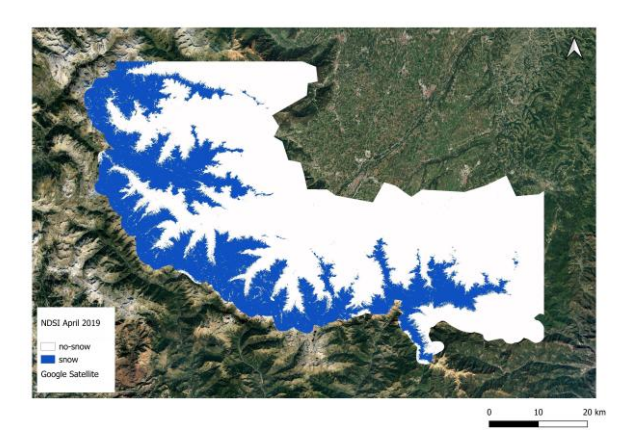


Figure 4.161 NDSI 2019 April Fix Threshold

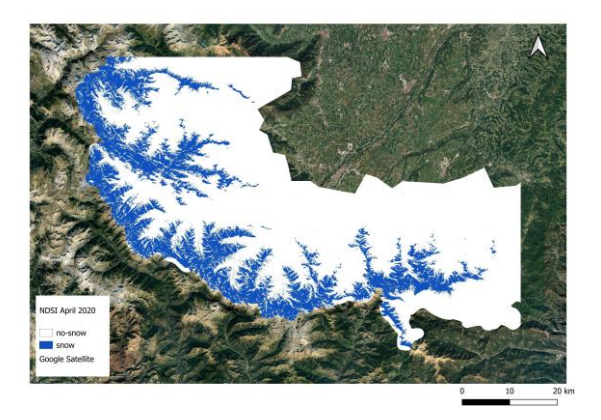


Figure 4.163 NDSI 2020 April Fix Threshold

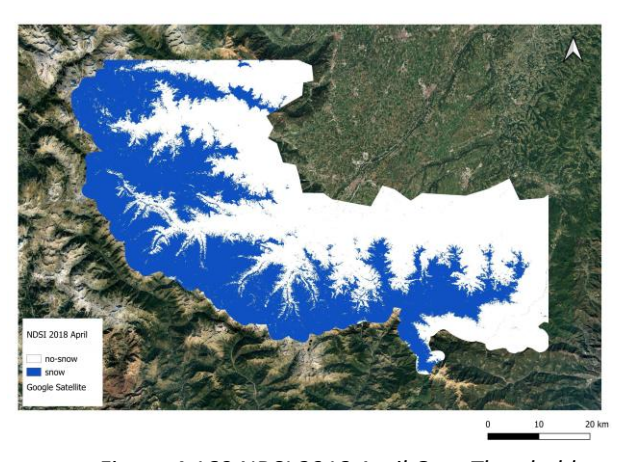


Figure 4.160 NDSI 2018 April Otsu Threshold

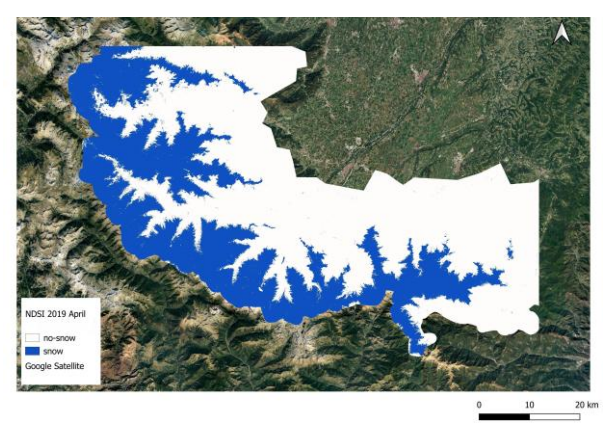


Figure 4.162 NDSI 2019 April Otsu Threshold

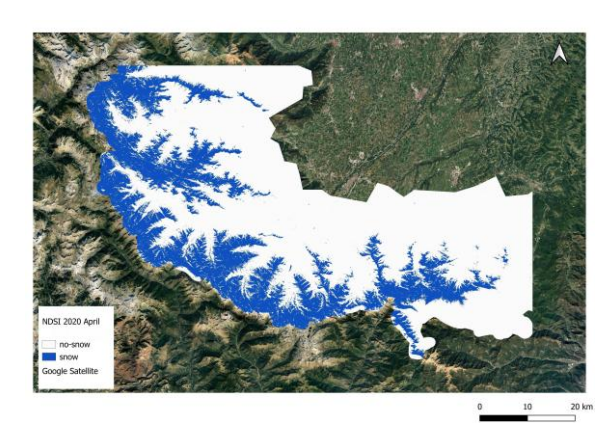


Figure 4.164 NDSI 2020 April Otsu Threshold

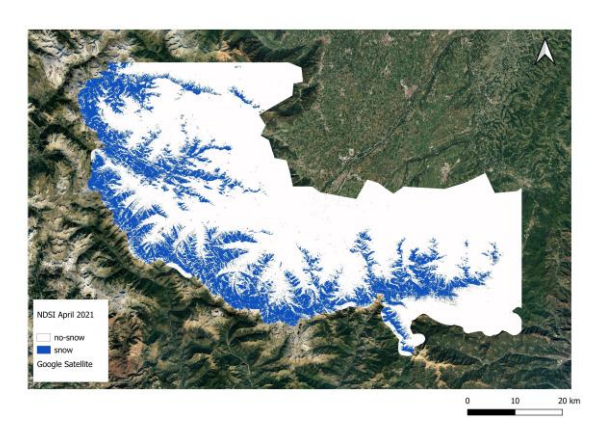


Figure 4.165 NDSI 2021 April Fix Threshold

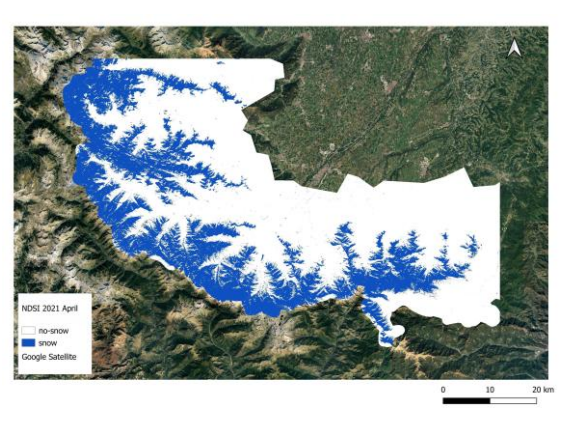


Figure 4.166 NDSI 2021 April Otsu Threshold

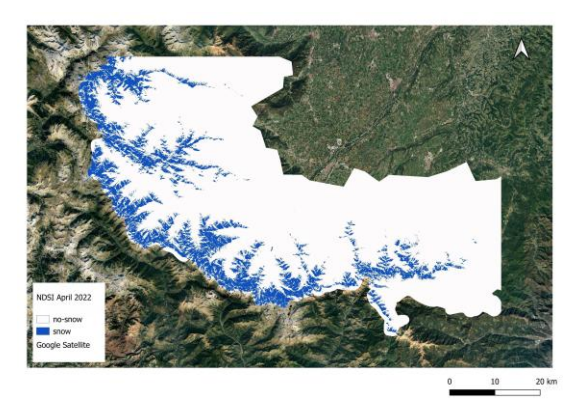


Figure 4.167 NDSI 2022 April Fix Threshold

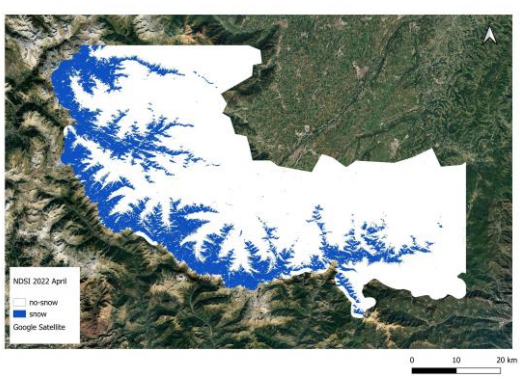


Figure 4.168 NDSI 2022 April Otsu Threshold

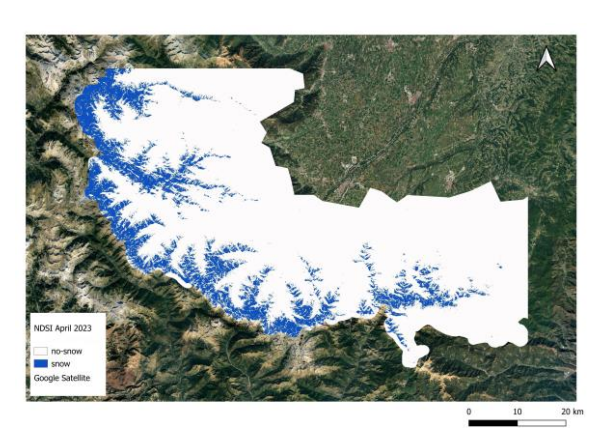


Figure 4.169 NDSI 2023 April Fix Threshold

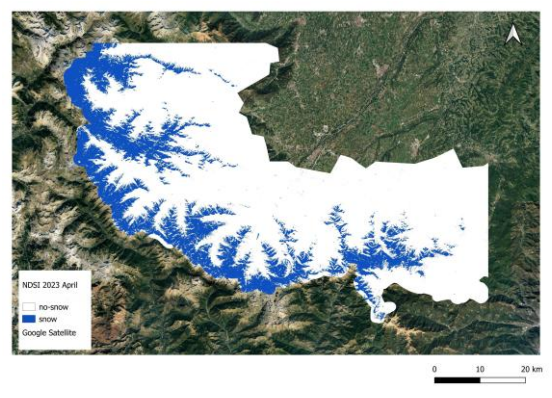


Figure 4.170 NDSI 2023 April Otsu Threshold

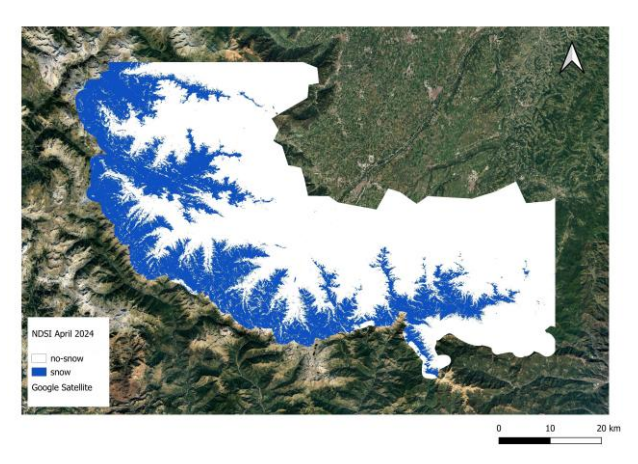


Figure 4.171 NDSI 2024 April Fix Threshold

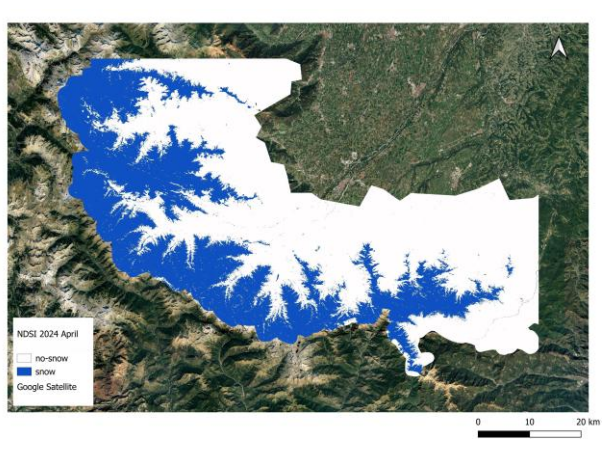


Figure 4.172 NDSI 2024 April Otsu Threshold

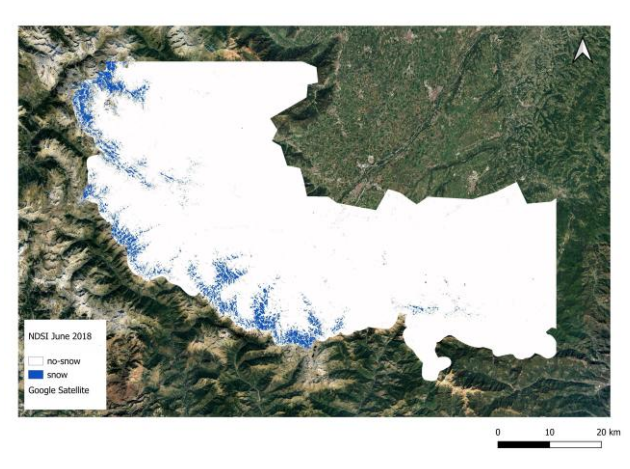


Figure 4.173 NDSI 2018 June Fix Threshold

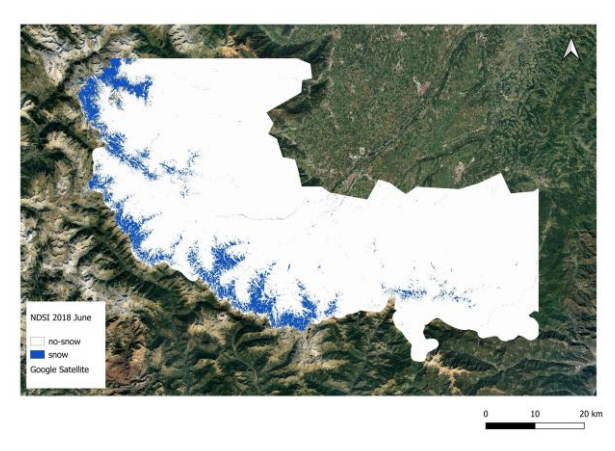


Figure 4.174 NDSI 2018 June Otsu Threshold

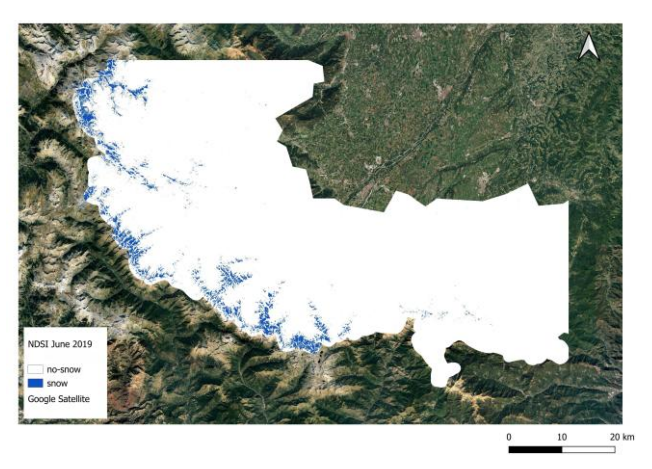


Figure 4.175 NDSI 2019 June Fix Threshold

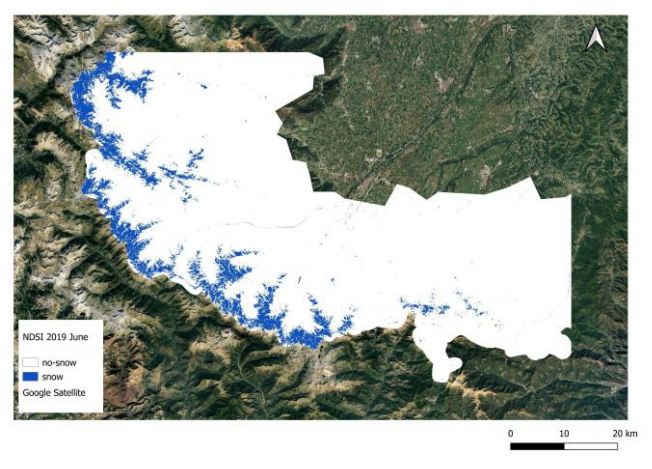


Figure 4.176 NDSI 2019 June Otsu Threshold

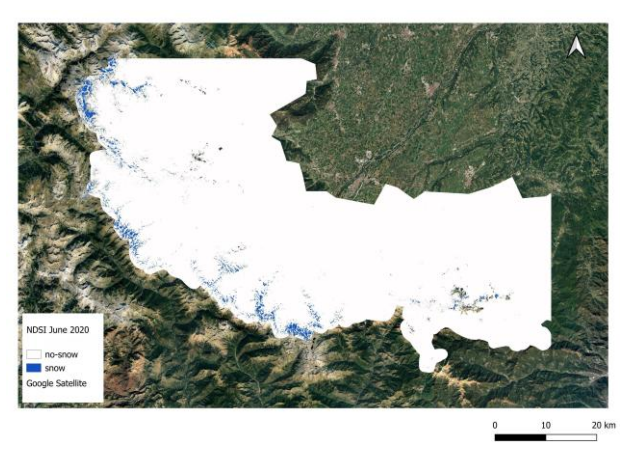


Figure 4.177 NDSI 2020 June Fix Threshold

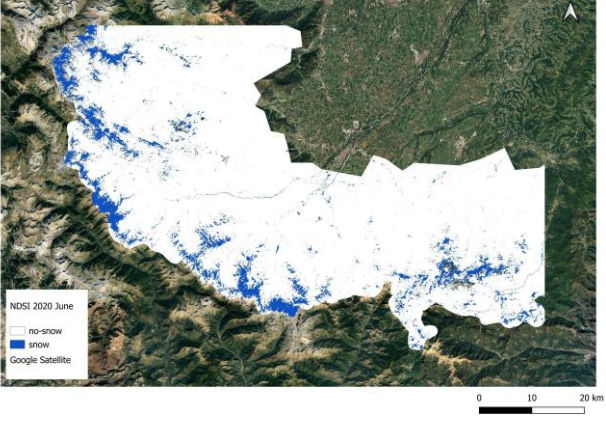


Figure 4.178 NDSI 2020 June Otsu Threshold

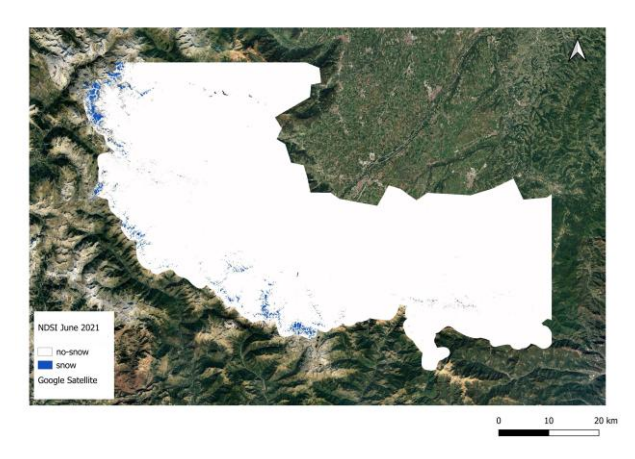


Figure 4.179 NDSI 2021 June Fix Threshold

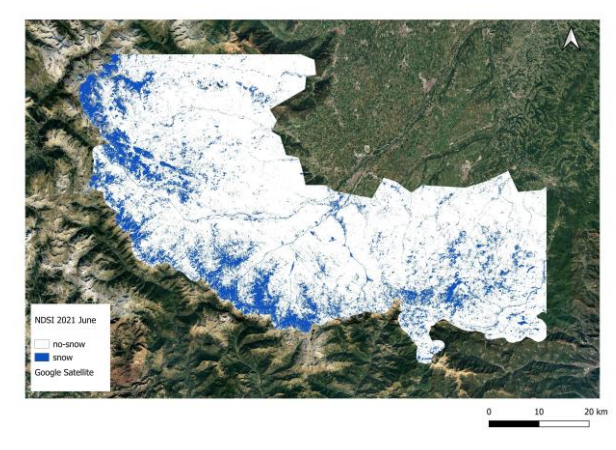


Figure 4.180 NDSI 2021 June Otsu Threshold

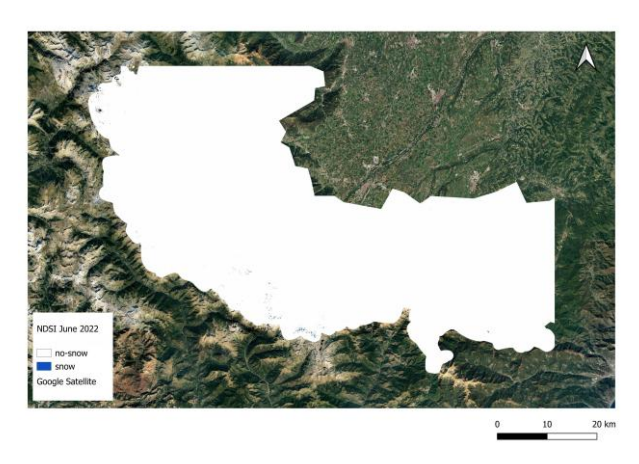


Figure 4.181 NDSI 2022 June Fix Threshold

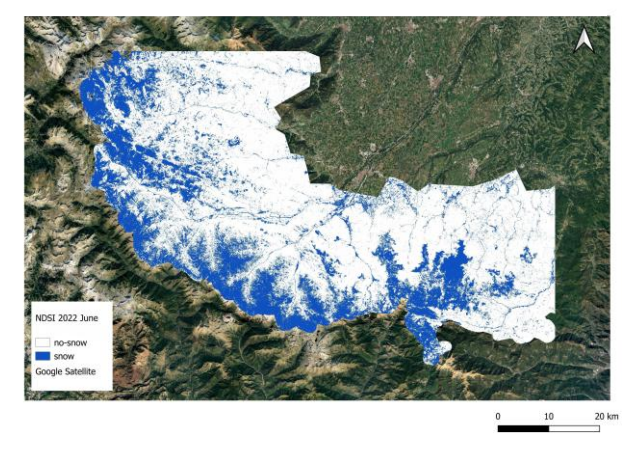


Figure 4.182 NDSI 2022 June Otsu Threshold

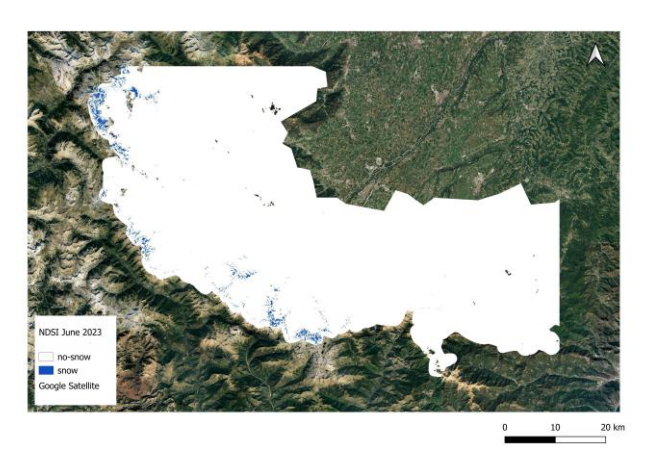


Figure 4.183 NDSI 2023 June Fix Threshold

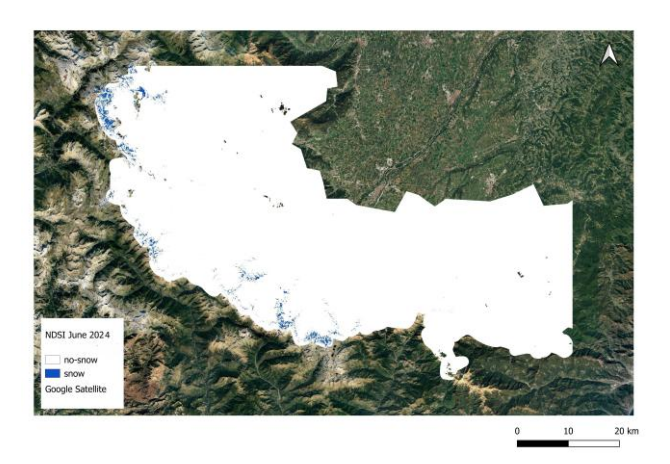


Figure 4.185 NDSI 2024 June Fix Threshold

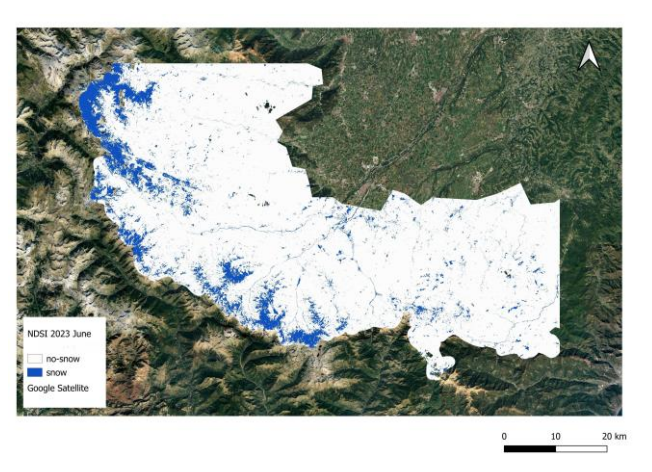


Figure 4.184 NDSI 2023 June Otsu Threshold

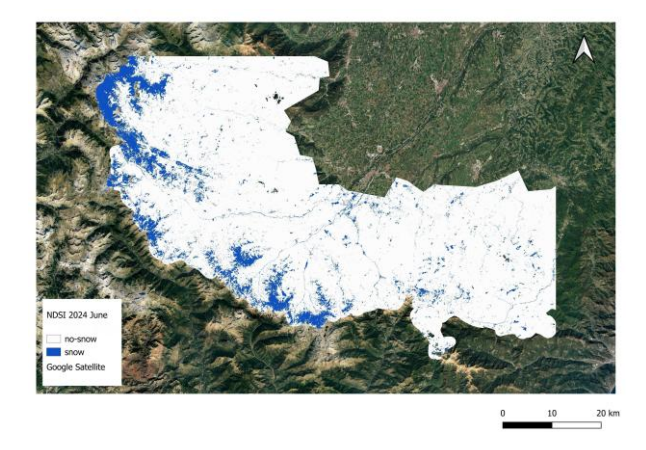
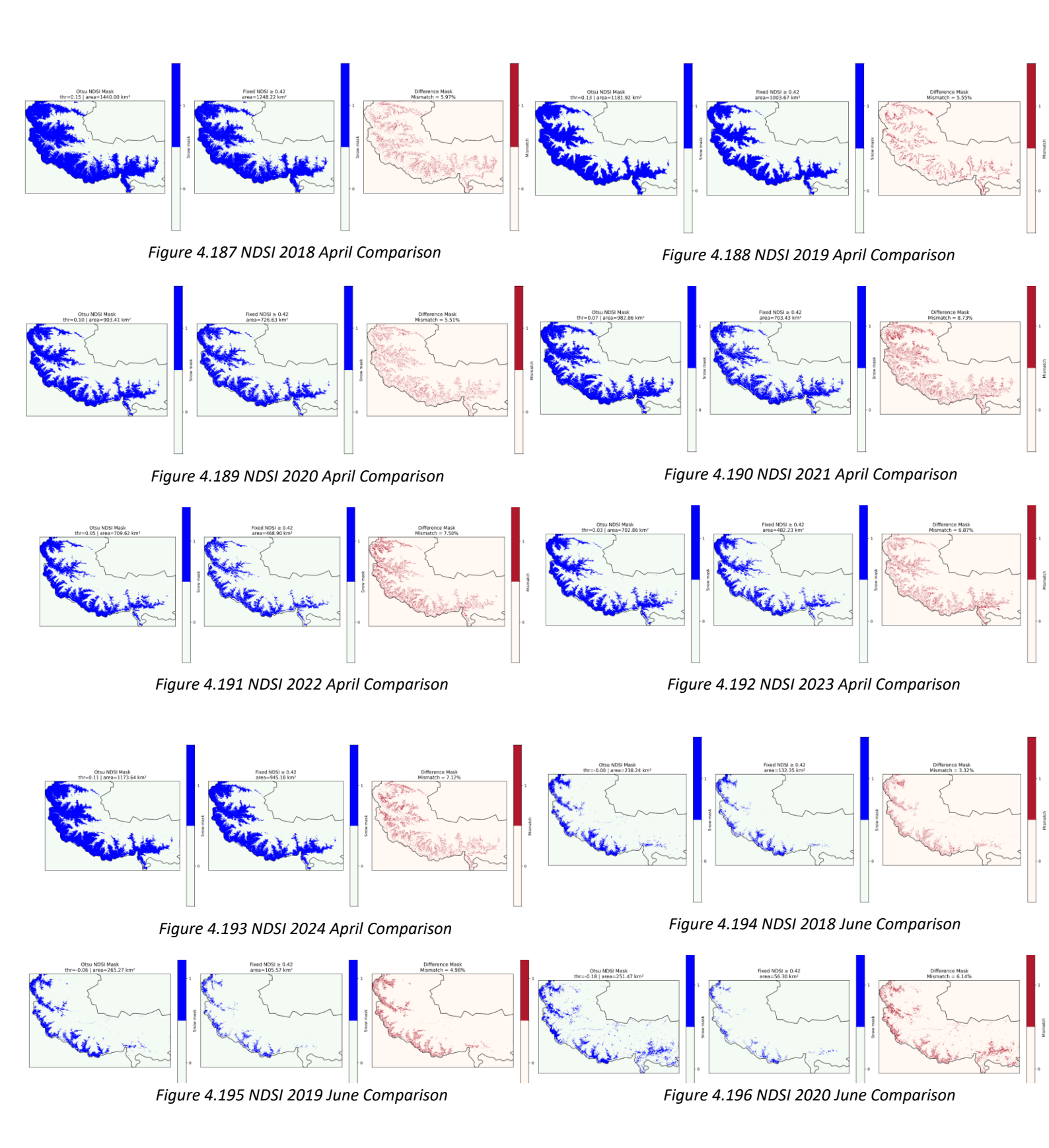


Figure 4.186 NDSI 2024 June Otsu Threshold



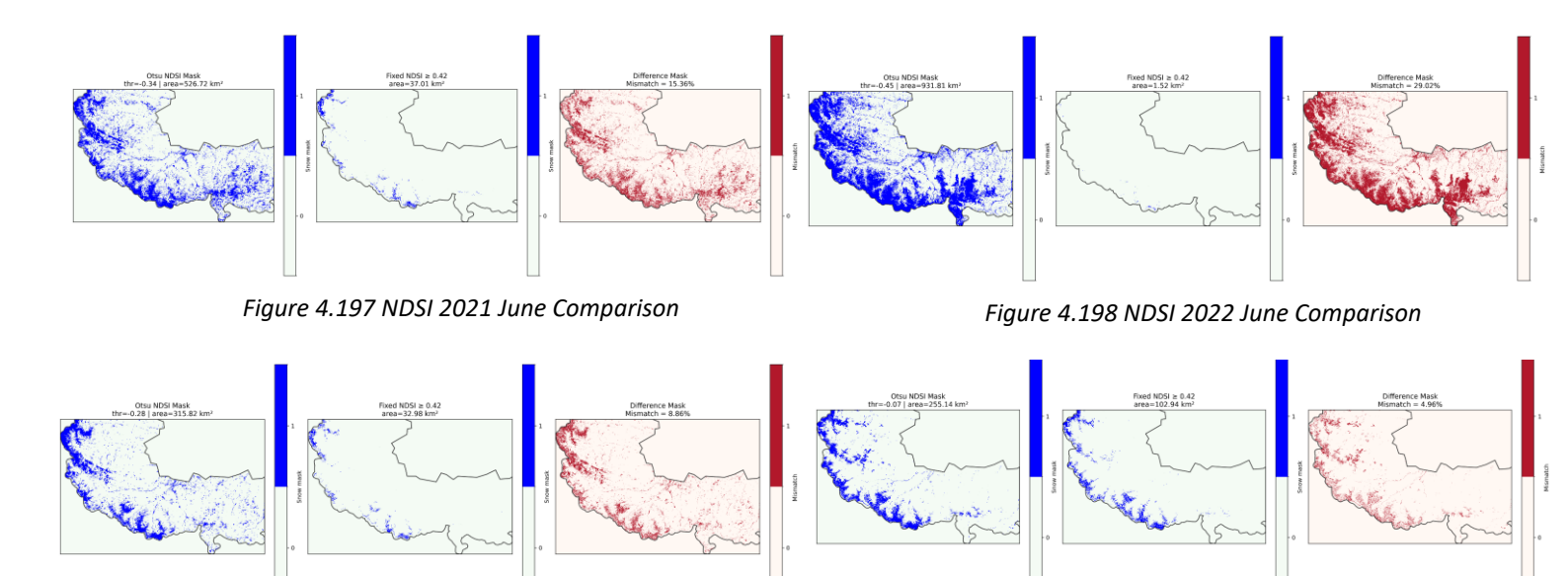


Figure 4.199 NDSI 2023 June Comparison

Figure 4.200 NDSI 2024 June Comparison

PLATFORM	YEAR	MONTH	OTSU THRESHOLD VALUE(NDSI)	Snow COVER AREA(Km^2) OTSU THRESHOLD	Snow COVER AREA(Km^2) THRESHOLD >0.42	Difference Mask Mismatch %
Sentinel Hub	2018	April	0.15	1440.00	1248.22	5.97
Sentinel Hub	2018	June	0.00	238.24	132.35	3.32
Sentinel Hub	2019	April	0.13	1181.92	1003.67	5.55
Sentinel Hub	2019	June	<mark>-0.06</mark>	265.27	105.57	4.98
Sentinel Hub	2020	April	0.10	903.41	726.63	5.51
Sentinel Hub	2020	June	<mark>-0.18</mark>	251.47	56.30	6.14
Sentinel Hub	2021	April	0.07	982.86	703.43	8.73
Sentinel Hub	2021	June	<mark>-0.34</mark>	526.72	37.01	15.36
Sentinel Hub	2022	April	0.05	709.62	468.90	7.50
Sentinel Hub	2022	June	<mark>-0.45</mark>	931.81	1.52	29.02
Sentinel Hub	2023	April	0.03	702.86	482.23	6.87
Sentinel Hub	2023	June	<mark>-0.28</mark>	315.82	32.98	8.86
Sentinel Hub	2024	April	0.11	1173.64	945.18	7.12
Sentinel Hub	2024	June	<mark>-0.07</mark>	255.14	102.94	4.96

4.16 Summary of NDSI classification results obtained from Sentinel Hub for April and June (2018–2024)

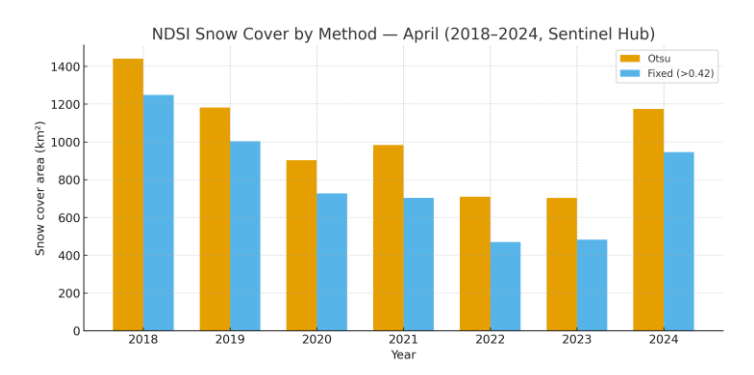


Figure 4.201 Sentinel Hub NDSI snow cover (km²) by method (Otsu vs fixed >0.42), April 2018–2024.

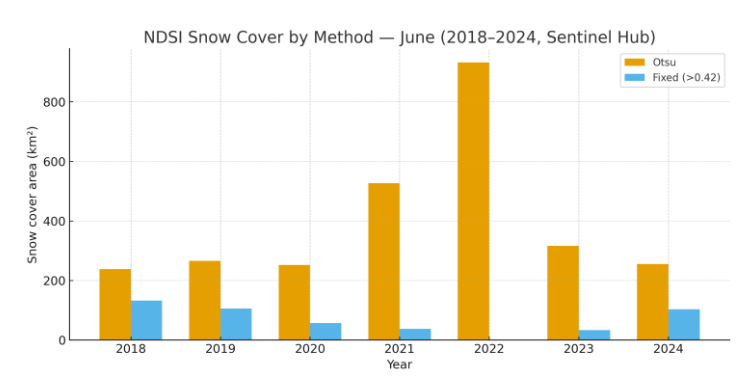


Figure 4.202 Sentinel Hub NDSI snow cover (km²) by method (Otsu vs fixed >0.42), April 2018–2024.

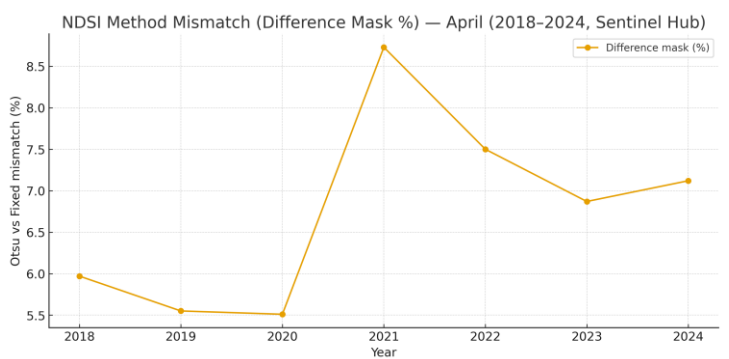


Figure 4.203 Otsu vs Fixed difference mask (%) for April (2018–2024).

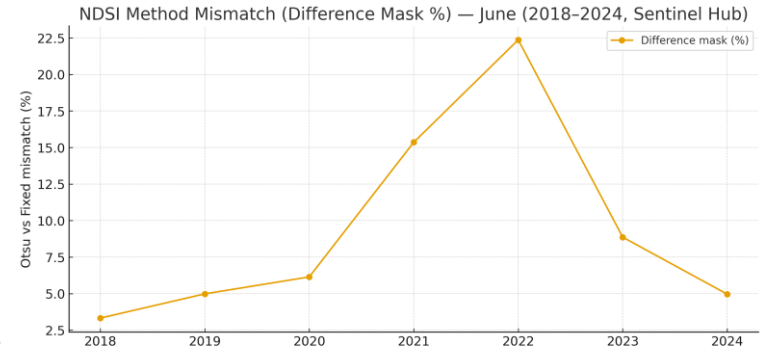


Figure 4.204 Otsu vs Fixed difference mask (%) for April (2018–2024).

The same dual-threshold approach used for GEE was applied to map April and June snow cover from 2018–2024 using Sentinel Hub (SH) Level-2A reflectance composites (≤15% cloud cover): a fixed cut (NDSI > 0.42) and an adaptive Otsu threshold calculated from each composite's NDSI histogram. April Otsu thresholds ranged from 0.05 (2022) to 0.15 (2018) throughout the series, indicating variations in snow persistence, illumination, and residual cloud/shadow contamination from year to year. While the fixed method produced lower extents (~469–1,248 km²), omitting some late-lying patches, Otsu estimated April snow-covered areas between ~710 km² (2022) and ~1,440 km² (2018) using these cuts. When snow, rock, and soil mixtures made class separability more difficult in 2022, method disagreement (difference mask), which was typically 5–8%, increased.

By June, snow contracted to glacial basins and shaded slopes. In years with very little cover, Otsu thresholds frequently drifted toward 0.00 and occasionally negative values (down to -0.45), capturing any remaining bright snow among a mixture of vegetation and bare ground. The fixed rule produced ~1.5–132 km², systematically underestimating fragmented late-season snow, whereas June Otsu areas ranged roughly ~32–238 km². In June, mismatches were usually between 3 and 9%, but under very low NDSI, they increased to about 29% (2022) when bright rock and wet soils confused the fixed cut. In summary, the fixed method provides temporal comparability but tends to underestimate late-season remnants, while the adaptive method best tracks transitional and heterogeneous snow.

Although Sentinel hub cloud/shadow handling and mosaic strategy (least-cloud pixel selection) result in slightly different magnitudes, Sentinel hub results follow the same seasonal pattern as GEE (April accumulation → June remnant patches). To help explain Sentinel hub slightly higher mismatches (up to ~30%) in the most transitional scenes, these choices slightly inflate April cover (cleaner bright-snow retrieval) and deflate June cover (stricter masking of marginal pixels) in comparison to GEE. When combined, the two platforms validate the effectiveness of a dual-threshold strategy: Fixed 0.42 for long-term comparability; Otsu for spatial nuance during transitional periods.

4.12 NDSI Validation with Fractional Snow Cover (FSC) using Google Earth Engine and Sentinel Hub

The Copernicus Fractional Snow Cover (FSC) product was used as the independent reference dataset to validate the snow-cover classification based on the Normalized Difference Snow Index (NDSI). The performance and consistency of NDSI thresholds applied to Sentinel-2 Level-2A imagery processed by both Google Earth Engine (GEE) and Sentinel Hub (SH) were investigated in this study using two different years: 2018 (shown by heavy snow accumulation and high albedo contrast) and 2022 (shown by a warmer and more variable snow season). Validation was conducted using standard accuracy metrics (Overall Accuracy, Precision, Recall, and F1-score) and a pixel-by-pixel comparison between the binary snow/no-snow masks generated by each threshold (ranging from 0.05 to 0.45), and FSC pixels with snow fraction ≥ 50%.

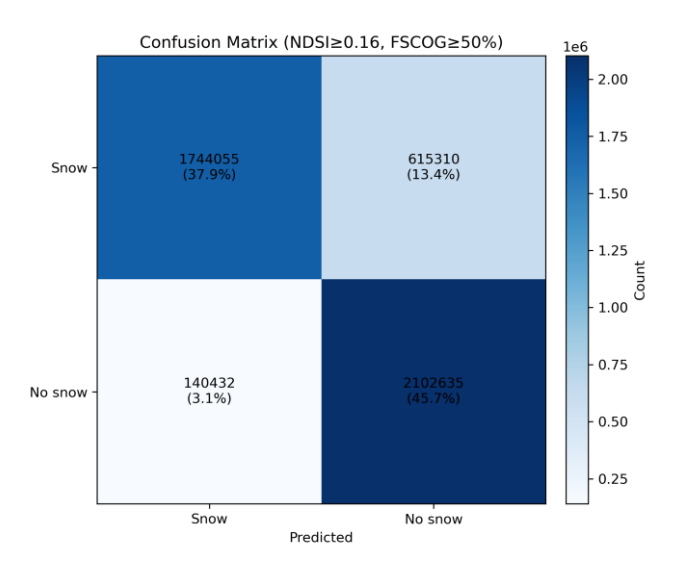


Figure 4.205 Confusion matrix of NDSI classification (t = 0.16) against Copernicus FSC ≥ 50 % for 2018, Google Earth Engine.

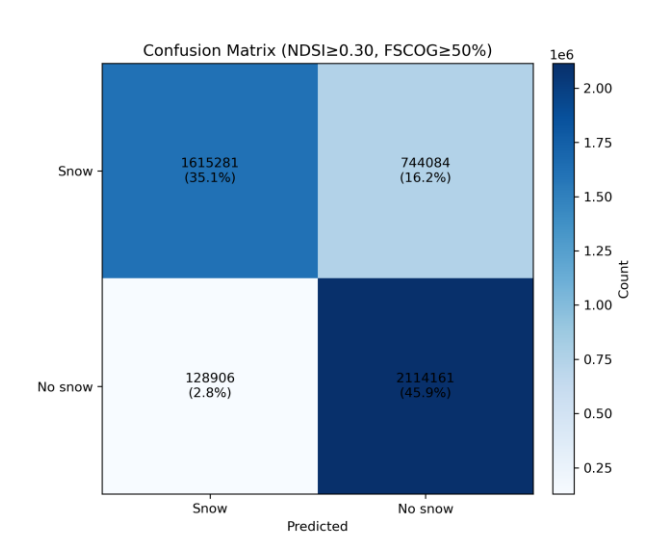


Figure 4.206 Confusion matrix of NDSI classification (t = 0.30) against Copernicus FSC ≥ 50 % for 2018, Google Earth Engine.

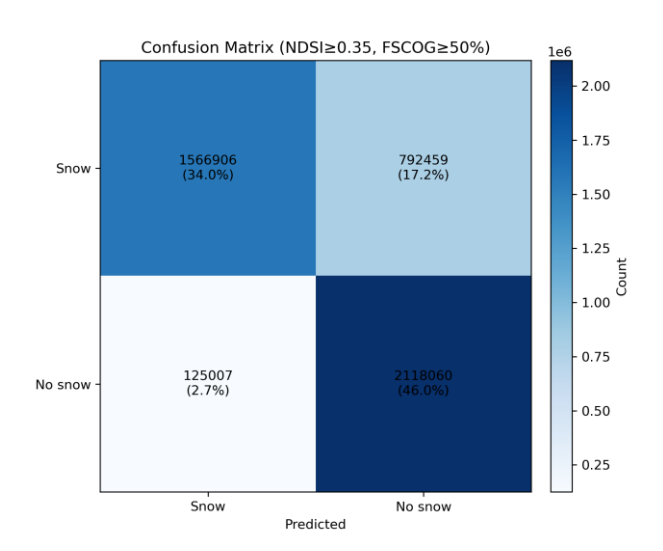


Figure 4.207 Confusion matrix of NDSI classification (t = 0.35) against Copernicus FSC ≥ 50 % for 2018, Google Earth Engine.

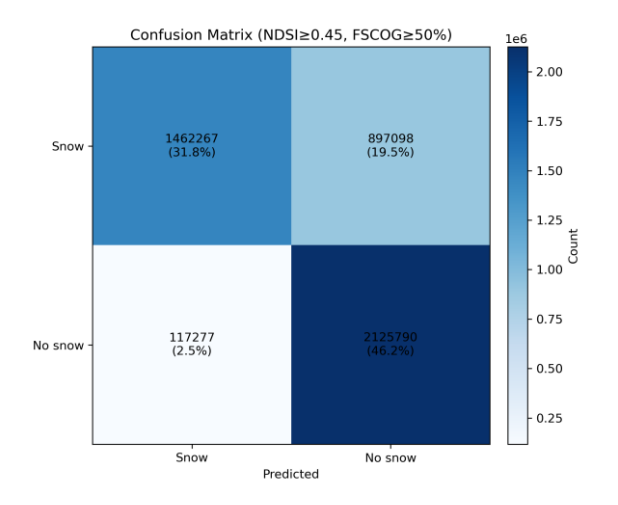


Figure 4.209 Confusion matrix of NDSI

classification (t = 0.45) against Copernicus FSC ≥ 50

% for 2018, Google Earth Engine.

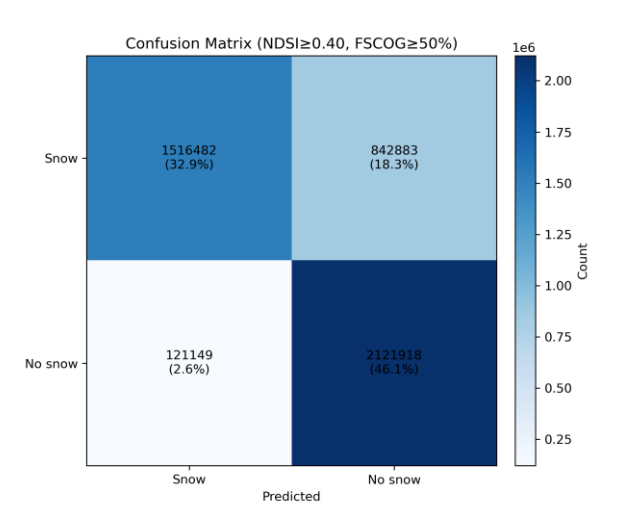


Figure 4.208 Confusion matrix of NDSI classification (t = 0.40) against Copernicus FSC \geq 50 % for 2018, Google Earth Engine.

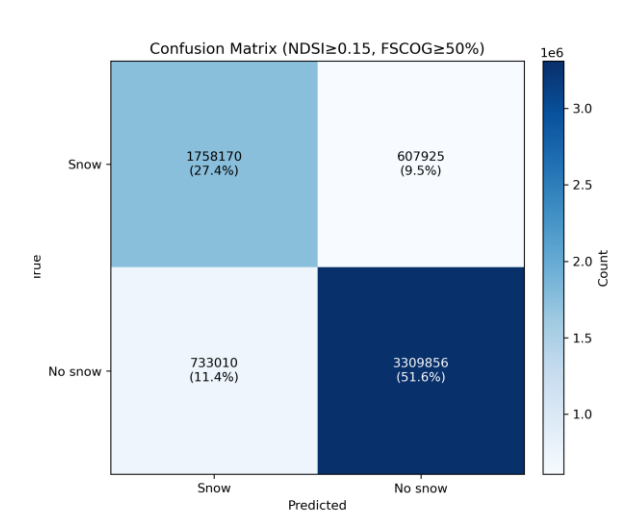


Figure 4.210 Confusion matrix of NDSI classification (t = 0.15) against Copernicus FSC ≥ 50 % for 2018, Sentinel Hub.

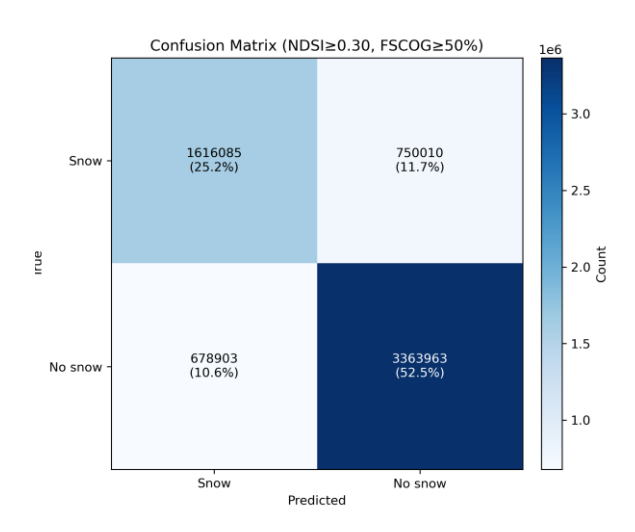


Figure 4.211 Confusion matrix of NDSI classification (t = 0.30) against Copernicus FSC \geq 50 % for 2018, Sentinel Hub.

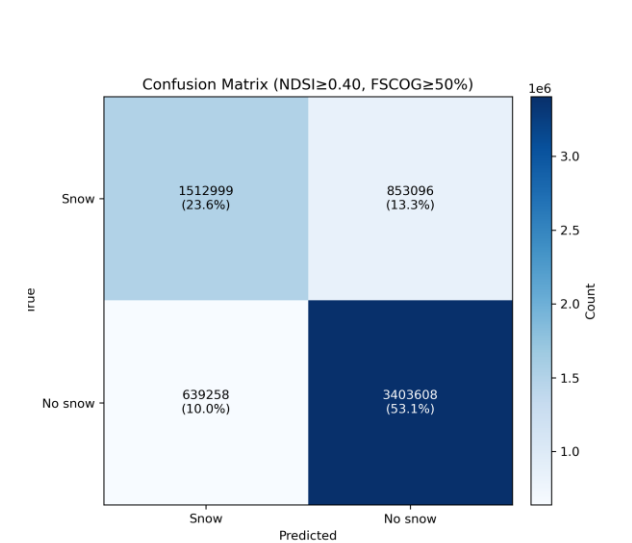


Figure 4.213 Confusion matrix of NDSI classification (t = 0.40) against Copernicus FSC \geq 50 % for 2018, Sentinel Hub.

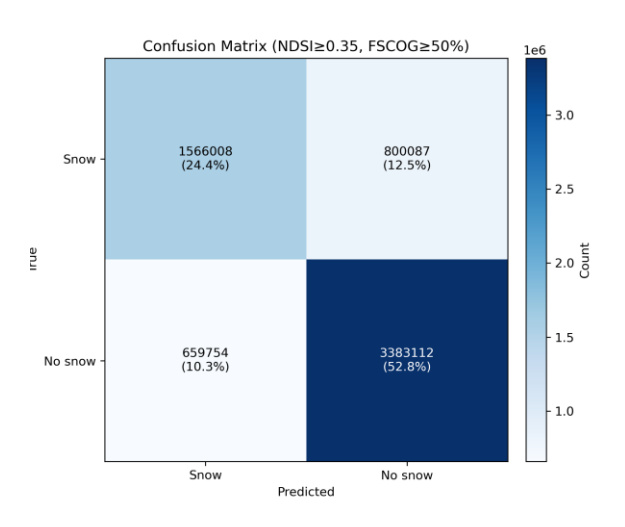


Figure 4.212 Confusion matrix of NDSI classification (t = 0.35) against Copernicus $FSC \ge 50$ % for 2018, Sentinel Hub.

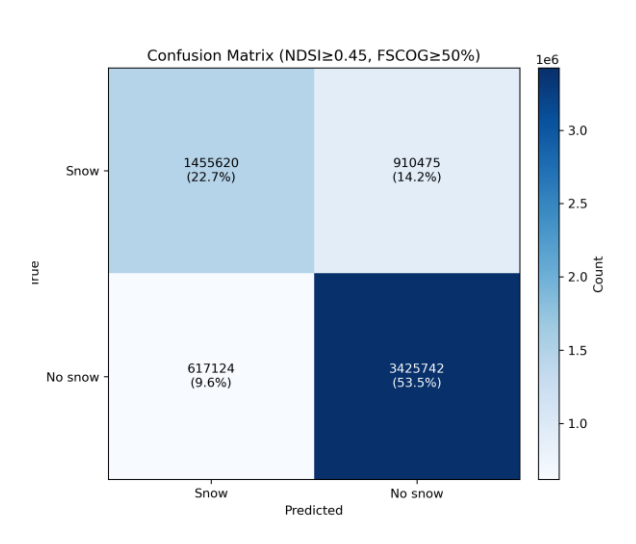


Figure 4.214 Confusion matrix of NDSI classification (t = 0.45) against Copernicus FSC ≥ 50 % for 2018, Sentinel Hub.

When snow cover was widespread and spectrally distinct, the GEE and Sentinel hub results for 2018 (Figures 4.205–4.209 and 4.210–4.214) clearly and consistently demonstrate a high classification reliability pattern. NDSI = 0.16 was determined to be the ideal threshold in GEE, resulting in balanced performance with F1 \approx 0.82 and Accuracy \approx 0.84. While Recall \approx 0.74 showed strong sensitivity to real snow pixels, Precision \approx 0.9 confirmed that false-snow detections were negligible.

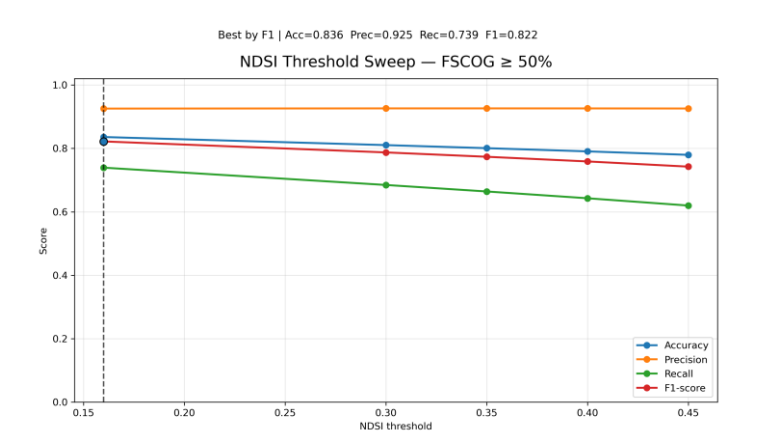


Figure 4.215 Threshold-sweep curve for 2018 NDSI classification (Accuracy, Precision, Recall, and F1) in Google Earth Engine.

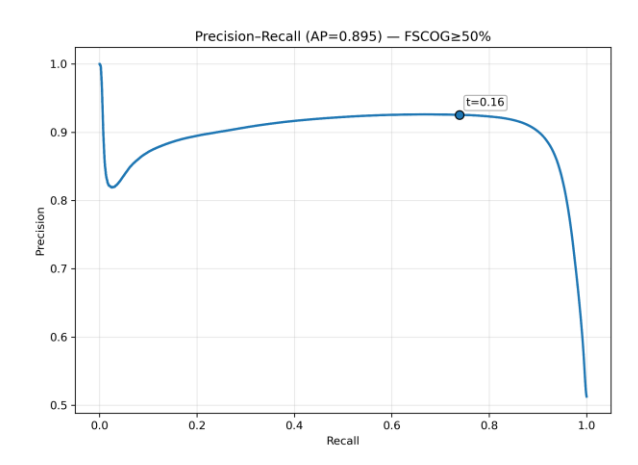


Figure 4.216 Precision—Recall curve for NDSI classification validated against Copernicus FSC \geq 50 % for 2018, Google Earth Engine (AP \approx 0.89).

The corresponding threshold-sweep curves (Figures 4.215–4.216) show the usual trade-off between commission and omission errors: raising thresholds increased Precision but progressively decreased Recall.

The confusion matrices (Figures 4.205–4.209) show a clear division between snow and non-snow classes.

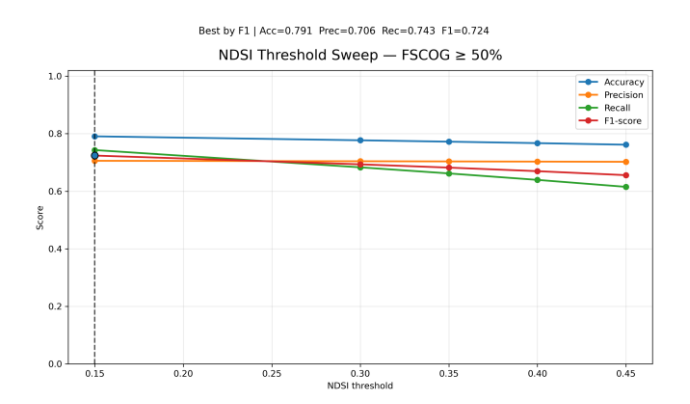


Figure 4.217 Threshold-sweep curve for 2018 NDSI classification (Accuracy, Precision, Recall, and F1) in Sentinel Hub.

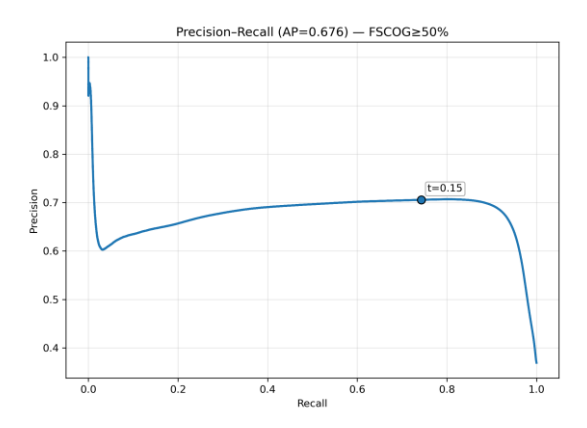


Figure 4.218 Precision—Recall curve for NDSI classification validated against Copernicus FSC \geq 50 % for 2018, Sentinel Hub (AP \approx 0.67).

The same behavior was observed in Sentinel Hub, where the best performing threshold (t = 0.15) produced F1 \approx 0.72 and Accuracy \approx 0.79 (Figures 4.217–4.218). Slightly lower scores in SH mainly stem from differences in cloud masking and the mosaicking strategy, which tends to remove bright mixed pixels near terrain shadows. Nevertheless, both platforms achieved strong agreement with the FSC reference, confirming the robustness of NDSI-based snow detection under clear, high-albedo conditions.

On the other hand, 2022 validation showed a sharp drop in classification performance and weaker separability (Figures 4.219–4.223 and 4.224–4.228). The ideal threshold for GEE moved downward to NDSI \approx 0.05, resulting in F1 \approx 0.48 and Accuracy \approx 0.64. Recall dropped significantly (\approx 0.3) while precision stayed high (\approx 0.9), suggesting significant under-detection of snow, particularly in fragmented or low-contrast areas. This imbalance is supported by the precision–recall curves (AP \approx 0.60), which show that higher commission error results from lower thresholds recovering more true-snow pixels. The majority of errors were false negatives, or missed snow patches in mixed terrain or under thin clouds, according to confusion matrices (Figures 4.219–4.223).

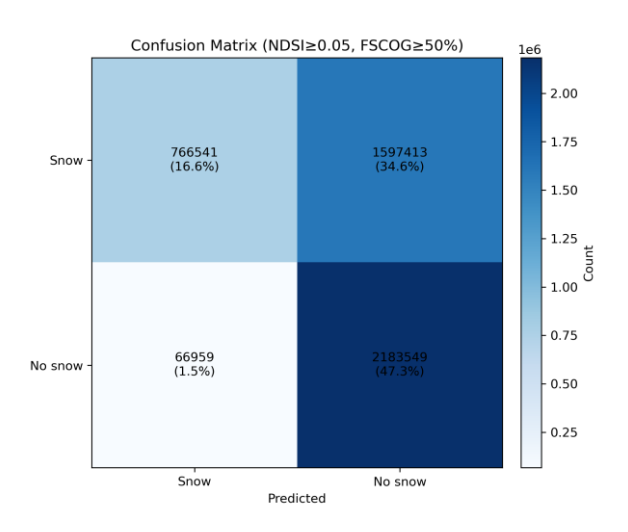


Figure 4.219 Confusion matrix of NDSI classification (t = 0.05) against Copernicus FSC ≥ 50 % for 2022, Google Earth Engine.

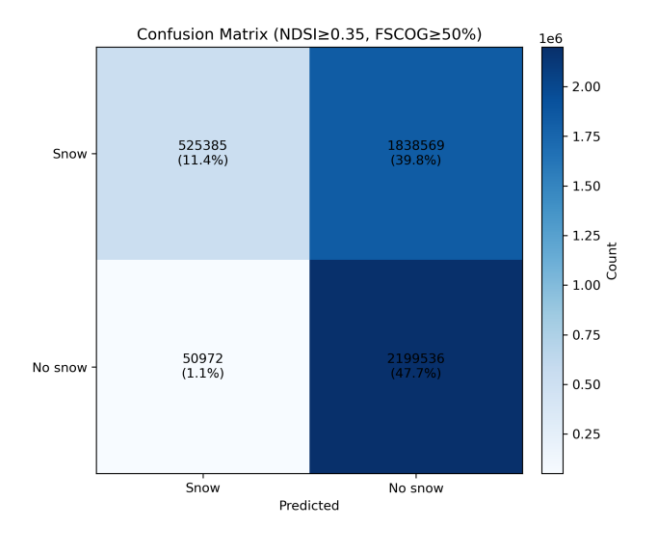


Figure 4.221 Confusion matrix of NDSI

classification (t = 0.35) against Copernicus FSC ≥ 50 %

for 2022, Google Earth Engine.

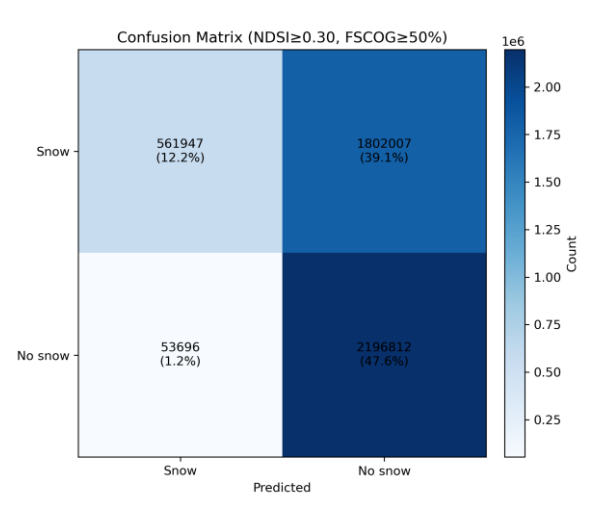


Figure 4.220 Confusion matrix of NDSI classification (t = 0.30) against Copernicus FSC ≥ 50 % for 2022, Google Earth Engine.

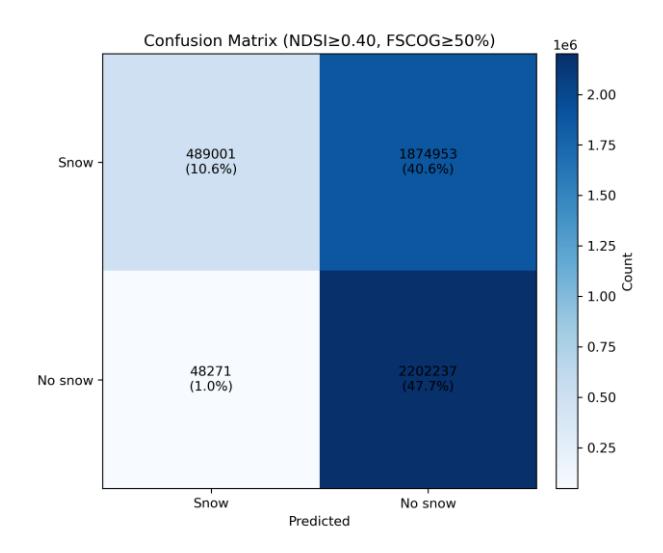


Figure 4.222 Confusion matrix of NDSI classification (t = 0.40) against Copernicus FSC \geq 50 % for 2022, Google Earth Engine.

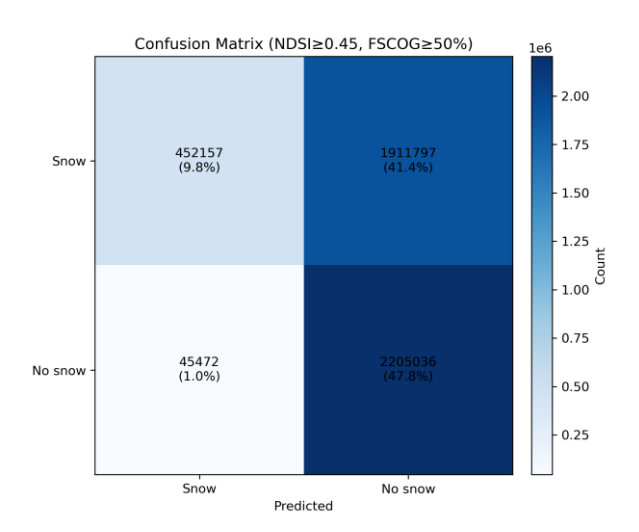


Figure 4.223 Confusion matrix of NDSI classification (t = 0.45) against Copernicus FSC ≥ 50 % for 2022, Google Earth Engine.

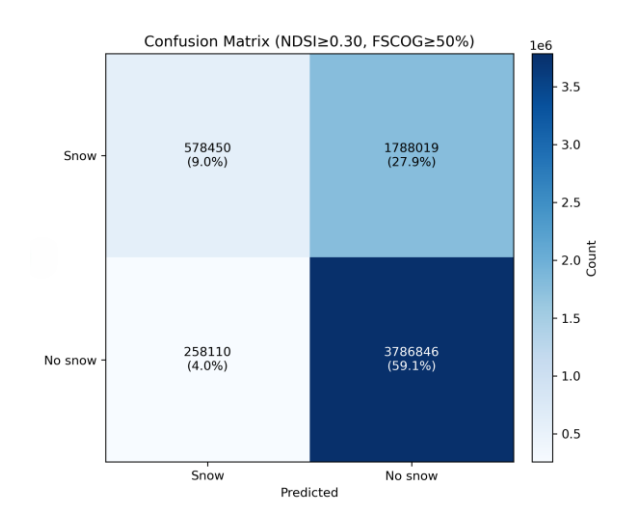


Figure 4.225 Confusion matrix of NDSI classification (t = 0.30) against Copernicus FSC \geq 50 % for 2022, Sentinel Hub.

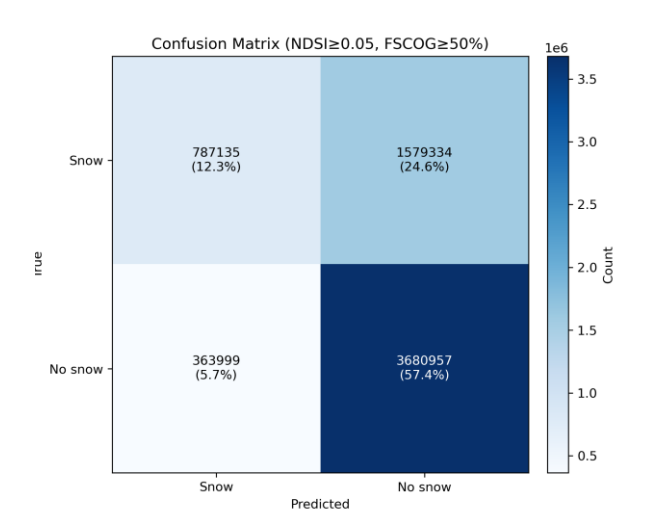


Figure 4.224 Confusion matrix of NDSI classification (t = 0.05) against Copernicus FSC \geq 50 % for 2022, Sentinel Hub.

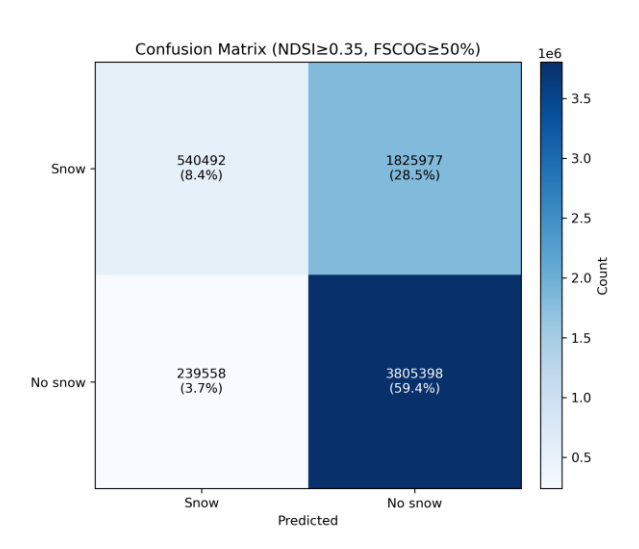


Figure 4.226 Confusion matrix of NDSI classification (t = 0.35) against Copernicus FSC \geq 50 % for 2022, Sentinel Hub.

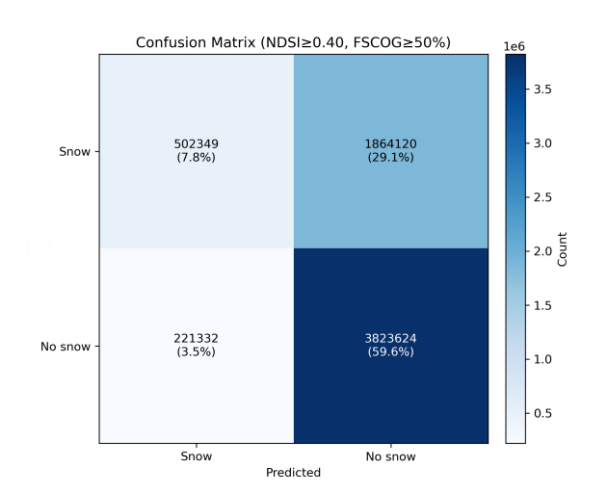


Figure 4.227 Confusion matrix of NDSI classification (t = 0.40) against Copernicus FSC \geq 50 % for 2022, Sentinel Hub.

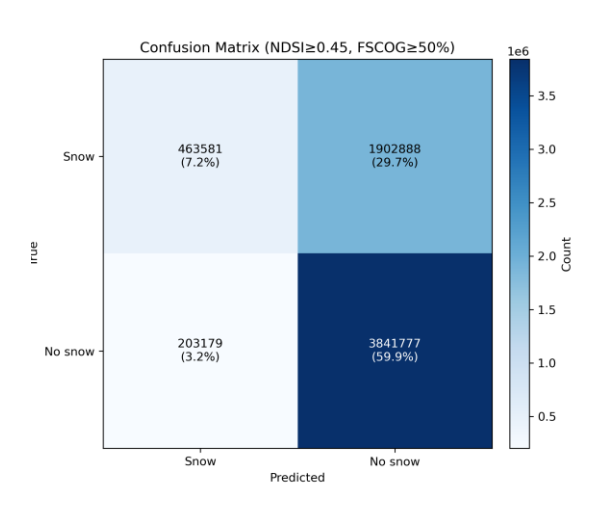


Figure 4.228 Confusion matrix of NDSI

classification (t = 0.45) against Copernicus FSC ≥ 50

% for 2022, Sentinel Hub.

Both physical and methodological factors contribute to the degradation: increased spectral confusion from wet soils, FSC uncertainties brought on by residual cloud contamination, and warmer temperatures that result in discontinuous snow cover. Sentinel Hub showed similar results, with the best F1 \approx 0.45 at NDSI = 0.05 and Accuracy \approx 0.70 (Figures 4.224–4.228). Although the SH mosaicking process was successful in minimizing artifacts, it also obscured minute snow remnants, as indicated by the lower recall (\approx 0.33) and moderate precision (\approx 0.68). In general, 2022 emphasizes how challenging threshold-based classification is during late-melt and transitional times when there is a considerable amount of spectral overlap between snow, rock, and moist soil.

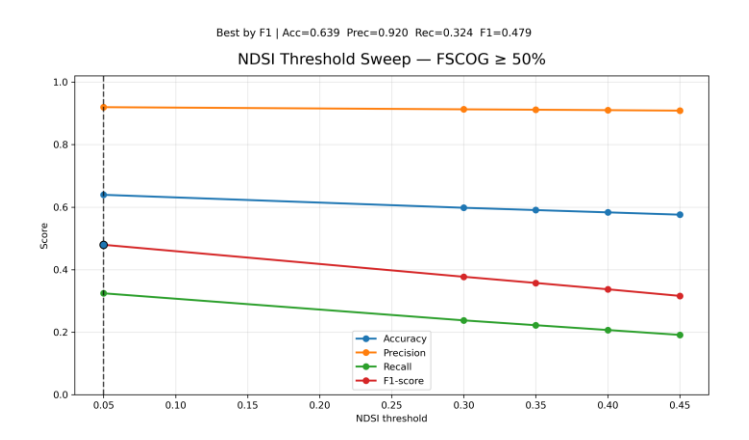


Figure 4.229 Threshold-sweep curve for 2022 NDSI classification (Accuracy, Precision, Recall, and F1) in Google Earth Engine.

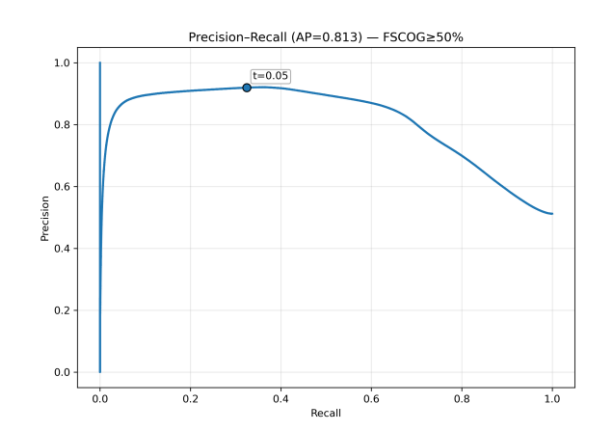


Figure 4.230 Precision—Recall curve for NDSI classification validated against Copernicus $FSC \ge 50$ % for 2022, Google Earth Engine (AP ≈ 0.81).

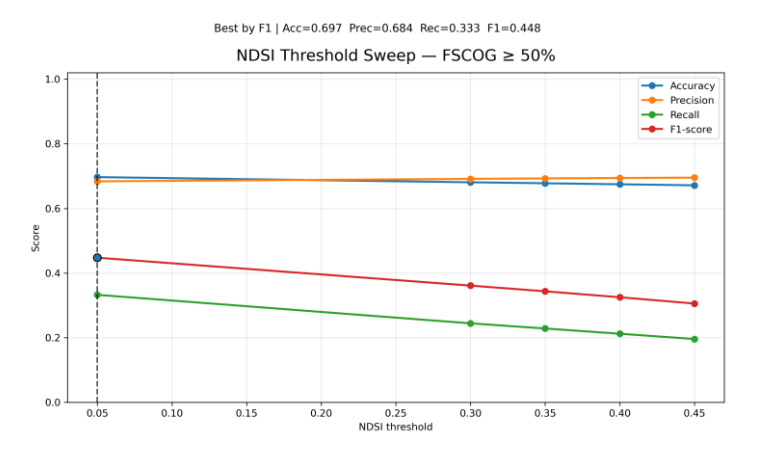


Figure 4.231 Threshold-sweep curve for 2022 NDSI classification (Accuracy, Precision, Recall, and F1) in Sentinel Hub.

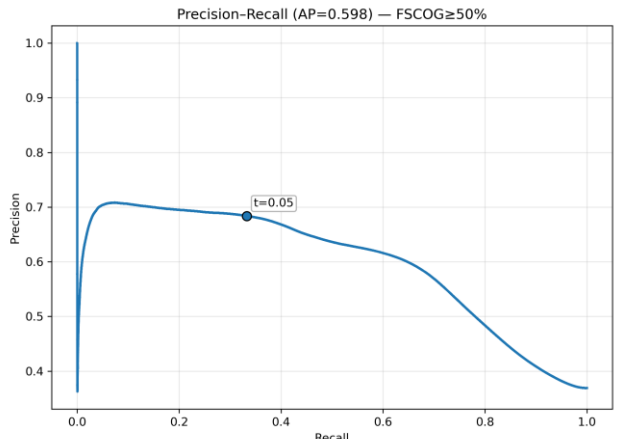


Figure 4.232 Precision–Recall curve for NDSI classification validated against Copernicus FSC \geq 50 % for 2022, Sentinel Hub (AP \approx 0.59).

Comparing the platforms from the two years shows consistent threshold behavior and complementary strengths. Similar optimal cut-offs (\approx 0.15–0.16 for 2018 and \approx 0.05 for 2022) were obtained in GEE and SH by the adaptive Otsubased selection, highlighting the fact that threshold variability is dominated by seasonal context rather than processing environment. Because of its histogrambased compositing, GEE tended to achieve slightly higher recall, capturing more fractional and sub-pixel snow areas; SH, on the other hand, maintained higher precision by strictly rejecting clouds and shadows. While adaptive thresholds are crucial for inter-annual analyses where spectral and meteorological variability alter snow reflectance patterns, fixed thresholds provide stability for long-term comparison, as evidenced by the stark year-to-year contrast (2018 vs. 2022). Both systems achieved satisfactory agreement with the FSC reference despite inherent discrepancies between instantaneous Sentinel-2 scenes and the temporally averaged Copernicus product.

All together, these findings demonstrate that a trustworthy quantitative framework for assessing alpine snow-cover dynamics is offered by NDSI threshold optimization and validation against FSC. While warm years with irregular snowfall, like 2022, diminish the dependability of any one threshold rule, high-snow years, like 2018, show strong spectral separability and high mapping accuracy. The benefits of multi-source approaches are further supported by the dual-platform validation: SH guarantees radiometric consistency and operational continuity, while GEE enables adaptive, large-scale monitoring with flexible compositing. Together, they show that a combination of fixed and adaptive NDSI thresholds can capture alpine snow cover's spectral variability and temporal persistence, offering a strong methodological basis for long-term studies of the Western Alps' climate and cryosphere.

4.13 Manual NDSI Validation (Google Earth Engine and Sentinel Hub, 2022)

A manual validation was conducted for April 2022 using Google Earth Engine (GEE) and Sentinel Hub (SH) in order to independently confirm the accuracy of the snow-cover classification derived from Sentinel-2 NDSI analysis. Using visual interpretation of high-resolution optical imagery, a total of manually labeled snow/no-snow points were gathered throughout the Maritime Alps region. The fixed threshold of NDSI \geq 0.42, which had been determined as the project team's operational cut-off for snow detection, was then used to compare each point against the binary NDSI classification outputs produced by both platforms.

Threshold Method	UA (non- snow)	UA (snow)	PA (non- snow)	PA (snow)	Overall Accuracy (OA)	Kappa (k)
Fixed (0.42)	93.8%	97.5%	97.6%	93.6%	95.6%	0.912

Table 4.17. User's and Producer's Accuracy for manual NDSI validation, April 2022, Google Earth Engine.

Threshold Method	Accuracy	Precision	Recall	F1 Score
Fixed (0.42)	95.6%	97.5%	93.6%	95.5%

Table 4.18. Summary of NDSI manual validation metrics (Accuracy, Precision, Recall, F1 Score), Google Earth Engine, April 2022.

Utilizing standard metrics such as Overall Accuracy (OA), Precision, Recall, F1-score, User's Accuracy (UA), Producer's Accuracy (PA), and Cohen's Kappa (κ), the manual validation adhered to the same accuracy assessment protocol used throughout this study. The goal was to measure the agreement between manually annotated reference points and automatically detected snow, as well as to assess the threshold-based approach's actual performance in field-representative settings.

Overall Accuracy = 95.6%, Precision = 97.5%, Recall = 93.6%, and F1 = 95.5% were the results of the validation for Google Earth Engine (Tables 4.17–4.18). There were very few misclassifications, and they mostly happened along shaded slopes and mixed terrain where snow reflectance decreases, according to the confusion matrix (Figure 4.233), which clearly shows a preponderance of true positives and true negatives. Errors were randomly distributed rather than concentrated in one area, as shown by the corresponding spatial distribution of validation points (Figure 4.234). These results show that when the snowpack is homogeneous and spectrally distinct in the early season, the fixed NDSI threshold of 0.42 is very dependable for broad-scale snow detection.

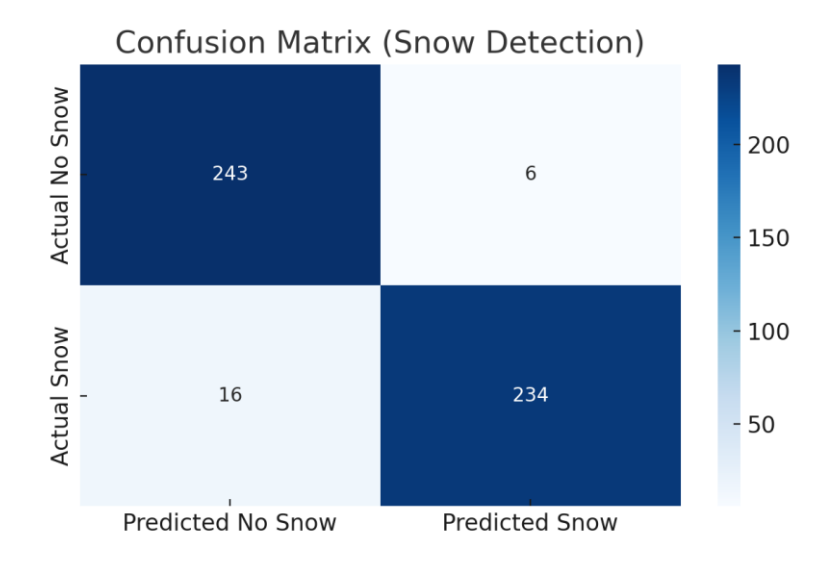


Figure 4.233. Confusion matrix for manual validation of NDSI classification (NDSI ≥ 0.42) using GoogleFigure 4.233. Confusion matrix for manual validation of NDSI classification (NDSI ≥ 0.42) using Google Earth Engine, April 202 Earth Engine, April 2022.

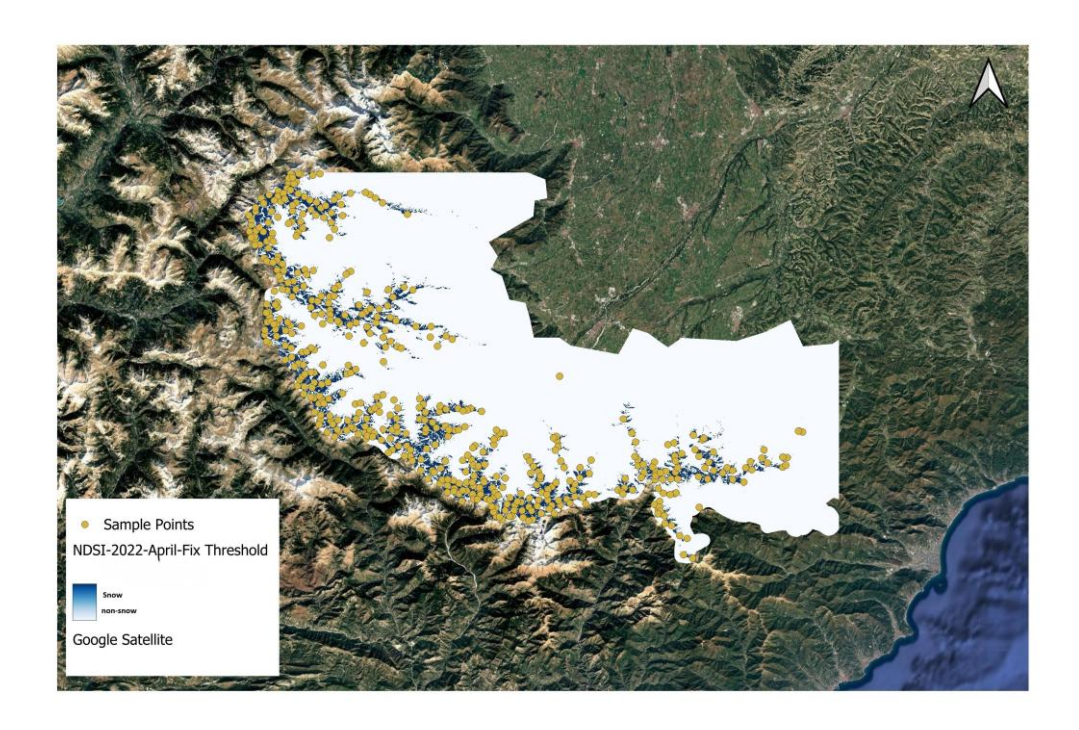


Figure 4.234. Spatial distribution of manual validation points used for NDSI assessment in April 2022, Google Earth Engine.

With Overall Accuracy = 98.8%, Precision = 98.8%, Recall = 97.2%, and F1 = 97.98%, Sentinel Hub's validation results were even higher (Tables 4.19-4.20). While the spatial visualization of sampling points (Figure 4.236) validates the dense and balanced coverage of snow and non-snow surfaces, the confusion matrix (Figure 4.233) demonstrates strong class separability. Excellent statistical agreement between the classified and manually interpreted datasets is indicated by the κ coefficient (0.96). Narrow shaded glacial basins and high-elevation ridges, where complicated topography and fluctuating illumination can lessen the NDSI contrast between snow and rock, were the primary locations for misclassifications.

Threshold Method	UA (non- snow)	UA (snow)	PA (non- snow)	PA (snow)	Overall Accuracy (OA)	Kappa (k)
Fixed (0.42)	97.2%	98.1%	98.8%	97.2%	98.0%	0.960

Table 4.19. User's and Producer's Accuracy for manual NDSI validation, April 2022,

Sentinel Hub.

Threshold Method	Accuracy	Precision	Recall	F1 Score
Fixed (0.42)	98.0%	98.78%	97.2%	97.98%

Table 4.20. Summary of NDSI manual validation metrics (Accuracy, Precision, Recall, F1 Score), Sentinel Hub, April 2022.

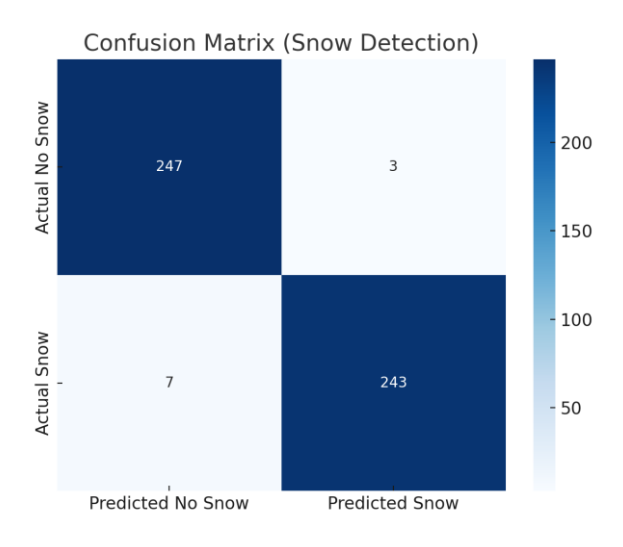


Figure 4.235. Confusion matrix for manual validation of NDSI classification (NDSI \geq 0.42) using Sentinel Hub, April 2022.

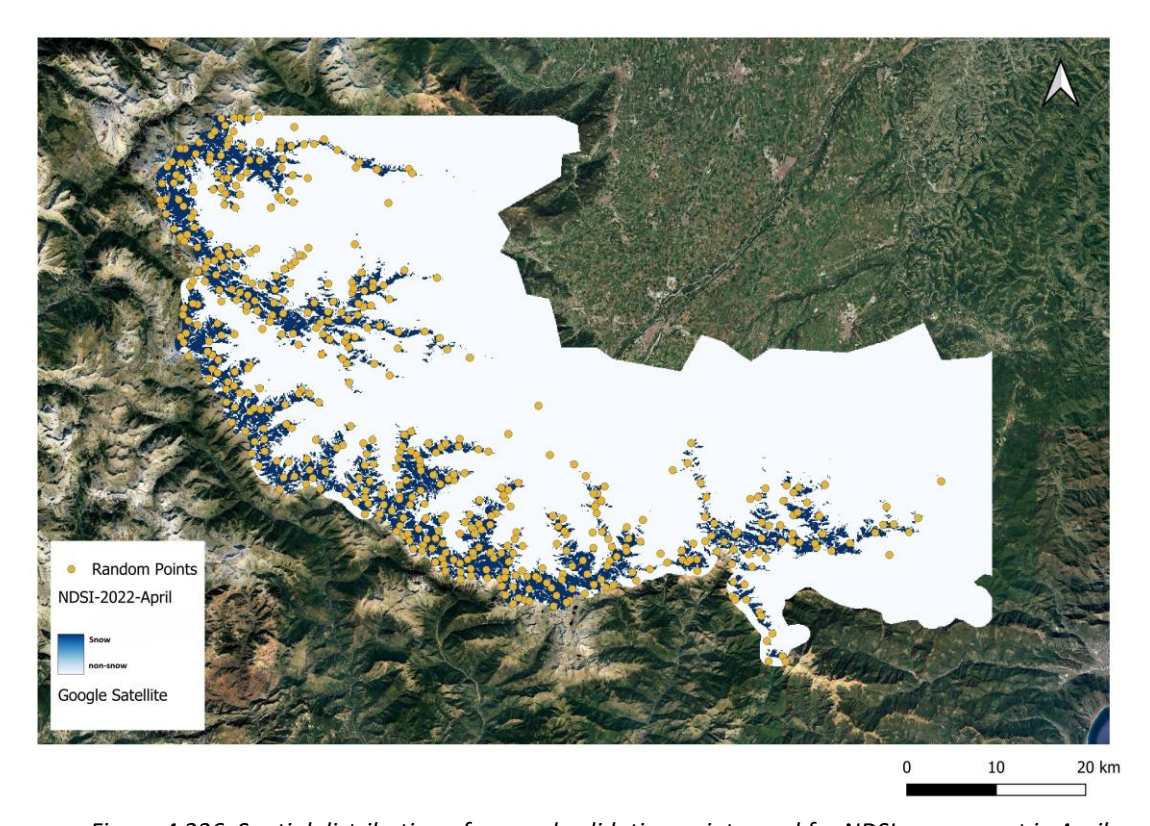


Figure 4.236. Spatial distribution of manual validation points used for NDSI assessment in April 2022, Sentinel Hub.

Sentinel Hub and GEE both achieved very high accuracy, according to the comparison (April 2022, fixed threshold); however, Sentinel Hub outperformed GEE by roughly 1.3% in precision and 3.6% in recall, with an overall 2.5% increase in F1-score. This illustrates the benefit of the Sentinel Hub cloud-masking and compositing technique, which lessens the influence of lingering clouds and terrain shadows that occasionally degrade GEE's mosaic composites. Although both systems are dependable, the slight performance difference indicates that GEE provides more flexibility for extensive temporal analyses, while SH is more appropriate for operational monitoring that is focused on accuracy.

Methodologically speaking, the manual validation offers solid independent confirmation of the dependability of the NDSI-based workflow. A fixed threshold (NDSI \geq 0.42) is suitable for early spring conditions in the Maritime Alps, where snow is continuous and highly reflective, as confirmed by the high accuracy attained in both platforms. The automated classification framework used for multi-year analyses is more reliable due to its cross-platform consistency.

In summary, manual validation confirms the high reliability and cross-platform stability of the NDSI threshold method. The results validate the automated assessments obtained with Copernicus FSC (Section 4.10) and demonstrate that the system performs accurately not only against satellite-based fractional data but also against human-interpreted ground-truth references. Sentinel Hub's slightly superior precision and recall highlight the benefits of optimized mosaicking and atmospheric correction workflows. Overall, the fixed-threshold NDSI configuration provides an effective and transferable solution for operational snow mapping under clear early-season conditions, ensuring methodological robustness for subsequent analyses of seasonal snow persistence and alpine cryosphere monitoring.

Discussion

5.1 NDVI Thresholding and Vegetation Dynamics

5.1.1 Fixed vs. Adaptive Thresholding

The research used fixed (NDVI ≥ 0.30) and adaptive Otsu thresholding methods to evaluate vegetation cover detection using Sentinel-2 imagery. The fixed threshold approach, derived from traditional methods (Tucker, 1979; Rouse et al., 1974), produced vegetation cover estimates that occasionally exceeded true values, particularly in April, when early-season greenness overlapped with residual snow. These results align with previous findings by (Huete et al. 2002) and (Forkel et al., 2019) which reported similar overestimations under mixed land-cover conditions.

The Otsu method (Otsu, 1979) which depends on histogram variance for optimizing the separation between vegetated and non-vegetated pixels demonstrated superior performance for detecting changes between annual periods and various environmental settings. The Otsu thresholds showed a broad range from 0.22 in April to 0.55 in June, capturing the transition from sparse vegetation to full canopy development. These results are consistent with alpine NDVI studies showing that vegetation dynamics are highly sensitive to the timing of snowmelt (Choler et al., 2021; Rösch et al., 2022).

5.1.2 Validation with CORINE 2018

Validation against CORINE Land Cover data highlighted the complementary strengths and weaknesses of both thresholding approaches.

The fixed threshold achieved higher Producer's Accuracy, successfully identifying most vegetated pixels, but showed lower User's Accuracy due to confusion where sparse or mixed pixels were incorrectly classified as vegetation. The Otsu method provided higher precision but lower recall, confirming the expected trade-off in land cover mapping between omission and commission errors (Congalton, 1991; Olofsson et al., 2014).

Despite moderate agreement ($\kappa \approx 0.3-0.4$), CORINE's 100-m resolution limited its use for pixel-level Sentinel-2 validation. These results highlight the need

for finer datasets, such as LUCAS, when assessing Sentinel-2 vegetation classifications.

5.1.3 Validation with LUCAS 2022

Accurate pixel-level validation was made possible by the LUCAS point survey. Recall ranged from 0.86 to 0.99, while precision (0.92–0.97) was highest when thresholds were between 0.30 and 0.34. Consistent with findings at the European scale, these results (OA \approx 0.93, F1 \approx 0.96) validate Sentinel-2 NDVI's strong ability to distinguish vegetation in alpine areas with variable soil and snow exposure (d'Addamio et al., 2021). However, in steep or shadowed terrain, the class imbalance between vegetated and non-vegetated pixels decreased recall.

5.1.4 Validation with Carta degli Habitat

Validation against *Carta degli Habitat* confirmed that NDVI binary classification can broadly represent vegetation zones but lacks habitat-level specificity. The low Kappa values ($\kappa = 0.10-0.15$) indicate that NDVI fails to capture detailed plant community composition, consistent with findings from Mediterranean and alpine protected areas (Pesaresi et al., 2020; Čajkovská et al., 2020). These results emphasize that NDVI is a valuable tool for monitoring general vegetation trends but should be complemented with habitat-specific indices for ecological studies.

5.1.5 Synthesis for NDVI

The NDVI validation experiments demonstrate that CORINE, LUCAS, and Carta degli Habitat serve as complementary references and that no single dataset can guarantee accuracy on its own. Large-scale thematic mapping is supported by CORINE, and precise pixel-level calibration and threshold optimization are made possible by LUCAS.

While adaptive Otsu techniques better capture spectral variability and phenological transitions, the fixed threshold approach guarantees temporal

consistency. When combined, they offer a dual framework that strikes a balance between ecological sensitivity and long-term comparability.

5.2 NDSI Thresholding and Snow Dynamics

5.2.1 Seasonal Dynamics

The dual-threshold method served as the method for detecting snow cover. The fixed thresholds (NDSI \geq 0.42) proved to be both reliable and straightforward to understand according to Hall et al. (Hall et al.,1995; Dozier, 1989), but tended to underestimate snow in fragmented conditions, especially in late-season months (June).

The Otsu thresholds showed dynamic changes based on annual conditions because they reached values below 0.20 and even negative numbers (e.g., June 2023) when bare soil and bright rocks became the main spectral indicators.

These findings confirm that adaptive thresholds effectively detect snow in transitional conditions but may introduce over-segmentation when wet soils or clouds share similar reflectance values.

5.2.2 Validation with FSC

Validation against the Copernicus Fractional Snow Cover (FSC) product demonstrated strong annual contrasts.

In 2018, the best results occurred at NDSI \geq 0.16 (OA = 0.84, F1 = 0.82), while 2022 yielded weaker performance (OA = 0.64, F1 = 0.48) with an optimal threshold near 0.05.

These variations reflect genuine snowpack differences between years, as well as the influence of FSC's fractional nature, which better captures accumulation periods than melt-out stages. Results align with previous cryosphere studies showing similar limitations in binary snow detection (Dumont et al., 2020; Mohammadi et al., 2023).

5.2.3 Manual Point-Based Validation

The random-point validation process inside the AOI area revealed positive and negative aspects of each method. The fixed threshold method achieved acceptable results when detecting large snow areas yet it did not detect small snow patches. The Otsu threshold method reduced the number of missed snow events but it led to incorrect snow detection in shaded cirque areas and steep slopes.

The research by (Parajka & Blöschl, 2008) confirms this trade-off because they showed that threshold selection generates the highest degree of uncertainty when mapping Alpine snow.

5.2.4 Synthesis for NDSI

The NDSI analysis shows that Otsu thresholds improve responsiveness to local snow and illumination conditions, while fixed thresholds guarantee inter-annual stability, allowing for trustworthy comparisons across years. Given the wide variations in snowpack characteristics and atmospheric effects, FSC validation confirms that no single threshold works best for all seasons.

To preserve accuracy and temporal coherence, these results highlight the need for flexible but comparable validation systems that combine binary and fractional references (Gascoin et al., 2020; Terrago et al., 2023).

5.3 Cross-Platform Comparison (GEE vs Sentinel Hub)

NDVI and NDSI results from GEE and Sentinel Hub showed strong coherence, with less than 15 % deviation in snow and vegetation area estimates. Differences mainly stemmed from distinct mosaicking and cloud-masking strategies. GEE facilitated automated workflows and flexible threshold testing, while Sentinel Hub offered higher precision due to its optimized atmospheric corrections and temporal compositing.

The two systems thus complement each other: GEE is ideal for large-scale, long-term studies, and Sentinel Hub excels in precision monitoring and visual consistency (Choler et al., 2021; Parisi et al., 2023).

5.4 Ecological and Climatic Implications

The dual analysis of vegetation (NDVI) and snow (NDSI) shows that alpine environments keep a strong connection between their cryosphere and biosphere systems. The results indicated the following findings:

The length of snow cover determines when plants start to grow in early spring (Marty et al., 2017; Kotlarski et al. 2022).

The NDVI trajectories reveal both short-term effects from snowmelt and slope instability and long-term thermophilization patterns (Lamprecht et al.,2018; Choler et al. 2021).

NDVI and NDSI require thresholding decisions for ecological interpretation because their responses change significantly based on the chosen threshold values.

The Maritime Alps demonstrated high sensitivity to threshold definitions because of their steep elevation changes and wide range of habitats. The classification of transitional habitats (snowbeds, alpine meadows, shrub–forest ecotones) demonstrates that their continuous spectral characteristics prevent them from being classified as simple binary categories.

5.5 Methodological Recommendations

- Adopt dual-threshold approaches as a standard practice in alpine Earth Observation (EO) studies. This combination ensures both inter-annual comparability (through fixed thresholds) and adaptability to variable conditions (through Otsu or other data-driven thresholds).
- Ensure validation diversity by integrating multiple reference datasets (e.g., CORINE, LUCAS, CdH, FSC). No single dataset provides complete reliability across scales; combining polygon-based, point-based, and fractional references reduces bias and improves robustness.
- Perform threshold optimization using precision—recall trade-offs and F1scores only when ground-truth or validated reference data are available.
 Reliable reference information is essential to evaluate true/false

- 4. classifications and avoid misleading accuracy assessments, especially under class imbalance conditions.
- 5. Incorporate machine learning and hybrid fractional methods (Vicente-Serrano et al., 2010; Tiede et al., 2021) to overcome binary classification limitations and to model gradual transitions (e.g., partial snow or mixed vegetation cover) that thresholding cannot fully capture.
- 6. Select thresholds according to study objectives:
- Use fixed thresholds for temporal comparisons and long-term trend analyses where stability and reproducibility are priorities.
- Use Otsu or adaptive thresholds for short-term or spatially heterogeneous analyses where illumination, moisture, or surface reflectance vary significantly.

Conclusion

This thesis investigated vegetation and snow dynamics in the Maritime Alps using Sentinel-2 satellite imagery, focusing on NDVI (Normalized Difference Vegetation Index) and NDSI (Normalized Difference Snow Index). The overarching aim was to evaluate how different thresholding strategies and validation datasets influence the accuracy and interpretability of alpine vegetation and snow-cover classifications. By employing both fixed and adaptive (Otsu) thresholds, the study systematically evaluated methodological trade-offs in binary classification of vegetation and snow cover. The results were validated against multiple reference datasets, including CORINE Land Cover 2018, LUCAS 2022, Carta degli Habitat, and the Copernicus Fractional Snow Cover (FSC) product.

The findings confirm that threshold selection strongly conditions ecological interpretation. Fixed thresholds (NDVI \geq 0.30, NDSI \geq 0.42) ensured comparability across years and alignment with legacy literature but systematically misrepresented transitional conditions overestimating vegetation in early spring and underestimating snow in patchy late-season cover. In contrast, adaptive Otsu thresholds flexibly adapted to spectral distributions, capturing inter-annual and seasonal variability more effectively, but occasionally introduced commission errors, particularly in ecotonal or topographically complex zones. This trade-off represents the central methodological contribution of the thesis, emphasizing that adaptive approaches increase responsiveness while fixed thresholds ensure temporal consistency.

Validation exercises provided critical insights. CORINE confirmed broad-scale agreement but highlighted scale mismatches. LUCAS offered high-resolution point-based validation, enabling threshold optimization and improving classification reliability. Carta degli Habitat extended the analysis to an ecological framework, illustrating both the potential and the limits of NDVI for habitat-level monitoring. The FSC product proved essential for snow validation, underscoring the utility of fractional approaches in capturing mixed-pixel conditions often overlooked by binary classification.

Methodologically, the comparison of Google Earth Engine and Sentinel Hub demonstrated that cloud platforms are not interchangeable but complementary.

Conclusion

GEE provided reproducibility and analytical depth through coding environments, while Sentinel Hub facilitated rapid visualization, API-based requests, and large-scale product generation. The consistency of outputs across platforms (with mismatches generally <15%) reinforces their reliability for climate-sensitive alpine monitoring. Future work should extend this dual-threshold framework to other alpine and Mediterranean regions to test its transferability under diverse snow-vegetation regimes.

Ecologically, the study revealed how vegetation greening trajectories and snow persistence are tightly linked. Snow duration emerged as a primary control on early-season NDVI, confirming long-term alpine observations (Marty et al., 2017; Kotlarski et al., 2022). Conversely, NDVI saturation in June highlighted the limitations of greenness indices in dense canopies, echoing known challenges in forested environments (Huete et al., 2002; Verrelst et al., 2015). These dynamics illustrate the vulnerability of alpine ecosystems to climate change, where warming-driven reductions in snow duration accelerate thermophilization and reshape habitat suitability (Lamprecht et al., 2018; Choler et al., 2021).

In conclusion, the research demonstrated that dual-threshold strategies, combined with diverse validation datasets, offer a robust framework for alpine vegetation and snow monitoring. While fixed thresholds preserve comparability across years, adaptive thresholds better represent dynamic environmental conditions. The integration of multiple reference datasets enhances accuracy assessment, while cross-platform processing increases reproducibility and scalability.

For the specific case study of the Maritime Alps, the combination of Google Earth Engine (GEE) with the Otsu adaptive threshold proved to be the most effective methodological choice. The Otsu method dynamically adjusts to variations in snow and vegetation reflectance, providing more realistic spatial distribution and reducing missed detections especially in transitional or heterogeneous terrain. Fixed thresholds, on the other hand, remain useful for long-term temporal comparisons where methodological consistency is prioritized.

Between the two processing platforms, GEE offered greater flexibility for reproducible workflows, threshold optimization, and integrated validation, while Sentinel Hub was particularly advantageous for fast visualization and

Conclusion

dissemination of results. Hence, a combined strategy using GEE for analytical processing and Sentinel Hub for operational product generation emerges as the most practical framework to support data-driven decision-making in alpine environmental management.

Looking forward, the study emphasizes the need to go beyond binary classifications by integrating fractional indices, machine learning, and multi-sensor data fusion. These approaches could capture the full spectrum of alpine landscape dynamics, from snowbed specialists to shrub encroachment, offering more nuanced indicators of ecosystem resilience. By providing both methodological lessons and ecological insights, this thesis contributes to advancing Earth Observation applications in one of Europe's most climate-sensitive mountain regions.

References

- Vojtěch Moravec, Yannis Markonis, Miroslav Trnka, Martin Hanel. (2023). Extreme hydroclimatic events compromise adaptation planning in agriculture based on long-term trends. ESS Open Archive. https://doi.org/10.22541/essoar.169903610.01052175/v1
- 2. A Huete a, K Didan a, T Miura a, E.P Rodriguez a, X Gao a, &, L.G Ferreira b. (2020). Overview of the radiometric and biophysical performance of the MODIS vegetation indices. *Remote Sensing of Environment*, 83(1–2), 195–213. https://doi.org/10.1016/S0034-4257(02)00096-2
- Adrián Melón-Nava. (2024). Recent Patterns and Trends of Snow Cover (2000–2023) in the Cantabrian Mountains (Spain) from Satellite Imagery Using Google Earth Engine. Remote Sensing, 16(19). https://doi.org/10.3390/rs16193592
- Adriana Romero, Department of Applied Mathematics and Analysis, Universität de Barcelona, Barcelona, Spain, &; Carlo Gatta; Gustau Camps-Valls. (2016). Unsupervised Deep Feature Extraction for Remote Sensing Image Classification. *IEEE Transactions on Geoscience and Remote Sensing*, 54(3), 1349–1362. https://doi.org/10.1109/TGRS.2015.2478379
- 5. Andrea Lamprecht, Philipp Robert Semenchuk, Klaus Steinbauer, Manuela Winkler, Harald Pauli. (2018). Climate change leads to accelerated transformation of high-elevation vegetation in the central Alps. *New Phytologist*, 220(2), 447–459. https://doi.org/10.1111/nph.15290
- Babak Mohammadi, Petter Pilesjö and Zheng Duan. (2023). The superiority of the Adjusted Normalized Difference Snow Index (ANDSI) for mapping glaciers using Sentinel-2 multispectral satellite imagery. GlScience & Remote Sensing, 60(1). https://doi.org/10.1080/15481603.2023.2257978
- 7. Baruth, B., Royer, A., Klisch, A., & Genovese, G. (2007). THE USE OF REMOTE SENSING WITHIN THE MARS CROP YIELD MONITORING SYSTEM OF THE EUROPEAN COMMISSION.

- 8. Beniston, M., Farinotti, D., Stoffel, M., Andreassen, L. M., Coppola, E., Eckert, N., Fantini, A., Giacona, F., Hauck, C., Huss, M., Huwald, H., Lehning, M., López-Moreno, J.-I., Magnusson, J., Marty, C., Morán-Tejéda, E., Morin, S., Naaim, M., Provenzale, A., ... Vincent, C. (2018). The European Mountain cryosphere: A review of its current state, trends, and future challenges. *The Cryosphere*, *12*(2), 759–794. https://doi.org/10.5194/tc-12-759-2018
- Bo-cai Gao. (1996). NDWI—A normalized difference water index for remote sensing of vegetation liquid water from space. *Remote Sensing of Environment*, 58(3), 257–266. https://doi.org/10.1016/S0034-4257(96)00067-3
- 10. Bonardi et al. (2010). (n.d.). The Influence of Climate Change on Alpine Geomorphological Processes" in: Geografia Fisica e Dinamica Quaternaria. 33(2), 167–174.
- Casazza, G., Barberis, G., & Minuto, L. (2005). Ecological characteristics and rarity of endemic plants of the Italian Maritime Alps. *Biological Conservation*, 123(3), 361–371. https://doi.org/10.1016/j.biocon.2004.12.005
- 12. Chang, C.-T., Chiang, J.-M., & Dai, J. (2023). Remote Sensing of Climate-Vegetation Dynamics and Their Effects on Ecosystems. *Remote Sensing*, 15(21), 5097. https://doi.org/10.3390/rs15215097
- 13. Chiara Graziani. (2024). ACLIMO Project: Deep Learning classification of aerial imagery for monitoring the effects of climate change on the mountain area of Maritime Alps [POLITECNICO DI TORINO]. https://webthesis.biblio.polito.it/33592/1/tesi.pdf
- 14. Choler, P., Bayle, A., Carlson, B. Z., Randin, C., Filippa, G., & Cremonese, E. (2021). The tempo of greening in the European Alps: Spatial variations on a common theme. *Global Change Biology*, *27*(21), 5614–5628. https://doi.org/10.1111/gcb.15820
- 15. CLAUDIO COMOGLIO, SARA RATTO and FRANCO BONETTO. (2003). The October 2000 flooding in Valle d'Aosta (Italy): Event description and landplanning measures for the risk mitigation. *International Journal of*

- River Basin Management, 1(2), 105–116. https://doi.org/10.1080/15715124.2003.9635197
- 16. Compton J. Tucker. (1979). Red and photographic infrared linear combinations for monitoring vegetation. *Remote Sensing of Environment*, 8(2), 127–150. https://doi.org/10.1016/0034-4257(79)90013-0
- 17. Darius Phiri, Matamyo Simwanda, Serajis Salekin, Vincent R. Nyirenda, Yuji Murayama and Manjula Ranagalage . (2020). Sentinel-2 Data for Land Cover/Use Mapping: A Review. *Remote Sensing*, 12(14). https://doi.org/10.3390/rs12142291
- Davide Notti, Daniele Giordan, Davide Bertolo, Fabiana Calò, Diego Reale, Simona Verde & Gianfranco Fornaro. (2023). State of activity classification of deep-seated gravitational slope deformation at regional scale based on Sentinel-1 data. *Landslides, Springer Nature Link, 20,* 2529–2544. https://doi.org/DOI%252010.1007/s10346-023-02114-7
- 19. Dirk Tiede a, Martin Sudmanns a, Hannah Augustin a, & Andrea Baraldi. (2021). Investigating ESA Sentinel-2 products' systematic cloud cover overestimation in very high-altitude areas. *Remote Sensing of Environment*, 252. https://doi.org/10.1016/j.rse.2020.112163
- 20. E. Belcore, M. Latella, M. Piras and C. Camporeale. (2024). Enhancing precision in coastal dunes vegetation mapping:ultra-high resolution hierarchical classification at theindividual plant level. *International Journal of Remote Sensing*, 45(13), 4527–4552. https://doi.org/10.1080/01431161.2024.2354135
- 21. Eric P. Crist; Richard C. Cicone. (1984). A Physically-Based Transformation of Thematic Mapper Data—The TM Tasseled Cap. *IEEE Transactions on Geoscience and Remote Sensing*, *GE-22*(3), 256–263. https://doi.org/10.1109/TGRS.1984.350619
- 22. ESA, 2023. (n.d.). *Copernicus Sentinel Missions Overview*. https://www.copernicus.eu/en/about-copernicus/infrastructure/discover-our-satellites

- 23. Francesco Parisi, Elia Vangi, Saverio Francini, Giovanni D'Amico, Gherardo Chirici, Marco Marchetti, Fabio Lombardi, Davide Travaglini, Sonia Ravera, Elena De Santis, Roberto Tognetti. (2023). Sentinel-2 time series analysis for monitoring multi-taxon biodiversity in mountain beech forests. Frontiers in Forests and Global Change, 6. https://doi.org/10.3389/ffgc.2023.1020477
- 24. Gascoin, S., Grizonnet, M., Bouchet, M., Salgues, G., & Hagolle, O. (2019). Theia Snow collection: High-resolution operational snow cover maps from Sentinel-2 and Landsat-8 data.
- 25. Giles M. Foody. (2002). Status of land cover classification accuracy assessment. *Remote Sensing of Environment*, 80(1), 185–201. https://doi.org/10.1016/S0034-4257(01)00295-4
- 26. Giulia Mazzotti, Richard Essery, Clare Webster, Johanna Malle, Tobias Jonas. (2019). Process-Level Evaluation of a Hyper-Resolution Forest Snow Model Using Distributed Multisensor Observations. Water Resources Research, 56(9). https://doi.org/10.1029/2020WR027572
- 27. György Büttner. (2014). CORINE Land Cover and Land Cover Change Products. In *Remote Sensing and Digital Image Processing* (Vol. 18, pp. 55–74). Springer.
- 28. Hall et al., 1995. *The Normalized-Difference Snow Index (NDSI): A Standard for Automated Snow Cover Mapping*. https://ntrs.nasa.gov/api/citations/20100031195/downloads/20100031195.pdf
- 29. Härer, S., Bernhardt, M., Siebers, M., & Schulz, K. (2018). On the need for a time- and location-dependent estimation of the NDSI threshold value for reducing existing uncertainties in snow cover maps at different scales. *The Cryosphere*, *12*(5), 1629–1642. https://doi.org/10.5194/tc-12-1629-2018
- Jesús Delegido ,Jochem VerrelstORCID, Luis AlonsoORCID and José Moreno.
 (2011). Evaluation of Sentinel-2 Red-Edge Bands for Empirical Estimation of Green LAI and Chlorophyll Content. Sensors, 11(7), 7063–7081. https://doi.org/10.3390/s110707063

- 31. Johannes H.C. Cornelissen, Peter M. Van Bodegom, Rien Aerts, Terry V. Callaghan, Richard S.P. Van Logtestijn, Juha Alatalo, F. Stuart Chapin, Renato Gerdol, Jon Gudmundsson, Dylan Gwynn-Jones, Anne E. Hartley, David S. Hik, Annika Hofgaard, Ingibjörg S. Jónsdóttir, Staffan Karlsson, Julia A. Klein, Jim Laundre, Borgthor Magnusson, Anders Michelsen, Ulf Molau, Vladimir G. Onipchenko, Helen M. Quested, Sylvi M. Sandvik, Inger K. Schmidt, Gus R. Shaver, Bjørn Solheim, Nadejda A. Soudzilovskaia, Anna Stenström, Anne Tolvanen, Ørjan Totland, Naoya Wada, Jeffrey M. Welker, Xinquan Zhao, M.O.L. (2007). Global negative vegetation feedback to climate warming responses of leaf litter decomposition rates in cold biomes. *Ecology Letters*, 10(7), 619–627. https://doi.org/10.1111/j.1461-0248.2007.01051.x
- 32. Jonathan Barichivich, Keith R. Briffa, Ranga Myneni, Gerard Van der Schrier, Wouter Dorigo, Compton J. Tucker, Timothy J. Osborn and Thomas M. Melvin. (2014). Temperature and Snow-Mediated Moisture Controls of Summer Photosynthetic Activity in Northern Terrestrial Ecosystems between 1982 and 2011. *Remote Sensing*, 6(2), 1390–1431. https://doi.org/10.3390/rs6021390
- 33. Kotlarski, S., Gobiet, A., Morin, S., Olefs, M., Rajczak, J., & Samacoïts, R. (2023). 21st Century alpine climate change. *Climate Dynamics*, *60*(1–2), 65–86. https://doi.org/10.1007/s00382-022-06303-3
- 34. Lucia Čahojová, Martin Ambroz, Ivan Jarolímek, Michal Kollár, Karol Mikula, Jozef Šibík & Mária Šibíková. (2022). Exploring Natura 2000 habitats by satellite image segmentation combined with phytosociological data: A case study from the Čierny Balog area (Central Slovakia). 12. https://doi.org/10.1038/s41598-022-23066-3
- 35. M. Drusch , U. Del Bello, S. Carlier a, O. Colin , V. Fernandez , F. Gascon, B. Hoersch , C. Isola , P. Laberinti , P. Martimort , A. Meygret , F. Spoto a, O. Sy , F. Marchese , & , P. Bargellini. (2012). Sentinel-2: ESA's Optical High-Resolution Mission for GMES Operational Services. *Remote Sensing of Environment*, 120, 25–36.
- 36. Magalì Matteodo, Klaus Ammann, Eric Pascal Verrecchia, Pascal Vittoz. (2016). Snowbeds are more affected than other subalpine–alpine plant

- communities by climate change in the Swiss Alps. *Ecology and Evolution*, *6*(19), 6969–6982. https://doi.org/10.1002/ece3.2354
- 37. Martin Sudmanns, Dirk Tiede, Hannah Augustin. (2019). Assessing global Sentinel-2 coverage dynamics and data availability for operational Earth observation (EO) applications using the EO-Compass. *International Journal of Digital Earth*, 13(7), 768–784. https://doi.org/10.1080/17538947.2019.1572799
- 38. Marty, C., Schlögl, S., Bavay, M., & Lehning, M. (2017). How much can we save? Impact of different emission scenarios on future snow cover in the Alps. *The Cryosphere*, *11*(1), 517–529. https://doi.org/10.5194/tc-11-517-2017
- 39. Martyna Wakulińska andAdriana Marcinkowska-Ochtyr. (2020). Multi-Temporal Sentinel-2 Data in Classification of Mountain Vegetation. *Remote Sensing*, *12*(17). https://doi.org/10.3390/rs12172696
- 40. Matiu, M., Crespi, A., Bertoldi, G., Carmagnola, C. M., Marty, C., Morin, S., Schöner, W., Cat Berro, D., Chiogna, G., De Gregorio, L., Kotlarski, S., Majone, B., Resch, G., Terzago, S., Valt, M., Beozzo, W., Cianfarra, P., Gouttevin, I., Marcolini, G., ... Weilguni, V. (2021). Observed snow depth trends in the European Alps: 1971 to 2019. *The Cryosphere*, *15*(3), 1343–1382. https://doi.org/10.5194/tc-15-1343-2021
- 41. Matthias Forkel, Wouter Dorigo, Gitta Lasslop, Emilio Chuvieco, Stijn Hantson, Angelika Heil, Irene Teubner, Kirsten Thonicke and Sandy P Harrison. (2019). Recent global and regional trends in burned area and their compensating environmental controls. *ERC Graphic lopscience_header.Png*. https://doi.org/10.1088/2515-7620/ab25d2
- 42. Michael Gottfried, Harald Pauli, Andreas Futschik, Maia Akhalkatsi, Peter Barančok, José Luis Benito Alonso, Gheorghe Coldea, Jan Dick, Brigitta Erschbamer, Marı'a Rosa Fernández Calzado, George Kazakis, Ján Krajči, Per Larsson, Martin Mallaun, Ottar Michelsen, Dmitry Moiseev, Pavel Moiseev, Ulf Molau, Abderrahmane Merzouki, Laszlo Nagy, George Nakhutsrishvili, Bård Pedersen, Giovanni Pelino, Mihai Puscas, ...Georg Grabherr. (2012). Continent-wide response of mountain vegetation to

- climate change. *Nature Climate Change*, *2*, 111–115. https://doi.org/10.1038/nclimate1329
- 43. N Gorelick, M Hancher, M Dixon, S Ilyushchenko, D Thau, R Moore. (2017). Google Earth Engine: Planetary-scale geospatial analysis for everyone. *Remote Sensing of Environment, 202,* 18–27. https://doi.org/10.1016/j.rse.2017.06.031
- 44. Official EEA website for CORINE products. https://www.eea.europa.eu/data-and-maps/data/copernicus-land-monitoring-service-corine
- 45. Orsolya Gyöngyi Varga , Robert Gilmore Pontius Jr 2\, Zsuzsanna Szabó1and Szilárd Szabó. (2020). Effects of Category Aggregation on Land ChangeSimulation Based on Corine Land Cover Data. *Remote Sensing*, 12(8). https://doi.org/10.3390/rs12081314
- 46. Otsu, N. (1979). A Tireshold Selection Method from Gray-Level Histograms.
- 47. Parajka, j, & Blöschl, G. (2008). The value of MODIS snow cover data in validating and calibrating conceptual hydrologic models. *Journal of Hydrology*, 358(3–4), 240–258. https://doi.org/10.1016/j.jhydrol.2008.06.006
- 48. Parastoo Mohseni. (2024). *Mapping Snow and Vegetation Coverage Using Multitemporal Open Satellite Imagery Case Study of Maritime Alps"* [POLITECNICO DI TORINO]. https://webthesis.biblio.polito.it/33594/
- 49. Pontus Olofsson a & , Giles M. Foody b, Martin Herold c, Stephen V. Stehman d, Curtis E. Woodcock a, Michael A. Wulder e. (2014). Good practices for estimating area and assessing accuracy of land change. Remote Sensing of Environment, 148, 42–57. https://doi.org/10.1016/j.rse.2014.02.015
- 50. Raphaël d'Andrimont, Astrid Verhegghen, & Guido Lemoine, Pieter Kempeneers, Michele Meroni, Marijn van der Velde. (2021). From parcel to continental scale A first European crop type map based on Sentinel-1

- and LUCAS Copernicus in-situ observations. *Remote Sensing of Environment*, 266. https://doi.org/10.1016/j.rse.2021.112708
- 51. Rosa Lasaponara ,Nicodemo Abate,Carmen Fattore,Angelo Aromando ,Gianfranco Cardettini and Marco Di Fonzo. (2022). On the Use of Sentinel-2 NDVI Time Series and Google Earth Engine to Detect Land-Use/Land-Cover Changes in Fire-Affected Areas. *Remote Sensing*, *14*(19). https://doi.org/10.3390/rs14194723
- 52. ROUSE JW. (1973). Monitoring vegetation systems in the Great Plains with ERTS. *Third NASA Earth Resources Technology Satellite Symposium*, 1973, 1, 309–317.
- 53. Russell G. Congalton. (1991). A review of assessing the accuracy of classifications of remotely sensed data. *Remote Sensing of Environment*, *37*(1), 35–46. https://doi.org/10.1016/0034-4257(91)90048-B
- 54. Russell G. Congalton, Kass Green. (n.d.). *Assessing the Accuracy of Remotely Sensed Data* (3rd ed., p. 346).
- 55. S. Puliti, J. Breidenbach, J. Schumacher, M. Hauglin, T.F. Klingenberg b, &, R. Astrup. (2021). Above-ground biomass change estimation using national forest inventory data with Sentinel-2 and Landsat. *Remote Sensing of Environment*, 265. https://doi.org/10.1016/j.rse.2021.112644
- 56. Shou-Ye Xue, Hai-Yan Xu, Cui-Cui Mu, Tong-Hua Wu, Wang-Ping Li, Wen-Xin Zhang, Irina Streletskaya , Valery Grebenets, Sergey Sokratov, Alexander Kizyakov , Xiao-Dong Wu. (2021). Changes in different land cover areas and NDVI values in northern latitudes from 1982 to 2015 Author links open overlay panel. Advances in Climate Change Research, 12(14), 456–465. https://doi.org/10.1016/j.accre.2021.04.003
- 57. Simone Pesaresi, Adriano Mancini, Giacomo Quattrini and Simona Casavecchia. (2020). Mapping Mediterranean Forest Plant Associations and Habitats with Functional Principal Component Analysis Using Landsat 8 NDVI Time Series. Remote Sensing, 12(7). https://doi.org/10.3390/rs12071132

- 58. Sven Kotlarski, Andreas Gobiet, Samuel Morin, Marc Olefs, Jan Rajczak & Raphaëlle Samacoïts. (n.d.). 21st Century alpine climate change. *Climate Dynamics*, 60(65–86), 10 May 2022. https://link.springer.com/article/10.1007/s00382-022-06303-3
- 59. Terzago, S., Bongiovanni, G., & Von Hardenberg, J. (2023). Seasonal forecasting of snow resources at Alpine sites. *Hydrology and Earth System Sciences*, *27*(2), 519–542. https://doi.org/10.5194/hess-27-519-2023
- 60. Thomas Nagler, Helmut Rott. Markus Hetzenecker, Jan Wuite and Pierre Potin . (2015). The Sentinel-1 Mission: New Opportunities for Ice Sheet Observations. *Remote Sensing*, 7(7), 9371–9389. https://doi.org/10.3390/rs70709371
- 61. Tiancai Zhou, W.H., Chongchong Ye, Jian Sun, Junnan Xiong, Jinniu Wang. (2020). Dynamics and Drivers of the Alpine Timberline on Gongga Mountain of Tibetan Plateau-Adopted from the Otsu Method on Google Earth Engine. Remote Sensing, 12(16). https://doi.org/10.3390/rs12162651
- 62. Vanessa Drolon, Antoine Rabatel, Pascal Sirguey, Philippe Maisongrande, Yves Arnaud, Etienne Berthier, Lucas Davaze, Jean-Pierre Dedieu and Marie Dumont. (2017). Annual and Seasonal Glacier-Wide Surface Mass Balance Quantified from Changes in Glacier Surface State: A Review on Existing Methods Using Optical Satellite Imagery. *Remote Sensing*, *9*(5), 507. https://doi.org/10.3390/rs9050507
- 63. Verrelst, J., Camps-Valls, G., Muñoz-Marí, J., Rivera, J. P., Veroustraete, F., Clevers, J. G. P. W., & Moreno, J. (2015). Optical remote sensing and the retrieval of terrestrial vegetation bio-geophysical properties A review. *ISPRS Journal of Photogrammetry and Remote Sensing*, 108, 273–290. https://doi.org/10.1016/j.isprsjprs.2015.05.005
- 64. V.V Salomonson & I Appel. (2004). Estimating fractional snow cover from MODIS using the normalized difference snow index. *Remote Sensing of Environment*, 89(3), 351–360. https://doi.org/10.1016/j.rse.2003.10.016

- 65. Zacharie Barrou Dumont, Simon Gascoin, César Deschamps-Berger, Florence Marti, Germain Salgues, Juan Ignacio López-Moreno, Jesús Revuelto, Timothée Michon, Paul Schattan and Olivier Hagolle. (2020). Estimating Fractional Snow Cover in Open Terrain from Sentinel-2 Using the Normalized Difference Snow Index. *Remote Sensing*, 12(8). https://doi.org/10.3390/rs1218290
- 66. **ARPA Piemonte, 2023** Regional Environmental Protection Agency of Piedmont, ItalyWebsite: http://www.arpa.piemonte.it/
- 67. **ESA (European Space Agency), 2015** Sentinel-2 User Handbook and related technical documentation

Website: https://sentinel.esa.int/

- 68. **ESA, 2019** Sentinel-2 MSI user guides and datasets
 Website: https://sentinel.esa.int/web/sentinel/user-guides/sentinel-2-msi
- 69. **ESA, 2023** Copernicus Sentinel missions overview Website: https://www.copernicus.eu/en/about-copernicus/infrastructure/discover-our-satellites
- 70. JRC (Joint Research Centre of the European Commission), 2023 LUCAS (Land Use/Cover Area frame Survey) database
 Website: https://ec.europa.eu/eurostat/web/lucas
- 71. Climate Engine

Website: https://climateengine.org

72. Official EEA website for CORINE products:

https://www.eea.europa.eu/data-and-maps/data/copernicus-land-monitoring-service-corine

73. Main page for CORINE Land Cover 2018 dataset:

https://land.copernicus.eu/pan-european/corine-land-cover/clc2018

74. NASA Earthdata LP DAAC (MODIS & VIIRS data)

https://earthdata.nasa.gov/eosdis/daacs/lp-daac

- 75. **Agri4Cast** (JRC's historical NDVI/statistics for agriculture) https://agri4cast.jrc.ec.europa.eu/DataPortal/
- 76. Sentinel Hub (EO Browser & APIs)

https://www.sentinel-hub.com/

(Direct EO Browser: https://apps.sentinel-hub.com/eo-browser/